

**SYNTHESIS AND CHARACTERIZATION OF A NOVEL
PALLADIUM NANOSTRUCTURED ENSEMBLE
SUPPORTED ON ANODIZED ALUMINA SUBSTRATES
FOR HYDROGEN SENSING APPLICATIONS**

by

Héctor Guillermo Méndez-Colberg

A dissertation submitted in partial fulfillment of the requirements for the degree of

DOCTOR OF PHILOSOPHY
in
CHEMICAL ENGINEERING

UNIVERSITY OF PUERTO RICO
MAYAGÜEZ CAMPUS
2015

Approved by:

María Martínez-Iñesta, Ph.D.
President, Graduate Committee

Date

Wilfredo Otaño-Rivera, Ph.D.
Member, Graduate Committee

Date

Agnes Padovani-Blanco, Ph.D.
Member, Graduate Committee

Date

David Suleiman-Rosado, Ph.D.
Member, Graduate Committee

Date

Paul Sundaram, Ph.D.
Graduate Studies Representative

Date

Aldo Acevedo-Rullán, Ph.D.
Chairperson of the Department

Date

ABSTRACT

Hydrogen is a versatile molecule used in many industrial processes. Hydrogen is flammable at concentrations between 4% to 75% v/v at atmospheric pressure with a tendency to leak. There are a variety of hydrogen sensors, each with its advantages and disadvantages. Resistor type sensors are the most simple and promising sensors since they can readily detect hydrogen at room temperature or higher. Palladium thin film technology can potentially yield selective, small, fast, and energy efficient hydrogen sensors. The principle of this technology is the concurrent electrical and structural changes in the Pd structure upon hydrogen absorption.

Synthesis methods for Pd based thin films are often expensive and energy consuming. In this work the solid-state reduction (SSR) synthesis method was established as energy and cost efficient way to obtain Pd, Ag₁₀Pd₉₀ and Pt₁₀Pd₉₀ films that can be used as hydrogen sensors. Film characterization included: X-ray Diffraction, Scanning Electron Microscopy, Atomic Force Microscopy, Profilemeter, Energy Dispersive X-Ray Spectroscopy and X-Ray Photoelectron Spectroscopy. The hydrogen response was studied at room temperature. The hydrogen sensing conditions were optimized based on the effects of the film morphology, oxidation of the sample, presence of oxygen, working voltage and residence time on the stability, sensitivity and response time.

The best synthesis conditions for SSR included liquid phase impregnation with addition of water during reduction. The best sensing results were obtained in a small

volume chamber, as it was determined that the response time depends on the residence time.

The response of pure Pd films was stable and precise from 0.01% to 2% v/v H₂/N₂ with sensitivities ranging from 0.6 to 8.3%. However, the signal is affected by structural changes that occur above 2% v/v H₂ that are related to the α to β Pd phase transition. The bimetallic films had an expanded range of detection due to a restriction on the phase transition lattice expansion. The Pt₁₀Pd₉₀ film exhibited the best sensing properties with a stable signal up to 50% v/v H₂, a high sensitivity (~10%) that was proportional to the hydrogen concentration up to 8% v/v H₂/N₂ and a fast response time in the 10 s order of magnitude.

RESUMEN

El hidrógeno es una molécula versátil que se utiliza en muchos procesos industriales. El hidrógeno es inflamable a concentraciones entre 4% a 75% v/v a presión atmosférica con una tendencia a tener fugas. Hay variedad de sensores de hidrógeno, cada uno con sus ventajas y desventajas. Sensores de tipo resistencia son los sensores más simples y prometedores ya que pueden detectar fácilmente hidrógeno a temperatura ambiente o mayor. Tecnología de películas delgadas de paladio pueden potencialmente producir sensores de hidrógeno selectivos, pequeños, rápidos, eficientes en energía. El principio de esta tecnología está en los cambios eléctricos y estructurales que concurren en la estructura de Pd tras la absorción de hidrógeno.

Métodos de síntesis para películas delgadas basadas en Pd son a menudo costosos y grandes consumidores de energía. En este trabajo el método de síntesis de reducción en estado sólido (SSR) se estableció como un medio costo-efectivo y eficiente en energía para obtener películas delgadas de Pd, Ag₁₀Pd₉₀ y Pt₁₀Pd₉₀ que se pueden utilizar como sensores de hidrógeno. La caracterización incluye: difracción de rayos X, microscopía electrónica de barrido, microscopía de fuerza atómica, perfilómetros, espectroscopía de rayos X por dispersión de energía, espectroscopía fotoelectrónica de rayos X. La respuesta de hidrógeno se estudió a temperatura ambiente. Las condiciones de detección de hidrógeno fueron optimizadas con base a los efectos que la morfología de la película, la oxidación de la muestra, la presencia de oxígeno, el voltaje de funcionamiento y tiempo de residencia tienen en la estabilidad, sensibilidad y tiempo de respuesta.

Las mejores condiciones de síntesis para SSR incluyen impregnación fase líquida con adición de agua durante la reducción. Los mejores resultados de detección se obtuvieron en una cámara de volumen pequeño, ya que se determinó que el tiempo de respuesta depende del tiempo de residencia.

La respuesta de las películas de Pd puro fue estable y precisa con sensibilidades que van de 0.6 a 8.3% para concentraciones de 0.01% a 2% v/v H₂/N₂. Sin embargo, la señal se ve afectada por los cambios estructurales relacionados con la transición de fase, de α a β , de Pd más allá de 2% v/v H₂. Las películas bimetálicas tenían una gama más amplia de detección debido a una restricción en la expansión del retículo que resulta de la transición de fase. La película Pt₁₀Pd₉₀ exhibió las mejores propiedades de detección con una señal estable hasta 50% v/v H₂, una alta sensibilidad (~ 10%) proporcional a la concentración de hidrógeno hasta 8% v/v H₂/N₂ y un tiempo de respuesta rápido en el orden de 10 s de magnitud.

*This work is dedicated to my family, especially to my queen and
princess... Ziara and Helena*

ACKNOWLEDGEMENTS

Firstly, I would like to acknowledge my advisor Dr. María Martínez-Iñesta for her guidance, motivation, and understanding during my research. Her patience and encouragement really helped me to achieve this goal. Besides my advisor, I would like to thank the members of my graduate committee, Dr. Wilfredo Otaño, Dr. David Suleiman, and Dr. Agnes Padovani for their perceptive comments and suggestions. Special acknowledgements to Dr. Wilfredo Otaño for lending me his resources at his laboratory, and for his support throughout the project.

More importantly, I thank my family for their unconditional support throughout the hard years that took to achieve this goal. Without them, none of this would have been possible. My lab mates, Jennie Feliciano M.S. and Keren Valentín M.S. for their work on the synthesis of the materials. Their work was the basis for mine. Mr. Ángel Zapata was of great help during the project since every time I needed technical counseling, he was there helping without hesitation. Very warm thanks to all of my friends who were always there during the hard thinking sessions, discussions, frustrations and during the relaxing periods of drinking and laughing.

Last but not least, thank you Ziara for your understanding and your outstanding support. This work is for you... and for Helena.

TABLE OF CONTENTS

1	INTRODUCTION	1
1.1	JUSTIFICATION.....	1
1.2	GENERAL AND SPECIFIC OBJECTIVES	2
1.3	BACKGROUND.....	4
1.3.1	<i>Pd Changes Upon Hydrogen Adsorption and Absorption.....</i>	<i>4</i>
1.3.2	<i>Synthesis Methods for Producing Pd Thin Films</i>	<i>6</i>
1.3.3	<i>Sensor Sensitivity and Response Time.....</i>	<i>7</i>
1.3.4	<i>Sensors</i>	<i>8</i>
1.4	CONCLUSIONS.....	21
1.5	REFERENCES.....	22
2	SYNTHESIS AND CHARACTERIZATION OF Pd, Pt/Pd AND Ag/Pd THIN FILMS USING SOLID-STATE REDUCTION (SSR) METHOD	28
2.1	INTRODUCTION	28
2.2	METHODOLOGY.....	29
2.2.1	<i>Synthesis for Pure Pd Films - Solid Impregnation.....</i>	<i>29</i>
2.2.2	<i>Synthesis for Pure and Bimetallic Films – Solution Impregnation</i>	<i>30</i>
2.2.3	<i>Characterization</i>	<i>31</i>
2.3	RESULTS AND DISCUSSION.....	32
2.3.1	<i>Pure Pd films - Solid Impregnation.....</i>	<i>32</i>
2.3.2	<i>Pure and Bimetallic Films - Solution Impregnation</i>	<i>36</i>

2.4	CONCLUSIONS.....	46
2.5	REFERENCES.....	47

**3 BASIC SENSING CHARACTERIZATION OF PD FILMS OBTAINED BY SSR:
EFFECT OF ELECTRODE CONNECTIVITY, PD CONCENTRATION, PARTIAL
REDUCTION AND PHASE CHANGE..... 50**

3.1	INTRODUCTION	50
3.2	METHODOLOGY.....	50
3.3	RESULTS AND DISCUSSIONS	52
3.3.1	<i>Effect of Electrode Connection.....</i>	<i>52</i>
3.3.2	<i>Effect of Partial Reduction.....</i>	<i>53</i>
3.3.3	<i>Effect of Pd Concentration.....</i>	<i>54</i>
3.3.4	<i>Effect of Phase Change on the Response.....</i>	<i>61</i>
3.4	CONCLUSIONS.....	65
3.5	REFERENCES.....	66

**4 OPTIMIZATION OF THE SENSING RESPONSE OF PD FILMS OBTAINED BY
SSR: EFFECT OF RESIDENCE TIME, SOLUTION IMPREGNATION, AND
VOLTAGE..... 67**

4.1	INTRODUCTION	67
4.2	METHODOLOGY.....	68
4.3	RESULTS	70
4.3.1	<i>Effect of Voltage.....</i>	<i>70</i>
4.3.2	<i>Effect of Impregnation Form and Film Morphology.....</i>	<i>73</i>
4.3.3	<i>Effect of Residence Time on Response Time</i>	<i>76</i>
4.4	CONCLUSIONS.....	85

4.5	REFERENCES.....	87
5	SENSING CHARACTERIZATION OF PD/PT AND PD/AG FILMS OBTAINED BY SSR.....	88
5.1	INTRODUCTION	88
5.2	METHODOLOGY.....	89
5.3	RESULTS AND DISCUSSION.....	89
5.4	CONCLUSIONS.....	96
5.5	REFERENCES.....	97
6	REDUCTION OF THE EFFECT OF ADSORBED OXYGEN ON THE PD BASED HYDROGEN SENSOR RESPONSE BY ADDITION OF A ZEOLITE LAYER	99
6.1	INTRODUCTION	99
6.2	METHODOLOGY.....	101
6.2.1	<i>Synthesis and Characterization of Pd sensors.....</i>	<i>101</i>
6.2.2	<i>Synthesis and Characterization of Zeolite P.....</i>	<i>101</i>
6.2.3	<i>Deposition of Zeolite P.....</i>	<i>101</i>
6.3	RESULTS AND DISCUSSION.....	102
6.3.1	<i>Effect of Oxygen on the Response</i>	<i>102</i>
6.3.2	<i>Effect of Zeolite P on the Hydrogen/Oxygen Pd Sensor Selectivity.....</i>	<i>107</i>
6.4	CONCLUSIONS.....	111
6.5	REFERENCES.....	112
7	CONCLUSIONS AND RECOMMENDATIONS.....	114

LIST OF FIGURES

FIGURE 1.1 PHASE DIAGRAMS FOR THE PALLADIUM HYDRIDE AT DIFFERENT H/PD RATIOS ⁵	5
FIGURE 2.1 SCHEMATIC SHOWING THE SSR METHOD	30
FIGURE 2.2 SEM IMAGES SHOWING THE PD FILM SURFACES ON THE REDUCTION SIDE (A) AND THE IMPREGNATION SIDE (B) FOR THE 5%PD SAMPLE.....	33
FIGURE 2.3 SEM IMAGE OF THE PD NANOWIRES OBTAINED AFTER REMOVAL OF THE AAM SUPPORT.....	33
FIGURE 2.4 SCHEMATIC REPRESENTING THE COMBINATION OF MORPHOLOGIES	33
FIGURE 2.5 X-RAY DIFFRACTION PATTERNS AT DIFFERENT HYDROGEN CONCENTRATIONS SHOWING WHERE PHASE CHANGES OCCUR FOR THE 5% PD SAMPLE.....	34
FIGURE 2.6 LONG EXPOSURE TO 0.5% H ₂ FOR A 5% PD SAMPLE	35
FIGURE 2.7 LONG EXPOSURE TO 1.25% H ₂ FOR A 5% PD SAMPLE.....	36
FIGURE 2.8 SEM MICROGRAPHS OF PURE Pd (1), Ag ₁₀ Pd ₉₀ (2), Pt ₁₀ Pd ₉₀ (3). COLUMN (A) SHOWS THE FILMS ON THE IMPREGNATION SIDE AND THE COLUMN (B) ON THE REDUCTION SIDE.....	39
FIGURE 2.9 Pd NANOWIRES FORMED AFTER DISSOLUTION WITH NaOH.....	39
FIGURE 2.10 METAL DISTRIBUTION OF Ag ₁₀ Pd ₉₀ (A), AND Pt ₁₀ Pd ₉₀ (B) FILMS ON THE IMPREGNATION SIDE OBTAINED BY EDS. THE STUDIED AREA IS SHOWED ON THE LEFT, Pd ON THE MIDDLE, AND THE SECOND METAL ON THE RIGHT.	40
FIGURE 2.11 XRD PATTERNS OF THE Pd BIMETALLIC FILMS ON THE IMPREGNATION SIDE OF A) Ag ₁₀ Pd ₉₀ , B) Pt ₁₀ Pd ₉₀	41
FIGURE 2.12 X-RAY DIFFRACTION PATTERNS WITH H ₂ CONCENTRATION FOR THE Ag ₁₀ Pd ₉₀ SAMPLE	42
FIGURE 2.13 X-RAY DIFFRACTION PATTERNS WITH H ₂ CONCENTRATION FOR THE Pt ₁₀ Pd ₉₀ SAMPLE	42
FIGURE 2.14 FULL XPS SPECTRA FOR THE Ag ₁₀ Pd ₉₀ SAMPLE	43
FIGURE 2.15 FULL XPS SPECTRA FOR THE Pt ₁₀ Pd ₉₀ SAMPLE.....	43
FIGURE 2.16 A) Pd AND B) Ag XPS SPECTRA OF THE Ag ₁₀ Pd ₉₀ SAMPLE.....	45
FIGURE 2.17 XPS SPECTRUM FOR THE Pt IN THE Pt ₁₀ Pd ₉₀ SAMPLE.....	45
FIGURE 3.1 PVC CHAMBER, ~7000 cm ³	51

FIGURE 3.2 HYDROGEN RESPONSE OF A 5%PD SAMPLE ROUGH FILM USING A 4000 SCCM TOTAL FLOW CONNECTED WITH (A) MICROPROBE W NEEDLES AND (B) CU WIRES ADHERED WITH AG PASTE.	53
FIGURE 3.3 RESPONSE OF 5%WT PD SAMPLE ROUGH FILM UNDER A TOTAL FLOW OF 4000 SCCM (A) WITH NO WATER ADDED DURING REDUCTION, (B) WITH WATER ADDED DURING REDUCTION, AND (C) PRETREATED WITH 5%V/V H ₂	54
FIGURE 3.4 HYDROGEN RESPONSE TO A 2.5% PD SAMPLE.....	55
FIGURE 3.5 HYDROGEN RESPONSE TO A 5% PD SAMPLE.....	55
FIGURE 3.6 HYDROGEN RESPONSE TO A 10% PD SAMPLE.....	56
FIGURE 3.7 SENSITIVITY VS. SQUARE ROOT OF H ₂ CONCENTRATION.	59
FIGURE 3.8 AVERAGE SENSITIVITY VARIATION AT DIFFERENT H ₂ CONCENTRATIONS BETWEEN VARIOUS SAMPLES.	59
FIGURE 3.9 AVERAGE RESPONSE TIME T ₉₀ AND STANDARD DEVIATION AT DIFFERENT HYDROGEN CONCENTRATIONS FOR SAMPLES WITH 2.5%, 5% AND 10% WT PD LOADINGS.....	60
FIGURE 3.10 SAMPLE EXPOSED TO VARIOUS CYCLES OF H ₂ SHOWING THE EFFECT OF PHASE TRANSITION ON THE RESPONSE IN CH-7000.....	62
FIGURE 3.11 HYSTERESIS BEHAVIOR OF A 5% PD SAMPLE.....	63
FIGURE 3.12 SAMPLE EXPOSED TO H ₂ CONCENTRATIONS HIGHER THAN 2% V/V.....	63
FIGURE 3.13 RESPONSE OF A 1.5%WT PD SAMPLE TO DIFFERENT HYDROGEN CONCENTRATIONS.....	64
FIGURE 4.1 POLYCARBONATE CHAMBER, V~43,000 CM ³	69
FIGURE 4.2 STAINLESS STEEL CHAMBER, V~90 CM ³	70
FIGURE 4.3 VOLTAGE DEPENDENCY ON SENSITIVITY AND T ₉₀ FOR A 5%WT PD SAMPLE OBTAINED BY SOLID-SSR.	72
FIGURE 4.4 VOLTAGE DEPENDENCE ON SENSITIVITY AND T ₉₀ FOR A SAMPLE SYNTHESIZED BY SOLUTION-SSR.....	73
FIGURE 4.5 SENSITIVITY VALUES COMPARED TO THE SURFACE RMS ROUGHNESS. VARIOUS SENSITIVITY AND ROUGHNESS MEASUREMENTS WERE PERFORMED ON EACH SAMPLE.....	74
FIGURE 4.6 RESPONSE TIME VALUES COMPARED TO THE SURFACE RMS ROUGHNESS. VARIOUS SENSITIVITY AND ROUGHNESS MEASUREMENTS WERE PERFORMED ON EACH SAMPLE.....	75
FIGURE 4.7 CYLINDER OF LENGTH <i>L</i> AND RADIUS <i>R</i> WITH GAS FLOWING IN Z-DIRECTION.....	79
FIGURE 4.8 STEADY-STATE CONCENTRATION ALONG Z AT DIFFERENT <i>PE</i> NUMBERS.	81

FIGURE 4.9 CHANGES IN THE CYLINDER CONCENTRATION IN Z WITH TIME AT DIFFERENT PE AND P .	82
FIGURE 4.10 SENSITIVITY AND RESPONSE TIME DEPENDENCE ON RESIDENCE TIME FOR A SOLID-SSR SAMPLE AT 1% H_2 .	84
FIGURE 4.11 SENSITIVITY AND RESPONSE TIME DEPENDENCE ON RESIDENCE TIME FOR A SOLUTION-SSR SAMPLE AT 1% H_2 .	85
FIGURE 5.1 SENSING RESPONSE OF A PURE PD SAMPLE TO HYDROGEN CONCENTRATIONS RANGING FROM 1% TO 4% (A) AND THE SENSING RESPONSE OF A SAMPLE UP TO 50% v/v H_2/N_2 (B).	91
FIGURE 5.2 SENSING RESPONSE OF A $PT_{10}PD_{90}$ SAMPLE TO HYDROGEN CONCENTRATIONS RANGING FROM (A) 1% TO 10% AND (B) 2% TO 50%v/v H_2/N_2 .	91
FIGURE 5.3 HYSTERESIS BEHAVIOR FOR A $PT_{10}PD_{90}$ SAMPLE.	93
FIGURE 5.4 SENSING RESPONSE OF A $AG_{10}PD_{90}$ FILM (A) FROM 1% TO 4% v/v H_2/N_2 AND (B) 1% TO 50% v/v H_2/N_2 .	95
FIGURE 6.1 GISMONDINE FRAMEWORK VIEWED ALONG THE A-AXIS ¹³ .	100
FIGURE 6.2 SAMPLE WITH 5%WT PD EXPOSED TO O_2 AFTER HYDROGEN EXPOSURE.	104
FIGURE 6.3 SAMPLE WITH 5%WT PD EXPOSED TO H_2/ N_2 AND H_2 /COMPRESSED AIR CYCLES.	105
FIGURE 6.4 SAMPLE WITH 5%WT PD EXPOSED TO N_2 AND AIR CYCLES.	106
FIGURE 6.5 XRD PATTERNS FOR ZEOLITE TYPE NA-P1 SAMPLE COMPARED TO THEORETICAL PATTERN.	108
FIGURE 6.6 SAMPLE WITH 5%WT PD EXPOSED TO CYCLES OF 1%v/v H_2 , N_2 AND O_2 DILUTED WITH N_2 , (A) NO ZEOLITE DEPOSITED, AND (B) ZEOLITE LAYER DEPOSITED.	109

LIST OF TABLES

TABLE 2.1 PERCENT CHANGE BETWEEN THE SURFACE ROUGHNESS WHEN COMPARED TO CLEAN A AAM	38
TABLE 3.1 SENSITIVITY VALUES FOR THE DIFFERENT SAMPLES	57
TABLE 4.1 RESPONSE TIME FOR 5%WT PD SAMPLES TO 1%V/V H ₂ IN CHAMBERS OF DIFFERENT VOLUMES.....	77
TABLE 4.2 RESULTS FOR T ₉₀ AND SENSITIVITY IN THE CH-7000 OF A 5%WT PD SAMPLE AT 1%V/V H ₂ AS A FUNCTION OF TOTAL FLOW. TO REDUCE THE EXPERIMENTAL SAMPLE VARIANCES, THIS EXPERIMENT WAS DONE ON ONE SAMPLE WITH CYCLING OF DIFFERENT FLOWS.	78
TABLE 4.3 INITIAL AND BOUNDARY CONDITIONS FOR EQUATION 4.5	79
TABLE 4.4 INITIAL AND BOUNDARY CONDITIONS FOR EQUATION 4.6	80
TABLE 4.5 RESULTS FOR T ₉₀ AND SENSITIVITY VARYING TOTAL FLOW FOR THE CH-90 CHAMBER AT 1% H ₂	84
TABLE 5.1 SENSITIVITY AT VARIOUS CONCENTRATIONS FOR THE PD-M SAMPLES (NS = NOT STABLE).	91
TABLE 5.2 RESPONSE TIME AT VARIOUS CONCENTRATIONS FOR THE PD AND PD-M SAMPLES (NS = NOT STABLE) ...	94
TABLE 6.1 CURRENT CHANGES FOR THE SAMPLE WITH AND WITHOUT ZEOLITE DEPOSITION. RESPONSE TIMES ARE SHOWN FOR HYDROGEN CYCLES AFTER OXYGEN EXPOSURE.....	110

1 INTRODUCTION

1.1 JUSTIFICATION

Hydrogen is a versatile molecule that is used in numerous processes in very diverse industries. Hydrogen is considered the cleanest fuel available because its combustion yields just water as a byproduct. It can be used to produce electricity in fuel cells, which are used in transportation and stationary power generation. Electrical generators use hydrogen as a coolant because of its thermal conduction properties. In the chemical industry, hydrogen is used in a wide range of hydrogenation reactions such as the production of ammonia, a chemical widely used in agricultural applications. In the petrochemical industry, hydrogen is required for crude oil refinements and in the food industry hydrogen is used for the hydrogenation of vegetable oils to produce saturated fats.

The United States Occupational Safety and Health Administration (OSHA) regulates the use of hydrogen because mixtures of hydrogen with air, oxygen, or other oxidizers are highly flammable over a wide range of compositions. The flammability limits based on the volume percent of hydrogen in air (at 14.7 psia) are 4.0% and 75.0% at atmospheric pressure. Hydrogen can burn in two major modes: deflagration and detonation. Deflagration is the ordinary form of burning; the flame travels through the mixture at subsonic speeds, and when the flame and shock wave travel through the mixture at supersonic speeds it is called detonation. In addition, hydrogen has a tendency to leak due to its small molecular size. Common workplace tasks such as cutting,

welding, drilling, and even static electricity could provide ignition sources that can cause dangerous explosions.

One standard safety measure is to use sensors that can detect hydrogen concentrations below the lower explosion limit. A chemical sensor is a device that produces a measurable signal in the presence of a chemical species or by changes in its concentration. Palladium (Pd) based sensors are of particular interest as hydrogen sensors because Pd can absorb large quantities of hydrogen into its lattice, up to 900 times its own volume, which significantly change its electrical properties. Palladium thin films, specifically, have shown high sensitivity and selectivity to hydrogen due, in part, to the increased surface to volume ratio.

In this chapter, the development of palladium thin films for hydrogen sensing is briefly reviewed.

1.2 GENERAL AND SPECIFIC OBJECTIVES

The general objective of this work is to develop and characterize metal-based electrochemical nanostructured sensors that can selectively detect H₂ at various concentrations for safety applications that can include H₂ leak detection and H₂ monitoring. The specific objectives are the following.

1. Synthesis of Pd and Pd based nanostructures.
 - a. The Pd nanostructures will be synthesized using commercially available anodized alumina membranes using the solid-state reduction method developed in our laboratory^{1,2}.

- b. The synthesis of nanostructures of mixtures of Pd with other key metals such as silver (Ag), platinum (Pt) using solid-state reduction will be developed.
 - c. Understand the solid-state reduction synthesis method and be able to explain the formation of the resulting nanostructures.
 2. Characterization of the supported nanostructures
 - a. Evaluation of crystal structure and phase changes upon hydrogen adsorption from X-ray diffraction data.
 - b. Analysis of sample morphology with scanning electron microscopy (SEM), and profilometer.
 - c. Elemental analysis of samples using energy dispersive X-ray spectroscopy (EDS) and X-ray photoelectron spectroscopy (XPS)
 3. Adaptation of the membrane supported nanostructures as H₂ sensing elements.
 4. Study the response of the membrane supported nanostructures to H₂ in flow test chambers.
 - a. Build various flow test chambers.
 - b. Evaluate the effect of changing test conditions such as gas flow rates, chamber volume, and voltage.
 - c. Evaluate the effect on the response with the incorporation of other metals.

- d. Understand the mechanisms that govern the sensor response and to be able to explain these mechanisms to state what makes them different from existing sensors.

1.3 BACKGROUND

1.3.1 Pd Changes Upon Hydrogen Adsorption and Absorption

The absorption of hydrogen in Pd has been studied extensively since the early observations done in 1866 by Graham³ and a comprehensive review was presented by Lewis in 1967.⁴ The thermodynamics and kinetics of the absorption phenomena were reviewed by Wicke in 1978⁵ and Flanagan in 1991⁶ More recently, in 2006, Jewell and Davis⁷ compared the computational and experimental work done on the adsorption and absorption of the palladium-hydrogen system.

Palladium has a face-centered-cubic (fcc) structure with a lattice parameter of 3.890 Å. Hydrogen adsorbs dissociatively on the Pd surface and diffuses into the metal lattice. When the gas phase hydrogen molecules, the surface adsorbed hydrogen atoms, and hydrogen absorbed within the Pd structure reach equilibrium, a palladium hydride is formed.⁸ The absorbed hydrogen atoms coordinate octahedrally with the Pd atoms expanding its fcc structure isotropically. The dilute hydride is called the α -phase and it has a lattice parameter of 3.894 Å at room temperature.⁹ At higher hydrogen concentrations (at a H/Pd ratio close to 0.1⁶ or about 7 torr at 300 K¹⁰), Pd undergoes another phase change to the β -phase, with a lattice parameter of 4.025 Å at room temperature. Figure 1.1 shows a typical phase diagram for the palladium hydride at various temperatures. The volume change associated with this phase transition is 10.4%.⁹

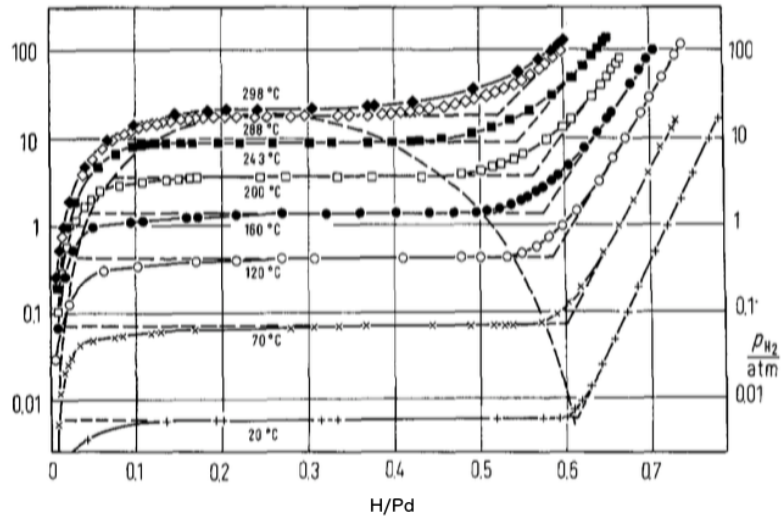


Figure 1.1 Phase diagrams for the palladium hydride at different H/Pd ratios⁵

These phase transitions can be observed in a hydrogen pressure-composition (P-H/Pd) curve of the Pd-hydrogen system as inflection points. The region where the pressure is invariant with hydrogen content, indicates the coexistence of the two solid hydride phases.¹¹ X-ray studies have shown that the miscibility gap between the two solid phases is narrowed when the crystallite size is decreased.^{12,13}

Hydrogen absorption also changes the resistivity of palladium. In the bulk, the resistivity of Pd increases proportionally to the concentration of absorbed hydrogen.^{4,5,14,15} This has been described using the Mott model.^{5,16,17} In this model the electrons of the absorbed hydrogen atoms fill the holes in the Pd d-bands. The resulting H cations weakly scatter conduction electrons giving rise to a small increase in the resistivity that is associated with the formation of the α -phase. As the holes in the d-band are completely filled, electrons occupy the s-band whose states are delocalized. This

causes a sharp increase in the resistivity that is associated with the formation of the β -phase.¹⁶

Studies with Pd alloys and bimetals have shown that the α to β phase transition is delayed to higher hydrogen concentrations in the presence of a second metal.^{10,18} This has been observed more frequently for Ni/Pd and Ag/Pd¹⁸⁻²³ but other combinations such as Cu/Pd²¹ and Ti/Pd²⁴ have also shown these effects. However, when the M:Pd ratio is approximately above 10:90, the solubility of hydrogen is significantly reduced²¹ and this reduces the resistivity changes with hydrogen.²⁵

The structural and electronic changes that Pd undergoes when it is exposed to hydrogen are the fundamental properties behind the mechanism of detection of the different hydrogen sensors reviewed here.

1.3.2 Synthesis Methods for Producing Pd Thin Films

Pure Pd and multi-metallic films for hydrogen sensing are commonly obtained by vacuum deposition methods²⁶ such as sputtering,^{27,28} electron beam evaporation^{10,29}, and thermal evaporation.³⁰⁻³² In sputtering a source is bombarded with a high-energy ionized gas, which ejects surface atoms that are then deposited on a new surface. In electron beam evaporation a target anode is bombarded with an electron beam produced using a charged filament cathode. The ejected atoms from the target are then deposited as a film on a substrate. In thermal evaporation a source is heated above its evaporation temperature and the vaporized atoms or molecules condense in the substrate's surface. With these techniques the film thickness, deposition rates, and microstructure can be controlled. More information about these techniques can be found in the books by Mattox.^{26,33}

1.3.3 Sensor Sensitivity and Response Time

Two of the main parameters used to compare the performance of sensors are sensitivity and response time.

1. Sensitivity

Sensitivity can be defined as the ratio of the absolute difference of the initial and final measured signal values and the initial value as described in the following equation:

$$S = \frac{|I_0 - I_f|}{I_0} \times 100 \quad (\text{Eq. 1.1})$$

where I_0 represents the initial signal and I_f represents the final signal value. Thus, a sensor with a high sensitivity can detect lower concentrations of hydrogen and can be used as a safety sensor.

2. Response times

The response time is defined as the time required to achieve a specific percentage change in the measured signal. Specific response times usually cited in the literature are: t_{90} which corresponds to the time required to achieve 90% change in the signal, t_{50} which is the time required to achieve 50% change in the signal and $t_{36.8}$ which is the time required to achieve a 36.8% change in the signal. The latter is based on relaxation time theory³⁴ and, according to this theory, this is the time to reach 36.8% (e^{-1}) of equilibrium.

The U.S. Department of Energy (DoE) established in 2011 a target for the response time of less than 1 second for a concentration range of 0.1 to 10%.^{35,36} However, the values of this parameter can vary significantly depending on the method used and the

experimental conditions as demonstrated in 2006 by Sawaguchi et al.³⁷ and in 2010 by Boon-Brett et al.³⁸

The response of a sensor is faster as the hydrogen concentration is increased. If the adsorption of hydrogen in Pd is described using a Langmuir adsorption model, the adsorption rate, r_a , is proportional to the square root of the H₂ partial pressure at low concentrations.³⁹ Therefore, assuming the adsorption step is rate limiting, as the hydrogen concentration is increased the adsorption rate increases and the response time of the sensor decreases.

Other important parameters used to evaluate the performance of sensors are recovery time, selectivity, signal stability and limits of detection, among others. A complete report on the requirements for hydrogen safety sensors was written by Buttner et al.⁴⁰

1.3.4 Sensors

Industrial scale hydrogen sensing has been achieved with technologies like gas chromatography and mass spectroscopy that are still in use today.⁴¹ The bulky and expensive equipment required by these techniques and their slow response time make them unsuitable for many applications.^{42,43} To meet the 2011 requirements of the DOE for hydrogen sensors they should be small, fast responding, sensitive, and their production should be cost effective. Reports in the last decades have shown that hydrogen sensors based on Pd thin films can potentially meet these requirements by controlling their morphology and sensor configuration.⁴⁴

Different Pd thin film hydrogen sensor technologies are reviewed below. Their mechanism of detection is based on the changes in the Pd electrical and structural

properties upon hydrogen absorption as discussed above. An attempt has been made to highlight the development of each type of sensor chronologically since their inception.

1. Metal Oxide Semiconductor (MOS) Type Sensor

A. Metal Oxide Semiconducting Transistor

Changes in the electrical properties of Pd upon absorption of hydrogen,^{4,20} inspired Lundström in 1975^{45,46} to be one of the first to use Pd films as hydrogen sensing elements in a metal-oxide-semiconductor (MOS) transistor device. In their sensor, a 10 nm thick Pd film was deposited through electron evaporation as a gate metal over a 10 nm silicon oxide layer on top of a silicon substrate. When a positive potential was applied to the gate, it produced a current between the source and the sink of the transistor. When hydrogen absorbed into the Pd film it diffused through the metal-insulator interface changing the work function and consequently the measured voltage. They were able to detect 320 ppm of hydrogen in air at 150 °C but the response time was very slow. Also, these sensors required oxygen to effectively remove the absorbed hydrogen and high temperatures in order to work.

B. Schottky diodes

Based on the early work by Lundström, Schottky diodes were developed as hydrogen sensing elements. At this time Schottky diodes were being studied for photovoltaic applications^{47,48}, and were explored for hydrogen sensing due to the simplicity of the Schottky diode assembly. Pd based Schottky diodes consist of a Pd thin film deposited on a thin insulating layer located on top of a semiconductor. One of the main differences with a MOS transistor is that it does not have a source and sink.

In these diodes the Fermi levels of the semiconductor and the metal are aligned resulting in a new work function that is called the Schottky barrier height. As in MOS transistors, hydrogen, when absorbed in the Pd film, changes this Schottky barrier height. The sensor response is given by the voltage change when the diode is operated with a constant current bias. A detailed review on Schottky diodes as sensing devices is given by Potje-Kamloth⁴⁹.

Shivaraman et al.⁵⁰ and Steele et al.⁵¹ were among the first to report the use of Schottky diodes as hydrogen sensing elements using palladium thin films as the active component in 1976. In 1979, Ito⁵² demonstrated that the diode current increased proportional to the hydrogen concentration in air at various temperatures (room temp to 84 °C). They also showed that increasing the temperature increased the sensitivity and decreased the response time of the sensing element. They concluded that the sensing response was due to the lowering of the Pd work function as hydrogen absorbed into the Pd structure.

Schottky diodes can also act as capacitors if the oxide layer is thicker, up to 100 nm, and are able to function as hydrogen sensing elements as reported by Steele⁵³ in 1976 and by Lundström in 1977.⁵⁴

Although Schottky diodes were capable of detecting leaks because of their high sensitivity, they were not as effective for hydrogen monitoring applications because there was a baseline drift in the signal as the sample was exposed to various sensing cycles^{55,56}. Armgarth and Nylander⁵⁷ resolved the issue by adding a 10 nm intermediate layer of alumina (Al₂O₃) between the Pd film and the SiO₂ film. They concluded that hydrogen interacted with the SiO₂ and hypothesized that migration of positively charged H atoms

through SiO₂, also known as ion drifting, affected the stability of the sensor. Reports by Hofstein⁵⁸, Revesz⁵⁹, and Mrstik⁶⁰ studied this phenomena in more detail.

Armgarth et al.⁶¹ also showed in 1982 that, in Schottky diodes, Pd was more effective than Pt as the gate metal for hydrogen detection at low concentrations in air but commented that the latter would be more effective at high concentrations. Fonash⁶² Ruths⁶³, and Keramati^{64,65} also studied the role of Pd films in Schottky diodes.

Hughes et al.¹⁹ addressed the baseline drift by using palladium-silver alloys in 1987. They showed that the baseline drift, caused by the blistering and/or peeling of the films due to phase changes, was eliminated using low concentrations of Ag (<10%) and the response time was improved. Choi et al.⁶⁶ found a similar result for Pt/Pd bimetallic films.

Schottky diodes are still being used as commercial hydrogen sensors because of their small size, durability and high sensitivity at concentrations below the explosion limit. However, oxygen is needed in these sensors to improve the recovery time and they need to operate at high temperatures for a fast response time and high sensitivity. There is, thus, a need for more versatile sensing elements that can also respond at lower temperatures in vacuum and inert atmospheres.⁴⁰

2. Surface Acoustic Wave Sensors

D'Amico et al.^{67,68} in 1982 introduced a new Pd film based sensor with a response based on the velocity changes undergone by surface acoustic waves (SAW) propagating on a piezoelectric YZ-LiNbO₃ film substrate. To make these sensors sensitive to hydrogen, the substrate is coated with a Pd film. Hydrogen absorption and desorption on

the Pd film affects the propagation velocity of an acoustic wave by changing its density and elastic properties and the changes are proportional to the hydrogen concentrations.

By adding a 720 nm Copper(II) phthalocyanine (CuPc) layer under a 20 nm Pd layer, Jakubik et al.⁶⁹ increased the sensitivity by 92% compared to conventional SAW sensors but had to operate at higher temperatures (70 °C vs 30 °C). With this modification these sensors were able to detect hydrogen concentrations from 50 ppm to 30,000 ppm.

SAW type sensors have the potential to detect hydrogen at a wide range of concentrations. However, their implementation as a commercial hydrogen sensing technology is still a challenge in terms of their long term stability and interference with other gases.⁷⁰ The response time with these sensors is also still slow ranging from 100 s to 25 min.

3. Optical Sensors

Butler⁷¹⁻⁷⁴ developed a new type of hydrogen optical sensing element by sputtering a single mode optical fiber with a 10 µm Pd film coating. As hydrogen is absorbed on Pd it expands, changing the effective optical path of the length of the optical fiber, which can be detected by interferometry.

Following Butler's work, Tabib-Azar⁷⁵ developed a new type of fiber optic hydrogen sensor consisting of a thin film of Pd deposited on the exposed core of a multimode optical fiber. The light traveling through the core excites evanescent fields at the surface of the core. When the sample is exposed to hydrogen, the expansion of the Pd film changes the refractive index and induces a strain in the fiber which influences the

phase of the guided light. The response time of these sensors was 20-30 s and could detect hydrogen concentrations in the range of 0.2-0.6% v/v H₂.

Zhao et al.⁷⁶ investigated the humidity effect on Pd₆₀Au₄₀ thin film based optical sensors. The bimetallic 20 nm films were deposited on glass substrates using radio frequency (RF) magnetron sputtering and its transmittance was measured as a function of humidity. As the humidity was increased, the response of the sensing element decreased to the point that the sensor was almost unresponsive. They attributed this effect to two possibilities: 1) blistering of the Pd film and 2) Pd catalyzed surface H₂O reactions that consumed H₂.

Optical sensors have the possibility to be implemented in explosive environments since there are no internal electrical signals that can cause ignition sources. In 2013 work was still being done to improve the stability of optical hydrogen sensing elements, which is still a major challenge.⁷⁷

4. Micromechanical Sensors

Following on the preliminary prototype by Britton et al.⁷⁸ and Okuyama et al.⁷⁹ on cantilever based hydrogen sensors, Baselt et al.⁸⁰ in 2003 conducted an extensive study on the design and the effects of environmental parameters on microelectromechanical hydrogen sensors. The sensor consisted of cantilever beams with a Pd₉₀Ni₁₀ 20 nm coating deposited by dual electron beam evaporation on a 5 nm Zr adhesion layer. As the Pd expands as a consequence of hydrogen absorption the cantilever is bent. The level of bending is measured by the capacitance between the cantilever and a stationary conductive lower plate. These sensors can detect hydrogen concentrations between 0.1 and 100%, however the response time is in the order of minutes.

5. Ferromagnetic Sensors

A new idea that is been developed by Chang et al.⁸¹, is to use a (5-40 nm) Co thin film under a (10-20 nm) Pd thin film as a ferromagnetic sensor. Hydrogen absorption shifts and narrows the ferromagnetic resonance of the Co film, which can be measured by microwave ferromagnetic resonance. According to Chang, this measurement method allows sensing of the hydrogen remotely.

6. Chemiresistors

Chemiresistors are devices that change their resistance when exposed to a gas or vapor. On Pd based chemiresistors, the resistance increases or decreases proportionally to the amount of hydrogen absorbed. Chemiresistor based sensors require low power and low temperatures in order to work and are fast responding (<15 s), accurate ($\pm <5\%$), and can detect hydrogen concentrations between 0.1-100%v/v.⁷⁰

Hughes and Schubert¹⁰ were among the first to probe Pd based MOS devices as chemiresistors and found that they could easily detect hydrogen. In 1992¹⁰ and 1995¹⁸ they studied Pd/Ni alloys chemiresistors and found that films with Ni concentrations higher than 8% delay the α to β -phase transition to $\sim 80\%$ v/v H₂ in nitrogen. This results in a stable baseline in the sensor signal and reduces blistering and delamination of the film caused primarily by the large volume expansion as the Pd goes through the β -phase transition. Nickel concentrations higher than 56%, however, made the sensor unresponsive to hydrogen. They concluded that these sensor elements could be used with a nickel concentration not higher than 10% and should be operated at 50 °C.

As the Pd goes through the α to β -phase transition the structure undergoes lattice strain deformation. The relaxation of these strains during hydrogen desorption is much

slower than their formation resulting in a hysteresis in a resistance-composition diagram.^{18,23,82,83} This effect affects the sensor stability. Lee et al.^{23,84} studied the effect of thickness and alloys on this hysteresis. They used Pd and Pd/Ni thin films ranging from 5-400 nm in thickness deposited by DC magnetron sputtering on silicon substrates with a 300 nm oxide layer to deposit. They showed that by decreasing the thickness of pure Pd films, the hysteresis in the sensitivity versus H₂ concentration curve decreases gradually, while adding Ni to the film eliminates it. Kim et al.²⁴ observed the same behavior by adding a titanium layer between a Pd thin film and an oxidized silicon substrate.

A. Response of Discontinuous Pd Nanostructures

In 2001, a widely cited article by Favier et al.⁸⁵ reported hydrogen sensors made from arrays of 50-300 nm Pd wires supported on graphite that had an inverse response to hydrogen than bulk Pd. They proved that the mechanism of detection was dominated by the closing of nanoscopic gaps in the wires due to the volume expansion associated with the Pd phase transition. These sensors had a response time of ~75 ms in 5% H₂. After this year the number of publications on hydrogen sensors has grown exponentially.⁷⁰

Inspired by Favier's results^{85,86} and on the early findings of Morris et. al.^{87,88}, Dankert et al.⁸⁹ proposed in 2002 a new way to explore the lattice expansion effect for hydrogen sensing. They fabricated discontinuous Pd films of 2-5 μm agglomerates by Joule heating over a sapphire substrate. The resistance of the sensing element decreases in the presence of hydrogen due to the induced lattice expansion provoked by the absorption which increases the number of conducting percolation pathways.

Following the work by Dankert, Xu et al.³⁰ synthesized Pd nanoparticles close to the percolation threshold forming a Pd film ~3.3 nm thick by thermal evaporation on

glass substrates. They demonstrated that by adding the siloxane self-assembled monolayer (SAM) between the glass substrate and the Pd film they could enhance the hydrogen sensing performance of the samples by improving response time and sensitivity. The Pd film on the siloxane covered glass showed an increase in conductance ($\Delta\sigma/\sigma_0$ with $\Delta\sigma=\sigma-\sigma_0$) as high as 68% and a t_{90} of 68 ms when exposed to 2% H₂. The SAM reduces the friction between the film and the substrate during the hydrogen induced lattice expansion therefore improving the responsiveness of the sensing element.

More recently, Wagner et al.⁹⁰ studied further the effect of nanoscopic gaps in 15 nm Pd films with meandering 14 nm island gaps deposited by sputtering on a sapphire substrate. These films show an enhanced percolation effect when exposed to up to 8% v/v H₂ with a resistance drop of ~5000%.

A. Effect of the Pd Film Substrate

Previous work in semiconductor-based devices had already concluded that hydrogen could be entrapped in SiO₂⁵⁷⁻⁶⁰, thus affecting their response. Adding layers on top of the SiO₂ minimized this effect but this phenomenon motivated the study of other substrates in chemiresistor sensors. The most relevant works are described below.

B. SWNTs as Substrates

Single wall carbon nanotubes (SWNTs) are nanometric materials with high mechanical strength and stiffness and large surface area. Depending on its asymmetry, SWNTs can be semiconducting, metallic or semimetallic. SWNTs used for chemical sensors are semiconducting because adsorbed molecules cause a charge transfer between the tubes and the molecules, thus changing the conductance of the nanotube.^{91,92}

One of the first studies on using SWNTs as substrates in chemiresistors for hydrogen sensing applications was done by Kong et al.⁹² in 2001. They functionalized the SWNTs with ~ 5 Å Pd thin films deposited by electron beam evaporation. They demonstrated that by modifying the SWNTs with Pd they could impart sensitivity to molecular hydrogen to an otherwise insensitive material. These sensing elements were able to detect hydrogen concentrations from 40 ppm to 400 ppm in air. The decrease in the conductance was reversible and the t_{50} response times were between 5 and 10 seconds.

In 2007 Sun et al.⁹³ developed one of the first flexible hydrogen sensing elements. A SWNTs film was grown by chemical vapor deposition on a 100 nm SiO₂ over Si substrate. The SWNT network was then transferred to a poly(ethylene terephthalate) sheet with a thin layer of epoxy resin and bilayers of Ti/Pd were used to form the electrodes. Finally, by electron beam evaporation, a 5 to 30 Å Pd film was deposited. The flexible sensors could detect hydrogen at concentrations as low as 30 ppm in air.

C. TiO₂ as Substrate

Titanium dioxide is an n-type semiconductor that is very stable at high temperatures and harsh environments.⁹⁴ Mor et al.³² developed sensors using perpendicularly aligned titania (TiO₂) nanotube arrays as a substrate over which a 10 nm discontinuous Pd film was deposited using thermal evaporation. The hydrogen atoms dissociatively adsorb and diffuse through the Pd films. The spillover hydrogen then adsorbs on the TiO₂ intertubular contact regions changing its electrical properties. They report a reduction in the resistance of the sensor by four orders of magnitude when exposed to 1000 ppm ($\sim 0.1\%$ v/v) of H₂ in N₂ at room temperature and a t_{90} of 30 s.

D. Anodic Aluminum Oxide as Substrate

Anodic aluminum oxides as substrates are of particular interest because of their ordered pore structure and density. These materials can be used as templates for the production of nanowires or as support for conducting or semiconducting materials to produce a wide range of electronic, magnetic, and optical devices.⁹⁵

By the end of 2005, Lu et al.⁹⁶ were one of the first researchers to use anodized aluminum oxide (AAO) as substrates for hydrogen sensing elements. Hexagonally closed packed AAO nanowells were prepared by anodization of high purity aluminum sheets. The nanowells had a diameter of 50 nm and were less than 100 nm deep. Pd films 10-50 nm thick were synthesized over these AAO nanowells by reduction of a Pd(OAc)₂ solution in Poly(DL-lactide). They concluded that AAO substrates are excellent for hydrogen sensing devices because its rough surface has a large surface area for the formation of the nanostructures, and because they are weakly conductive. They demonstrated that by varying the anodization time of the AAO substrates they could change the response time and the sensitivity of the sensing element at room temperature. Higher anodization times increase the surface area. This also increases the Pd surface area and therefore, the Pd hydrogen adsorption capacity resulting in larger sensitivity values. However, this could lead to slower response times as later shown in work done by the same group.³⁹

Ding et al.⁹⁷ in 2006 used Radio Frequency sputtering to deposit Pd thin films of different thicknesses 45-110 nm in AAO templates. They concluded that thinner films were more sensitive and had faster response times than thicker films. They stated that

AAO templates were also ideal substrates because porous surfaces provide better adhesion of the nanostructures.

In 2007 Wang and Feng²² synthesized zigzag microstructured Ag/Pd 200 nm films in alumina substrates that could detect hydrogen concentrations up to 4% v/v with good response times and sensitivity. As others before, they conclude that Ag/Pd films are more stable than their pure Pd counterpart.

Rumiche et al.³⁹ combined Xu's³⁰ siloxane SAM technique and Lu's⁹⁶ nanowell substrates to produce fast and highly sensitive Pd thin films in AAO. They report response times based on relaxation theory³⁴ ($t_{36.8}$) as low as 1.15 s.

Meanwhile, Taşaltın et al.⁹⁸ investigated the temperature dependence on the hydrogen sensing properties of 60 nm Pd thin films supported on AAO templates deposited by thermal evaporation. As the temperature is increased, the sensitivity of the sensing element decreased but the response time was faster. High diffusivity rates account for the fast response at higher temperatures, but no explanation is given in their report to the smaller sensitivity at higher temperatures. However, this can be explained by examining Sieverts' law, which states that the natural logarithm of the hydrogen solubility decreases linearly with increasing temperature at a given hydrogen partial pressure.^{4,5}

E. Effect of Film Morphology on the Response

The Pd film's roughness and thickness can affect the response of the sensors. For these studies silicon nitride was used as a substrate due to its insulating properties and its ability to function as a barrier to hydrogen diffusion.^{99,100}

RaviPrakash et al.⁴³ investigated the role of Pd thin film roughness in hydrogen sensing elements. They used p-doped silicon wafers with a 500 Å layer of silicon nitride to prevent trapping of H₂ in the silicon substrate. Two 3000 Å thick Pd film morphologies were obtained by sputter deposition: one smooth film resulting from depositing at a pressure equal to 5 mTorr and one rough film deposited at 25 mTorr. The smooth surface is a densely packed columnar structure, while the rougher film is a void filled faceted columnar structure. The sensors were tailored such that both films had the same initial resistance value and approximately the same thickness. They observed that the rough film had a higher resistivity, a slower response, and lower sensitivity than the smooth film. The lower sensitivity was attributed to the higher resistivity of the rough films.

The slower response was attributed to the higher binding energy of the hydrogen atoms adsorbed on the grain boundaries and defects that slows the kinetics of the desorption step.

Ramanathan et al.⁴² reported a crossover behavior of the sensing mechanism of Pd thin films, deposited on Silicon Nitride substrates by sputtering, with varying film thickness. Films thinner than 5 nm showed a decrease in the resistance of the film when exposed to hydrogen due to swelling of Pd. Thicker films (>5 nm), on the other hand, showed an increase in the resistance of the film. They explained that in thicker films the grains are interconnected yielding a response mechanism analogous to the bulk.

1.4 CONCLUSIONS

The development of Pd thin films as part of the hydrogen sensing technology was briefly reviewed since its inception. It is evident that there are many types of Pd thin film hydrogen based sensors, each of which has its advantages and disadvantages depending on its intended application.

Metal-oxide semiconductors although slowly responding and working only at high temperatures are very sensitive to low hydrogen concentrations. In addition, their small size and durability make them very appealing. Surface acoustic wave sensors can detect a wide range of hydrogen concentrations but their stability and interference with temperature and other gases still poses a challenge. Optical fiber type sensors can be useful in explosive environments and can detect high hydrogen concentrations; their fabrication however is complicated. Resistor type sensors are the most simple and are the most promising sensors since they can readily detect hydrogen at room temperature or higher. The possibility of adding a second metal expands the concentration range of these types of sensors even though sensitivity is sacrificed.

1.5 REFERENCES

- (1) Quiñones, L.; Grazul, J.; Martínez-Iñesta, M. M. Synthesis of Platinum Nanostructures in Zeolite Mordenite Using a Solid-State Reduction Method. *Materials Letters* **2009**, *63* (30), 2684–2686.
- (2) Feliciano, J.; Martínez-Iñesta, M. M. Synthesis and Characterization of Pd, Cu, and Ag Nanowires in Anodic Alumina Membranes Using Solid State Reduction. *Materials Letters* **2012**, *82*, 211–213.
- (3) Graham, T. On the Absorption and Dialytic Separation of Gases by Colloid Septa. *Philosophical Transactions of the Royal Society of London* **1866**, *156*, 399–439.
- (4) Lewis, F. A. *The Palladium Hydrogen System*; Academic Press, 1967.
- (5) Wicke, E.; Brodowsky, H.; Züchner, H. Hydrogen in Palladium and Palladium Alloys. *Topics in Applied Physics* **1978**, *29*, 73–155.
- (6) Flanagan, T. B.; Oates, W. A. The Palladium-Hydrogen System. *Annu. Rev. Mater. Res.* **1991**, *21*, 269–304.
- (7) Jewell, L.; Davis, B. Review of Absorption and Adsorption in the Hydrogen–Palladium System. *Applied Catalysis A: General* **2006**, *310*, 1–15.
- (8) Conrad, H.; Ertl, G.; Latta, E. E. Adsorption of Hydrogen on Palladium Single Crystal Surfaces. *Surface Science* **1974**, *41* (2), 435–446.
- (9) Aben, P. C.; Burgers, W. G. Surface Structure and Electrochemical Potential of Palladium While Absorbing Hydrogen in Aqueous Solution. *Trans. Faraday Soc.* **1962**, *58*, 1989–1992.
- (10) Hughes, R. C.; Schubert, W. K. Thin Films of Pd/Ni Alloys for Detection of High Hydrogen Concentrations. *J. Appl. Phys.* **1992**, *71* (1), 542–544.
- (11) Lewis, F. A. The Hydrides of Palladium and Palladium Alloys. *Platinum Metals Rev* **1960**, *4* (4), 132–137.
- (12) Eastman, J.; Thompson, L.; Kestel, B. Narrowing of the Palladium-Hydrogen Miscibility Gap in Nanocrystalline Palladium. *Phys. Rev., B Condens. Matter* **1993**, *48* (1), 84–92.
- (13) Narehood, D. G.; Kishore, S.; Goto, H.; Adair, J. H.; Nelson, J. A.; Gutiérrez, H. R.; Eklund, P. C. X-Ray Diffraction and H-Storage in Ultra-Small Palladium Particles. *International Journal of Hydrogen Energy* **2009**, *34* (2), 952–960.
- (14) Garcia, E. Y.; Loffler, D. G. Electrical Resistivities of Iridium, Palladium, Rhodium, and Tungsten at Temperatures Between 295 and 1100 K. *Journal of Chemical & Engineering Data* **1985**, *30* (3), 304–305.
- (15) Sakamoto, Y.; Takai, K.; Takashima, I.; Imada, M. Electrical Resistance Measurements as a Function of Composition of Palladium-Hydrogen (Deuterium) Systems by a Gas Phase Method. *J. Phys.: Condens. Matter* **1996**, *8*, 3399–3411.
- (16) Bambakidis, G.; Smith, R.; Otterson, D. Electrical Resistivity Versus Deuterium Concentration in Palladium. *Physical Review* **1969**, *177* (3), 1044–1048.
- (17) Mott, S. N. F.; Jones, H. *The Theory of the Properties of Metals and Alloys*; Oxford University Press: London, 1958.

- (18) Hughes, R.; Schubert, W.; Buss, R. Solid- State Hydrogen Sensors Using Palladium- Nickel Alloys: Effect of Alloy Composition on Sensor Response. *J. Electrochem. Soc.* **1995**, *142*, 249–254.
- (19) Hughes, R. C.; Schubert, W. K.; Zipperian, T. E.; Rodriguez, J. L.; Plut, T. A. Thin-Film Palladium and Silver Alloys and Layers for Metal-Insulator-Semiconductor Sensors. *J. Appl. Phys.* **1987**, *62* (3), 1074–1083.
- (20) Lewis, F. A. The Hydrides of Palladium and Palladium Alloys. *Platinum Metals Rev* **1961**, *5* (1), 21–25.
- (21) Lewis, F. A. The Palladium-Hydrogen System. *Platinum Metals Rev* **1982**, *26* (3), 121–128.
- (22) Wang, M.; Feng, Y. Palladium–Silver Thin Film for Hydrogen Sensing. *Sensors & Actuators: B. Chemical* **2007**, *123* (1), 101–106.
- (23) Lee, E.; Lee, J. M.; Lee, E.; Noh, J.-S.; Joe, J. H.; Jung, B.; Lee, W. Hydrogen Gas Sensing Performance of Pd–Ni Alloy Thin Films. *Thin Solid Films* **2010**, *519* (2), 880–884.
- (24) Kim, K. R.; Noh, J.-S.; Lee, J. M.; Kim, Y. J.; Lee, W. Suppression of Phase Transitions in Pd Thin Films by Insertion of a Ti Buffer Layer. *J Mater Sci* **2010**, *46* (6), 1597–1601.
- (25) Barton, J. C.; Green, J. A. S.; Lewis, F. A. Changes of Electrode Potential and Electrical Resistance as a Function of the Hydrogen Content of Some Pd+Ni and Pd+Rh Alloys. *Trans. Faraday Soc.* **1966**, *62*, 960–970.
- (26) Mattox, D. M. *Handbook of Physical Vapor Deposition (PVD) Processing*, 1st ed.; Andrew, W., Ed.; William Andrew, 2010.
- (27) Joshi, R. K.; Krishnan, S.; Yoshimura, M.; Kumar, A. Pd Nanoparticles and Thin Films for Room Temperature Hydrogen Sensor. *Nanoscale Res Lett* **2009**, *4* (10), 1191–1196.
- (28) Tong, H. D.; vanden Berg, A. H. J.; Gardeniers, J. G. E.; Jansen, H. V.; Gielens, F. C.; Elwenspoek, M. C. Preparation of Palladium–Silver Alloy Films by a Dual-Sputtering Technique and Its Application in Hydrogen Separation Membrane. *Thin Solid Films* **2005**, *479* (1-2), 89–94.
- (29) Amin-Ahmadi, B.; Idrissi, H.; Galceran, M.; Colla, M. S.; Raskin, J. P.; Pardoën, T.; Godet, S.; Schryvers, D. Effect of Deposition Rate on the Microstructure of Electron Beam Evaporated Nanocrystalline Palladium Thin Films. *Thin Solid Films* **2013**, *539*, 145–150.
- (30) Xu, T.; Zach, M. P.; Xiao, Z. L.; Rosenmann, D.; Welp, U.; Kwok, W. K.; Crabtree, G. W. Self-Assembled Monolayer-Enhanced Hydrogen Sensing with Ultrathin Palladium Films. *Appl. Phys. Lett.* **2005**, *86* (20), 203104.
- (31) Taşaltın, N.; Öztürk, S.; Kılınc, N.; Ziya Öztürk, Z. Temperature Dependence of a Nanoporous Pd Film Hydrogen Sensor Based on an AAO Template on Si. *Appl. Phys. A* **2009**, *97* (4), 745–750.
- (32) Mor, G. K.; Varghese, O. K.; Paulose, M.; Ong, K. G.; Grimes, C. A. Fabrication of Hydrogen Sensors with Transparent Titanium Oxide Nanotube-Array Thin Films as Sensing Elements. *Thin Solid Films* **2006**, *496* (1), 42–48.
- (33) Mattox, D. M. *The Foundations of Vacuum Coating Technology*; Elsevier, 2003.

- (34) Laidler, K. J. *Chemical Kinetics*; 1965.
- (35) Buttner, W.; Burgess, R.; Post, M.; Rivkin, C. Summary and Findings From the NREL/DOE Hydrogen Sensor Workshop (June 8, 2011). **2012**.
- (36) Hydrogen, Fuel Cells & Infrastructure Technologies Program. *www.nrel.gov*. p 280.
- (37) Sawaguchi, N.; Nishibori, M.; Tajima, K.; Shin, W.; Izu, N.; Murayama, N.; Matsubara, I. Practical Test Methods for Hydrogen Gas Sensor Response Characterization. *Electrochemistry* **2006**, *74* (4), 315–320.
- (38) Boon-Brett, L.; Black, G.; Moretto, P.; Bousek, J. A Comparison of Test Methods for the Measurement of Hydrogen Sensor Response and Recovery Times. *International Journal of Hydrogen Energy* **2010**, *35* (14), 7652–7663.
- (39) Rumiche, F.; Wang, H. H.; Hu, W. S.; Indacochea, J. E.; Wang, M. L. Anodized Aluminum Oxide (AAO) Nanowell Sensors for Hydrogen Detection. *Sensors & Actuators: B. Chemical* **2008**, *134* (2), 869–877.
- (40) Buttner, W. J.; Post, M. B.; Burgess, R.; Rivkin, C. An Overview of Hydrogen Safety Sensors and Requirements. *International Journal of Hydrogen Energy* **2011**, *36* (3), 2462–2470.
- (41) Soundarajan, P.; Schweighardt, F. Hydrogen Sensing and Detection. *Hydrogen Fuel: Production, Transport, and Storage*, CRC Press, Boca Raton **2009**, 495–534.
- (42) Ramanathan, M.; Skudlarek, G.; Wang, H. H.; Darling, S. B. Crossover Behavior in the Hydrogen Sensing Mechanism for Palladium Ultrathin Films. *NanoTech* **2010**, *21* (12), 125501.
- (43) RaviPrakash, J.; McDaniel, A. H.; Horn, M.; Pilione, L.; Sunal, P.; Messier, R.; McGrath, R. T.; Schweighardt, F. K. Hydrogen Sensors: Role of Palladium Thin Film Morphology. *Sensors & Actuators: B. Chemical* **2007**, *120* (2), 439–446.
- (44) Korotcenkov, G. *Handbook of Gas Sensor Materials: Properties, Advantages and Shortcomings for Applications Volume 2: New Trends and Technologies*; Springer Science & Business Media, 2013.
- (45) Lundström, I.; Shivaraman, S.; Svensson, C.; Lundkvist, L. A Hydrogen-Sensitive MOS Field-Effect Transistor. *Appl. Phys. Lett.* **1975**, *26* (2), 55–57.
- (46) Lundström, K. I.; Shivaraman, M. S.; Svensson, C. M. A Hydrogen-Sensitive Pd-Gate MOS Transistor. *J. Appl. Phys.* **1975**, *46* (9), 3876–3881.
- (47) Green, M. A.; King, F. D.; Shewchun, J. Minority Carrier MIS Tunnel Diodes and Their Application to Electron- and Photo-Voltaic Energy Conversion—I. Theory. *Solid-State Electronics* **1974**, *17* (6), 551–561.
- (48) Peckerar, M.; Lin, H. C.; Kocher, R. L. Open Circuit Voltage of MIS Schottky Diode Solar Cells. *Electron Devices Meeting* **1975**, 213–216.
- (49) Potje-Kamloth, K. Semiconductor Junction Gas Sensors. *Chem. Rev.* **2008**, *108* (2), 367–399.
- (50) Shivaraman, M. S.; Lundström, I.; Svensson, C.; Hammarsten, H. Hydrogen Sensitivity of Palladium--Thin-Oxide--Silicon Schottky Barriers. *Electronics Letters* **1976**, *12* (18), 483–484.

- (51) Steele, M. C.; MacIver, B. A. Palladium/Cadmium-Sulfide Schottky Diodes for Hydrogen Detection. *Appl. Phys. Lett.* **1976**, *28* (11), 687–688.
- (52) Ito, K. Hydrogen-Sensitive Schottky Barrier Diodes. *Surface Science* **1979**, *86*, 345–352.
- (53) Steele, M. C. Hydrogen-Sensitive Palladium Gate MOS Capacitors. *J. Appl. Phys.* **1976**, *47* (6), 2537–2538.
- (54) Lundström, I.; Shivaraman, M. S.; Svensson, C. Chemical Reactions on Palladium Surfaces Studied with Pd-MOS Structures. *Surface Science* **1977**, *64* (2), 497–519.
- (55) Lundström, I. Hydrogen Sensitive MOS-Structures: Part 1: Principles and Applications. *Sensors and Actuators* **1981**, *1*, 403–426.
- (56) Lundström, I.; Söderberg, D. Hydrogen Sensitive Mos-Structures Part 2: Characterization. *Sensors and Actuators* **1982**, *2*, 105–138.
- (57) Armgarth, M. A Stable Hydrogen-Sensitive Pd Gate Metal-Oxide Semiconductor Capacitor. *Appl. Phys. Lett.* **1981**, *39* (1), 91–92.
- (58) Hofstein, S. R. Stabilization of MOS Devices. *Solid-State Electronics* **1967**, *10* (7), 657–670.
- (59) Revesz, A. G. The Role of Hydrogen in SiO₂ Films on Silicon. *J. Electrochem. Soc.* **1979**, *126* (1), 122–130.
- (60) Mrstik, B.; McMarr, P.; Saks, N.; Rendell, R.; Klein, R. Hydrogen Permeability in Thermally Grown Films of SiO₂ on Silicon Substrates. *Phys. Rev., B Condens. Matter* **1993**, *47* (7), 4115–4118.
- (61) Armgarth, M. Palladium and Platinum Gate Metal-Oxide-Semiconductor Capacitors in Hydrogen and Oxygen Mixtures. *Appl. Phys. Lett.* **1982**, *41* (7), 654–655.
- (62) Fonash, S. J.; Huston, H.; Ashok, S. Conducting Mis Diode Gas Detectors: the Pd/SiO_x/Si Hydrogen Sensor. *Sensors and Actuators* **1981**, *2*, 363–369.
- (63) Ruths, P. F.; Ashok, S.; Fonash, S. J.; Ruths, J. M. A Study of Pd/Si MIS Schottky Barrier Diode Hydrogen Detector. *IEEE Trans. Electron Devices* **1981**, *28* (9), 1003–1009.
- (64) Keramati, B.; Zemel, J. N. Pd-Thin-SiO₂-Si Diode. I. Isothermal Variation of H₂-Induced Interfacial Trapping States. *J. Appl. Phys.* **1982**, *53* (2), 1091–1099.
- (65) Keramati, B.; Zemel, J. N. Pd-Thin-SiO₂-Si Diode. II. Theoretical Modeling and the H₂ Response. *J. Appl. Phys.* **1982**, *53* (2), 1100–1109.
- (66) Choi, S. Y.; Takahashi, K.; Matsuo, T. No Blister Formation Pd/Pt Double Metal Gate MISFET Hydrogen Sensors. *IEEE Electron Device Lett.* **1984**, *5* (1), 14–15.
- (67) D'Amico, A.; Palma, A.; Verona, E. Hydrogen Sensor Using a Palladium Coated Surface Acoustic Wave Delay-Line; IEEE; pp 308–311.
- (68) D'Amico, A. Palladium-Surface Acoustic Wave Interaction for Hydrogen Detection. *Appl. Phys. Lett.* **1982**, *41* (3), 300–301.
- (69) Jakubik, W. P.; Urbańczyk, M. W.; Kochowski, S.; Bodzenta, J. Bilayer Structure for Hydrogen Detection in a Surface Acoustic Wave Sensor System. *Sensors & Actuators: B. Chemical* **2002**, *82* (2), 265–271.

- (70) Hübert, T.; Boon-Brett, L.; Black, G.; Banach, U. Hydrogen Sensors – a Review. *Sensors & Actuators: B. Chemical* **2011**, *157* (2), 329–352.
- (71) Butler, M. A. Optical Fiber Hydrogen Sensor. *Appl. Phys. Lett.* **1984**, *45* (10), 1007–1009.
- (72) Butler, M. A. Fiber Optic Sensor for Hydrogen Concentrations Near the Explosive Limit. *J. Electrochem. Soc.* **1991**, *138* (9), L46–L47.
- (73) Butler, M. A.; Buss, R. J. Kinetics of the Micromirror Chemical Sensor. *Sensors & Actuators: B. Chemical* **1993**, *11* (1-3), 161–166.
- (74) Butler, M. A. Micromirror Optical-Fiber Hydrogen Sensor. *Sensors & Actuators: B. Chemical* **1994**, *22* (2), 155–163.
- (75) Tabib-Azar, M.; Sutapun, B.; Petrick, R.; Kazemi, A. Highly Sensitive Hydrogen Sensors Using Palladium Coated Fiber Optics with Exposed Cores and Evanescent Field Interactions. *Sensors & Actuators: B. Chemical* **1999**, *56* (1), 158–163.
- (76) Zhao, Z.; Knight, M.; Kumar, S.; Eisenbraun, E. T.; Carpenter, M. A. Humidity Effects on Pd/Au-Based All-Optical Hydrogen Sensors. *Sensors & Actuators: B. Chemical* **2008**, *129* (2), 726–733.
- (77) Strohfeltd, N.; Tittl, A.; Giessen, H. Long-Term Stability of Capped and Buffered Palladium-Nickel Thin Films and Nanostructures for Plasmonic Hydrogen Sensing Applications. *Optical Materials Express* **2013**, *3* (2), 194–204.
- (78) Britton, C.; Jones, R.; Oden, P.; Hu, Z.; Warmack, R.; Smith, S.; Bryan, W.; Rochelle, J. Multiple-Input Microcantilever Sensors. *Ultramicroscopy* **2000**, *82* (1-4), 17–21.
- (79) Okuyama, S.; Mitobe, Y.; Okuyama, K.; Matsushita, K. Hydrogen Gas Sensing Using a Pd-Coated Cantilever. *Jpn. J. Appl. Phys.* **2000**, *39* (Part 1, No. 6A), 3584–3590.
- (80) Baselt, D.; Fruhberger, B.; Klaassen, E.; Cemalovic, S.; Britton, C.; Patel, S.; Mlsna, T.; McCorkle, D.; Warmack, B. Design and Performance of a Microcantilever-Based Hydrogen Sensor. *Sensors & Actuators: B. Chemical* **2003**, *88* (2), 120–131.
- (81) Chang, C. S.; Kostylev, M.; Ivanov, E. Metallic Spintronic Thin Film as a Hydrogen Sensor. *Appl. Phys. Lett.* **2013**, *102* (14), 142405.
- (82) Fazle Kibria, A.; Sakamoto, Y. Hysteresis of Pressure-Composition and Electrical Resistance-Composition Isotherms of Palladium-Silver Alloys-Hydrogen System. *Materials Science and Engineering: B* **1998**, *53* (3), 256–261.
- (83) Wei, X.; Wei, T.; Xiao, H.; Lin, Y. S. Nano-Structured Pd-Long Period Fiber Gratings Integrated Optical Sensor for Hydrogen Detection. *Sensors & Actuators: B. Chemical* **2008**, *134* (2), 687–693.
- (84) Lee, E.; Lee, J. M.; Koo, J. H.; Lee, W.; Lee, T. Hysteresis Behavior of Electrical Resistance in Pd Thin Films During the Process of Absorption and Desorption of Hydrogen Gas. *International Journal of Hydrogen Energy* **2010**, *35* (13), 6984–6991.

- (85) Favier, F.; Walter, E. C.; Zach, M. P.; Benter, T.; Penner, R. M. Hydrogen Sensors and Switches From Electrodeposited Palladium Mesowire Arrays. *Science* **2001**, *293* (5538), 2227–2231.
- (86) Walter, E. C.; Favier, F.; Penner, R. M. Palladium Mesowire Arrays for Fast Hydrogen Sensors and Hydrogen-Actuated Switches. *Anal. Chem.* **2002**, *74* (7), 1546–1553.
- (87) Wu, F.; Morris, J. E. The Effects of Hydrogen Absorption on the Electrical Conduction in Discontinuous Palladium Films. *Thin Solid Films* **1994**, *246* (1), 17–23.
- (88) Morris, J. E. Effects of Hydrogen Absorption on the Electrical Conduction of Discontinuous Palladium Thin Films. *International Journal of Electronics* **1996**, *81* (4), 441–447.
- (89) Dankert, O.; Pundt, A. Hydrogen-Induced Percolation in Discontinuous Films. *Appl. Phys. Lett.* **2002**, *81* (9), 1618–1620.
- (90) Wagner, S.; Hamm, M.; Pundt, A. Huge Hydrogen-Induced Resistive Switching in Percolating Palladium Thin Films. *Scripta Materialia* **2013**, *69* (10), 756–759.
- (91) Kong, J.; Franklin, N. R.; Zhou, C.; Chapline, M. G.; Peng, S.; Cho, K.; Dai, H. Nanotube Molecular Wires as Chemical Sensors. *Science* **2000**, *287* (5453), 622–625.
- (92) Kong, J.; Chapline, M. G.; Dai, H. Functionalized Carbon Nanotubes for Molecular Hydrogen Sensors. *Adv. Mater.* **2001**, *13* (18), 1384–1386.
- (93) Sun, Y.; Wang, H. H. High-Performance, Flexible Hydrogen Sensors That Use Carbon Nanotubes Decorated with Palladium Nanoparticles. *Adv. Mater.* **2007**, *19* (19), 2818–2823.
- (94) Aswal, D. K.; Gupta, S. K. *Science and Technology of Chemiresistor Gas Sensors*; Nova Publishers, 2007.
- (95) Li, F.; Zhang, L.; Metzger, R. M. On the Growth of Highly Ordered Pores in Anodized Aluminum Oxide. *Chem. Mater.* **1998**, *10* (9), 2470–2480.
- (96) Lu, J.; Yu, S.; Wang, H. H. Ultrafast Pd/AAO Nanowell Hydrogen Sensor. *MRS Proceedings* **2005**, 0900–O10–09.1.
- (97) Ding, D.; Chen, Z.; Lu, C. Hydrogen Sensing of Nanoporous Palladium Films Supported by Anodic Aluminum Oxides. *Sensors & Actuators: B. Chemical* **2006**, *120* (1), 182–186.
- (98) Taşaltın, N.; Öztürk, S.; Kılınc, N.; Yüzer, H.; Öztürk, Z. Z. Fabrication of Vertically Aligned Pd Nanowire Array in AAO Template by Electrodeposition Using Neutral Electrolyte. *Nanoscale Res Lett* **2010**, *5* (7), 1137–1143.
- (99) Benoit, D.; Regolini, J.; Morin, P. Hydrogen Desorption and Diffusion in PECVD Silicon Nitride. Application to Passivation of CMOS Active Pixel Sensors. *Microelectronic Engineering* **2007**, *84* (9-10), 2169–2172.
- (100) Chen, P. J.; Wallace, R. M. Deuterium Transport Through Device Structures. *J. Appl. Phys.* **1999**, *86* (4), 2237–2244.

2 SYNTHESIS AND CHARACTERIZATION OF Pd, Pt/Pd AND Ag/Pd THIN FILMS USING SOLID-STATE REDUCTION (SSR) METHOD

2.1 INTRODUCTION

Palladium (Pd) and palladium alloys (M/Pd) are materials of interest due to their high hydrogen (H₂) adsorption capacity. As films, they are used as hydrogen sensors¹⁻⁵, as well as other applications such as H₂ separation membranes,⁶ membrane reactors for hydrogenation and dehydrogenation^{7,8}, and others⁹⁻¹¹.

Pure and multimetallic films for these applications are commonly obtained by vacuum processes such as sputtering¹²⁻¹⁴, electron beam evaporation^{4,15}, chemical vapor deposition^{16,17}, and atomic layer deposition¹⁸. Through these techniques the film thickness, deposition rates, and microstructure can be controlled. However, these techniques require specialized equipment and high energy¹⁹. These films can also be obtained through more economical non-vacuum processes such as electrodeposition and electroless deposition.^{20,21} With these techniques you also have control of the film thickness and composition by adjusting the identity and concentration of the reactants in solution but there is an excess of unreacted species that result from the process.

In this chapter the solid-state reduction (SSR) synthesis technique^{22,23} is explored as an alternative to obtain Pd and Pd bimetallic films. The technique consists on the impregnation of a pure metal precursor and its solid-state reduction using sodium borohydride. This method has been shown to yield pure Pd, Cu, and Ag nanowires.²³ Here the technique was applied to allow the formation of pure Pd and bimetallic film structures.

Within SSR, two impregnation methods were studied: solid impregnation and solution impregnation. Solid impregnation uses the minimum water possible and allows better diffusion of the precursor into the membrane, which is restricted by the surface tension of the water on the surface. This method, however, cannot be used effectively to impregnate more than one metal and leads to inhomogeneous films, and hence, solution impregnation was also studied.

2.2 METHODOLOGY

2.2.1 Synthesis for Pure Pd Films - Solid Impregnation

A mass of 0.0054 g of $\text{Pd}(\text{NO}_3)_2 \cdot x\text{H}_2\text{O}$ (Alfa-Aesar, 99.9% metal basis) was placed in powder form over one side of commercial Anodic Alumina Membranes (Whatman, Anodisc 25mm with an average pore diameter of 200 nm) to obtain a metal loading of 5% wt Pd. After deposition, the samples were left at room conditions for 30 minutes. This results in adsorption of sufficient ambient water by the hydrophilic $\text{Pd}(\text{NO}_3)_2 \cdot x\text{H}_2\text{O}$ to completely dissolve. Then, the wet precursor was carefully dispersed through the membrane and then left standing for 30 more minutes. This side of the membrane is referred to as the impregnation side.

Afterwards a small pellet of solid sodium borohydride (~0.006 g) [NaBH_4 98%mm—Alfa Aesar] was spread on the opposite side of the membrane (reduction side) making sure that the entire surface was covered. To improve the reduction process a small amount of water (~2 μL) was added to the NaBH_4 pellet as illustrated in Figure 2.1. Immediately the membrane changed to a dark grey color indicating that the metal was reduced. After reduction, the samples were washed three times for 30 minutes in a large bath of cold distilled water.

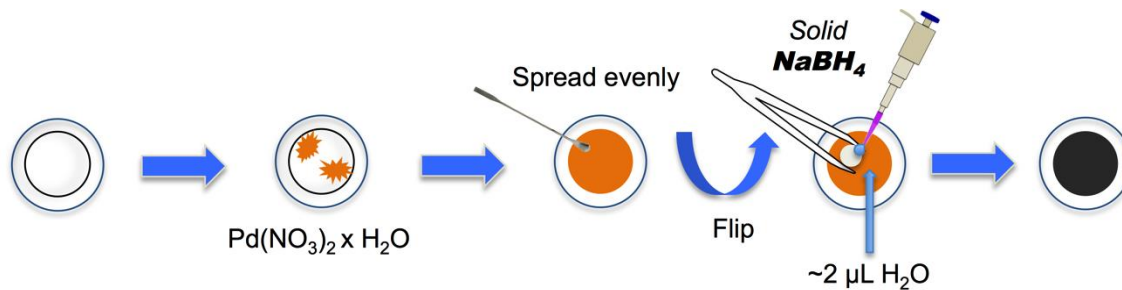


Figure 2.1 Schematic showing the SSR method

2.2.2 Synthesis for Pure and Bimetallic Films - Solution Impregnation

For the Pd sample, 0.0048 g of palladium nitrate hydrate [$\text{Pd}(\text{NO}_3)_2 \cdot \text{H}_2\text{O}$ Alfa-Aesar] were dissolved in 9 μL of deionized water. The solution was sonicated for 5 minutes and 3 μL of this solution were impregnated over one side of a commercial Anodic Alumina Membrane (AAM) (Whatman[®] Anodisc 13mm, pore size 0.02 μm) to achieve a 5% wt Pd loading. The sample was then dried at room conditions for 2 minutes and for 10 minutes in an oven at 80 °C. Metal reduction was attained by spreading a small pellet (~6 mg) of solid sodium borohydrate [NaBH_4 98% mm-Alfa Aesar] with 2 μL of deionized water on the opposite side to the impregnation. The samples were dipped in cold deionized water in three intervals of 30 minutes to remove any excess NaBH_4 . The sample was then dried overnight at 80 °C.

The bimetallic films were synthesized following similar steps maintaining a 5% wt total metal concentration and a $\text{M}_{10}\text{Pd}_{90}$ composition. The solution for the $\text{Ag}_{10}\text{Pd}_{90}$ sample had 0.0016 g of silver nitrate [AgNO_3 , Alfa Aesar] and 0.0200 g of $\text{Pd}(\text{NO}_3)_2 \cdot \text{H}_2\text{O}$ dissolved in 42 μL of deionized water. The solution for the $\text{Pt}_{10}\text{Pd}_{90}$ film had 0.0013 g of tetraammineplatinum(II) nitrate [$\text{Pt}(\text{NH}_3)_4(\text{NO}_3)_2$, Sigma Aldrich] and

0.0068 g of Pd(NO₃)₂•H₂O dissolved in 16 μL of deionized water. For both samples only 3 μL of the solutions were impregnated to achieve the desired concentrations. The final 10:90 ratio of the M:Pd metals was chosen because it has been suggested in the literature that this ratio is the one suited for hydrogen sensing applications.^{4,24}

2.2.3 Characterization

The crystallinity of the Pd, Ag₁₀Pd₉₀, and Pt₁₀Pd₉₀ films was determined by X-ray diffraction (XRD) on a Rigaku Ultima III diffractometer unit using CuKα radiation operating at 40 kV and 44 mA. The α to β palladium structure transition of the Pd, Ag₁₀Pd₉₀, Pt₁₀Pd₉₀ samples were also studied with the Rigaku Reactor X attachment by flowing hydrogen at different concentrations with a total gas flow of 152 mL/min and a total pressure of 1 atm. Each run was taken in intervals of 5 minutes to ensure that the sample reached equilibrium. A scanning speed of 1-2.5°/min and a 0.02° step size was used to obtain the diffraction patterns in the 30° - 50° 2θ range.

The morphology and homogeneity of the films were obtained on a JEOL-JSM – 6390 Scanning Electron Microscope (SEM) equipped with an Energy Dispersive Spectrometer. X-ray Photoelectron Spectra (XPS) were obtained on a PHI 5000 Versa Probe using a monochromatic AlKα X-Ray Source. Binding energies were calibrated using as reference the Pd 3d 5/2 peak at 335.2 eV obtained from the spectrum of a pure Pd sample.

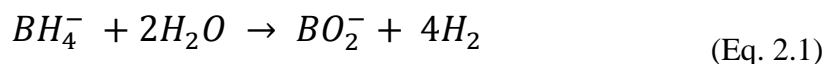
An Atomic Force Microscope (AFM) Veeco di CPII AP0100A and a KLA-Tencor Alpha-Step IQ Surface Profiler was used to study the samples' surface thickness and roughness using a scan length of 1000 μm, a scan speed of 5 μm/s with a sampling rate of 50 Hz, and a cut-off filter value of 250 μm for the profiler.

2.3 RESULTS AND DISCUSSION

2.3.1 Pure Pd films - Solid Impregnation

Figure 2.2 shows the different surface morphologies that result from the SSR method, the reduction side (A) and the impregnation side (B). They show that for both sides, a Pd film covered the entire surface of the AAM. They also show that a coarse film was formed on the reduction side and a continuous film was formed on the impregnation side. The films have an average thickness of $1.1 \pm 0.4 \mu\text{m}$ on the reduction side and $1.0 \pm 0.3 \mu\text{m}$ on the impregnation side according to AFM experiments. For this sample the root mean squared (RMS) roughness obtained by AFM of the film on the impregnation side is $0.131 \pm 0.042 \mu\text{m}$ and $0.232 \pm 0.028 \mu\text{m}$ on the reduction side.

The reaction below²⁵ describes how the reducing agent reacts with water to produce hydrogen,



In our synthesis method the solid NaBH_4 reacts with the absorbed water of the Pd loaded membrane thus producing hydrogen. This hydrogen can then reduce the Pd precursor dispersed on the other side of the AAM membrane. This reaction is presumably very abrupt on the reduction side, where the water concentration is higher, resulting in a coarser film.

As previously observed,²³ during the process nanowires 300 nm in diameter and 5 μm in length were formed inside the membrane pores as shown in Figure 2.3. This image was obtained after dissolution of the AAM with 10 M NaOH. Figure 2.4 is a schematic showing how the samples' different morphologies are arranged within the membrane.

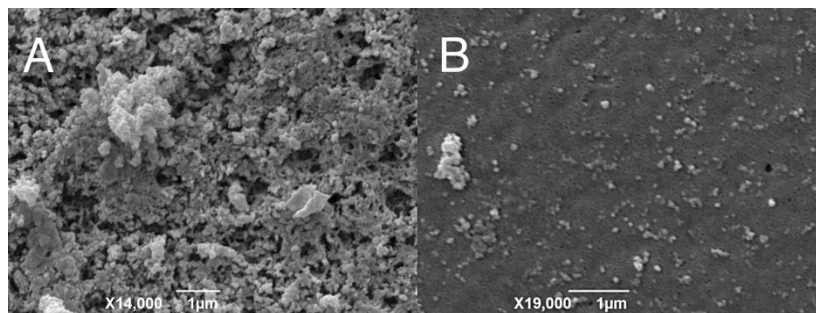


Figure 2.2 SEM images showing the Pd film surfaces on the reduction side (A) and the impregnation side (B) for the 5%Pd sample.

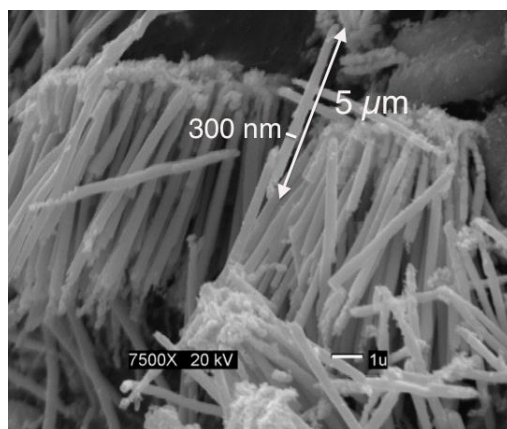


Figure 2.3 SEM image of the Pd nanowires obtained after removal of the AAM support

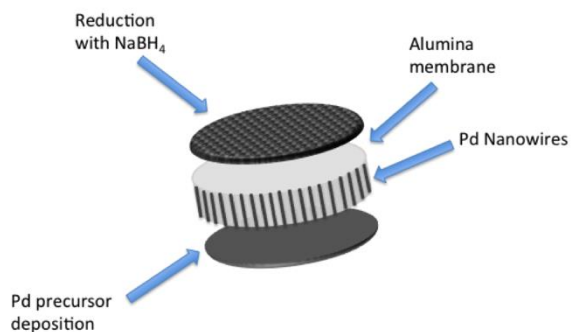


Figure 2.4 Schematic representing the combination of morphologies

To understand the phase behavior upon hydrogen absorption of these films, the XRD patterns of the 5% Pd sample were obtained at various H_2 concentrations (Figure 2.5). The peaks observed at low concentrations correspond to the typical bulk Pd fcc

peaks at $2\theta = 40.1^\circ$ and 46.5° corresponding to the (111) and (200) planes. The α to the β phase transition begins to occur at 1% v/v H_2 and is approximately complete at 2% v/v. For bulk Pd the two phases coexist between 1 to 2% v/v H_2 ^{26,27}.

Bragg's law states that the wavelength of the incident X-rays is proportional to the lattice spacing between the atoms and the sine of the scattering angle as shown in Equation 2.2.

$$n\lambda = 2d \sin \theta \quad (\text{Eq. 2.2})$$

For cubic structures, such as the Pd structure, the lattice parameter a can be calculated from Bragg's law:

$$a = \frac{n\lambda\sqrt{h^2 + k^2 + l^2}}{2 \sin \theta} \quad (\text{Eq. 2.3})$$

Therefore, as the incident angle decreases, the lattice parameter increases. Using equation 2.3, it is found that the lattice parameter for the sample in Figure 2.5 increases from 3.889 Å to 4.022 Å which are close to the accepted values in the literature.²⁸

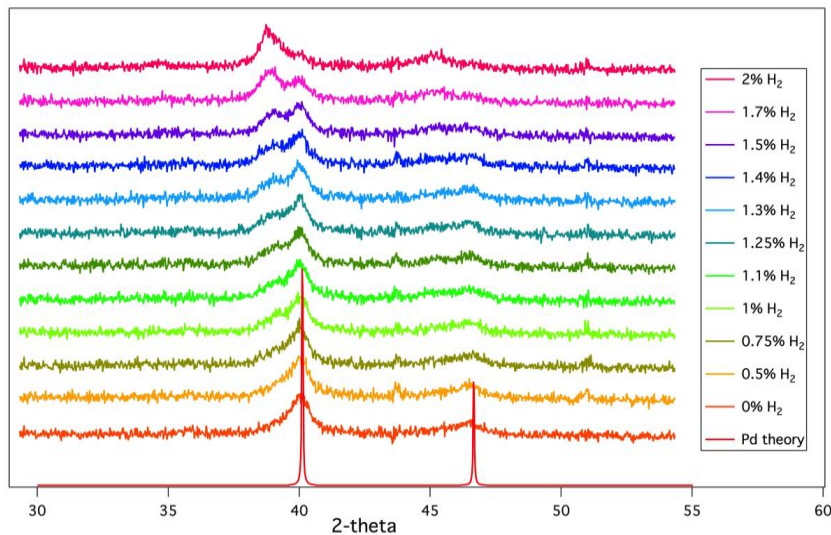


Figure 2.5 X-ray diffraction patterns at different hydrogen concentrations showing where phase changes occur for the 5% Pd sample.

To study the effect of time on the Pd structure at a specific concentration, XRD patterns of the 5% Pd sample were obtained when exposed to 0.5% v/v H₂ (Figure 2.6) and 1.25% v/v H₂ (Figure 2.7) for 25 minutes in intervals of 2.7 min using the same total gas flow. It can be seen that at 0.5% v/v H₂ the structure is at equilibrium at all times and no structural changes occur after long exposure. At 1.25% v/v H₂ the presence of the β phase is evident after 2.7 min and reaches equilibrium at 5.4 min. The time it takes for formation of the β -phase in Pd bulk samples depends on surface conditions and can take hours or even days.^{29,30} The formation of the β -phase within minutes in our samples is because H₂ can better penetrate through the rough surface of our samples as explained by Blackford et al.²⁹

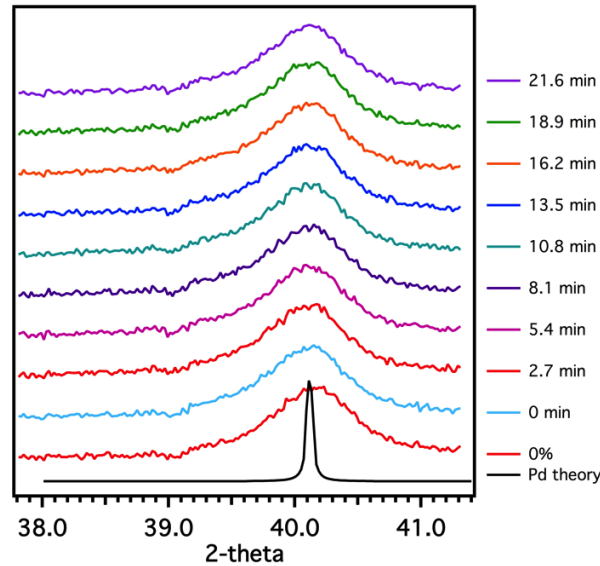


Figure 2.6 Long exposure to 0.5% H₂ for a 5% Pd sample

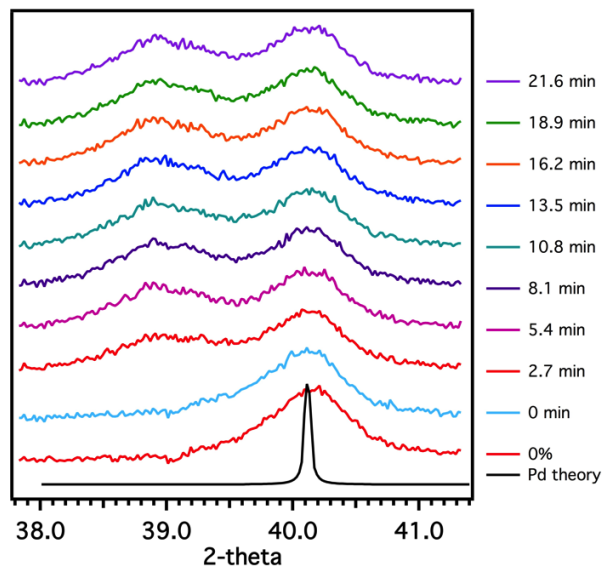


Figure 2.7 Long exposure to 1.25% H₂ for a 5% Pd sample

These diffraction patterns do not show alumina peaks because our supports do not have peaks in this angle range. Furthermore these Pd peaks are broad, which is unexpected for a highly crystalline substance. This is due to artifacts by the use of an attachment needed for the flow-through experiments, the Reactor X (Appendix A). The Pd XRD peaks of the samples obtained without this attachment are well-defined intense peaks as observed in Appendix B. However, using the reactor resulted in broad peaks that are shown in Figures 2.5, 2.6 and 2.7. We believe that the massiveness of the reactor affects the amount of X-rays that the detector receives thus affecting the signal of the instrument.

2.3.2 Pure and Bimetallic Films - Solution Impregnation

Figure 2.8 shows that, when the metal precursors are added in solution, films are also formed on both sides of the AAM. For all the samples, and contrary to what was found with solid impregnation, coarser films were formed on the impregnation side while

smoother films were formed on the reduction side. For this sample the average root mean squared (RMS) roughness of the film on the impregnation side is $0.210 \pm 0.023 \mu\text{m}$ and $0.102 \pm 0.016 \mu\text{m}$ on the reduction side.

With solid impregnation, the water concentration is higher on the reduction side while, with solution impregnation, the concentration is higher on the impregnation side. This reinforces the idea that the reaction in equation 2.1 occurs more violently on the side with the higher water concentration yielding coarser films. Nanowires were also formed inside the AAM pores in all the samples as reported with the solid impregnation (Figure 2.9). These nanowires have diameters similar to those obtained by solid impregnation ($\sim 300\text{nm}$) but their average length ($\sim 1 \mu\text{m}$) is much smaller and their morphology and shape are greatly affected. This suggests a repression of their growth when using solution impregnation.

Table 2.1 shows the surface roughness percent change of the samples when compared to the roughness of a clean AAM, $0.157 \pm 0.027 \mu\text{m}$. The surface roughness of the impregnation side is consistently $\sim 30\%$ rougher than the clean AAM. However, the surface roughness on the reduction side varies significantly which also suggests the repression effect on the growth of the films on this side.

Table 2.1 Percent change between the surface roughness when compared to clean a AAM

	Orig. SSR	Solution form	Solution form	Solution form
		Sample 1	Sample 2	Sample 3
Reduction side	-18.3%	-8.8%	-35.2%	-20.9%
Impregnation side	-10.4%	39.9%	34.1%	34.4%

Figure 2.10 shows the EDS elemental mapping of $M_{10}Pd_{90}$ bimetallic films. These qualitative results show a homogenous metal distribution on the surface of the films in all samples. However, Ag (Figure 2.10A) has a higher relative M/Pd content on the surface compared to Pt. This might be a result of the tendency of the Ag atoms to segregate to the surface when alloyed with Pd³¹⁻³³ and to the poor interaction of the Ag with the alumina support³¹. For the Pt/Pd combination no surface segregation of the solute has been reported.³⁴

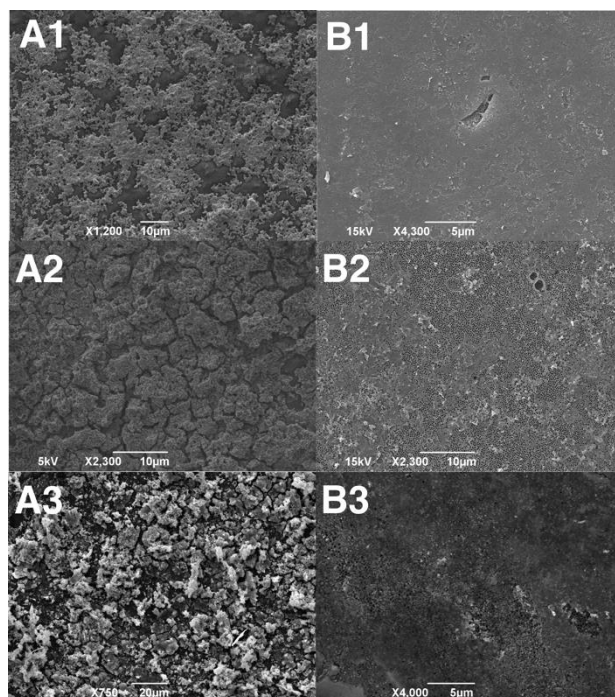


Figure 2.8 SEM micrographs of pure Pd (1), Ag₁₀Pd₉₀ (2), Pt₁₀Pd₉₀ (3). Column (A) shows the films on the impregnation side and the column (B) on the reduction side.

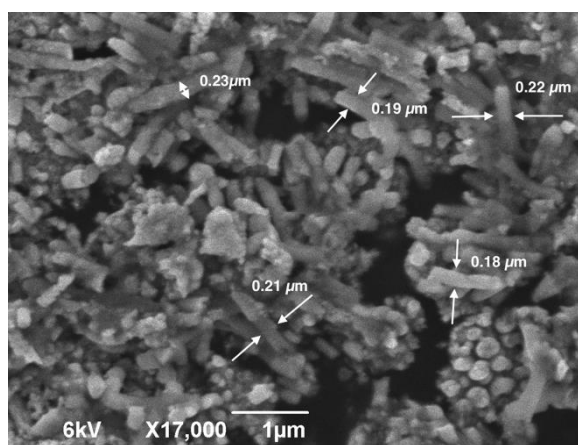


Figure 2.9 Pd nanowires formed after dissolution with NaOH.

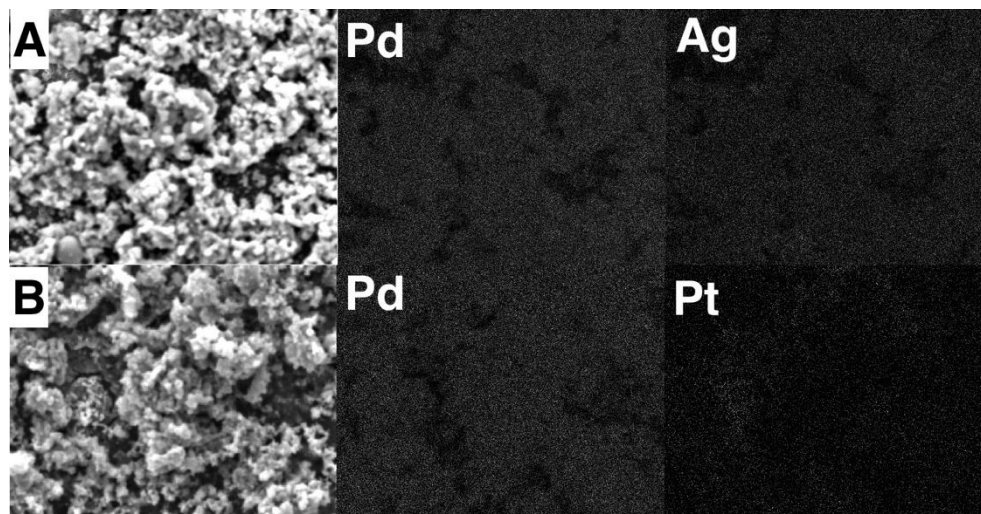


Figure 2.10 Metal distribution of $\text{Ag}_{10}\text{Pd}_{90}$ (A), and $\text{Pt}_{10}\text{Pd}_{90}$ (B) films on the impregnation side obtained by EDS. The studied area is showed on the left, Pd on the middle, and the second metal on the right.

Figure 2.11 shows the X-ray diffraction (XRD) patterns for the two M/Pd samples at the impregnation side and in all samples the Pd $\langle 111 \rangle$ and Pd $\langle 200 \rangle$ peaks are in their characteristic positions suggesting that Pd is in its metallic fcc configuration. For the $\text{Ag}_{10}\text{Pd}_{90}$ sample (Figure 2.11A), a peak at $2\theta = 38.3^\circ$ lies between the characteristic Pd $\langle 111 \rangle$ peak and the characteristic Ag $\langle 111 \rangle$ peak which suggests the partial formation of a Ag/Pd alloy.³⁵ No characteristic or Pt peaks were observed for the $\text{Pt}_{10}\text{Pd}_{90}$ samples possibly due to overlap with Pd peaks.

The phase transition of the $\text{Ag}_{10}\text{Pd}_{90}$ and $\text{Pt}_{10}\text{Pd}_{90}$ films were also studied as shown in Figure 2.12 and Figure 2.13, respectively. The phase transition of the $\text{Ag}_{10}\text{Pd}_{90}$ occurs between 0.5% v/v and 1.5% v/v H_2 but the lattice expansion is restricted as evidenced by the location of the β phase peak at a higher angle. The phase transition of the $\text{Pt}_{10}\text{Pd}_{90}$ film is shifted to higher concentrations (1.5% v/v H_2 to 3% v/v H_2) and the lattice expansion is also restricted. This is consistent with results of other bimetallic films

reported by Hughes et al.^{4,36} where Ag/Pd films were used to suppress the lattice expansion of Pd based Schottky diodes and also in Ni/Pd based resistors, as discussed in Section 1.3.1.

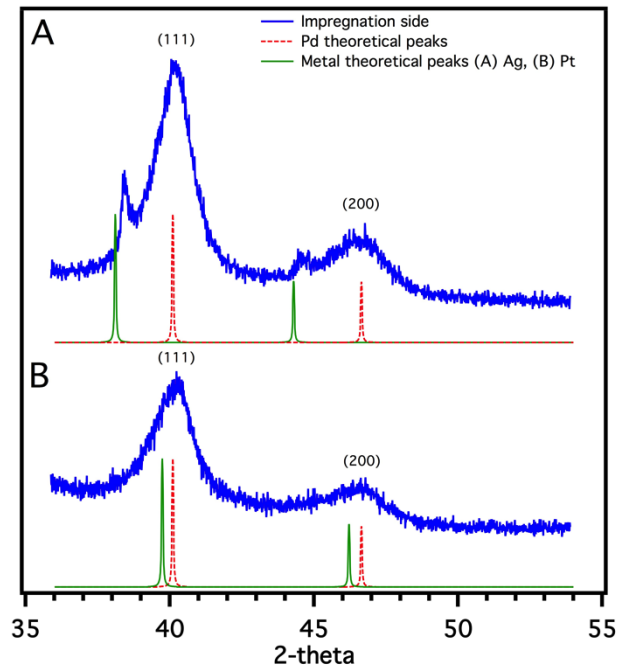


Figure 2.11 XRD patterns of the Pd bimetallic films on the impregnation side of A) Ag₁₀Pd₉₀, B) Pt₁₀Pd₉₀.

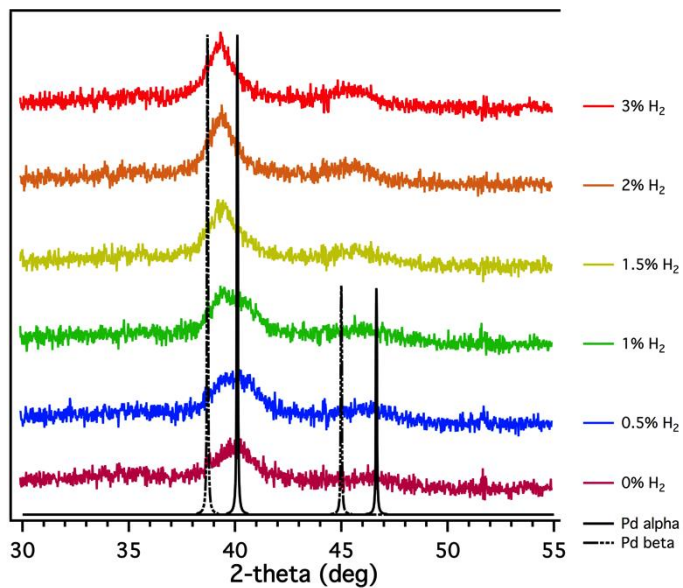


Figure 2.12 X-ray diffraction patterns with H₂ concentration for the Ag₁₀Pd₉₀ sample

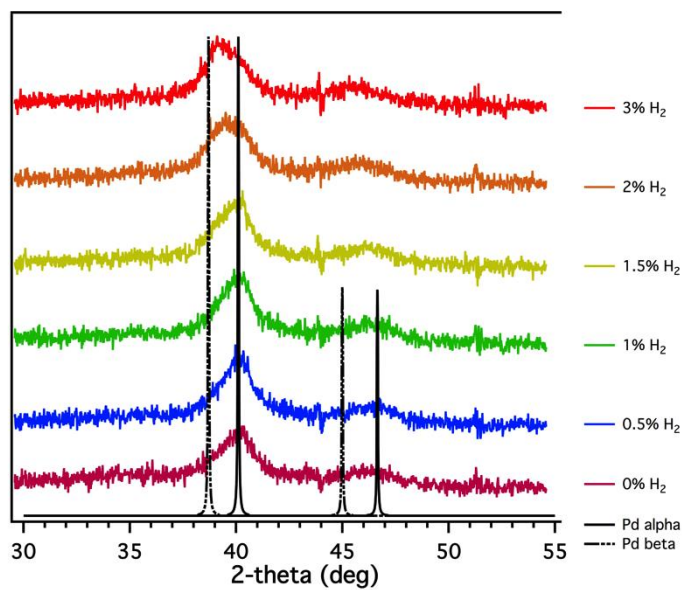


Figure 2.13 X-ray diffraction patterns with H₂ concentration for the Pt₁₀Pd₉₀ sample

XPS experiments were done to study the efficiency of the synthesis method. Full scan XPS spectra did not show the presence of boron, sodium, or nitrogen suggesting that

the washing procedure is appropriate to remove any remaining solids as shown in Figure 2.14 for Ag/Pd and Figure 2.15 for Pt/Pd.

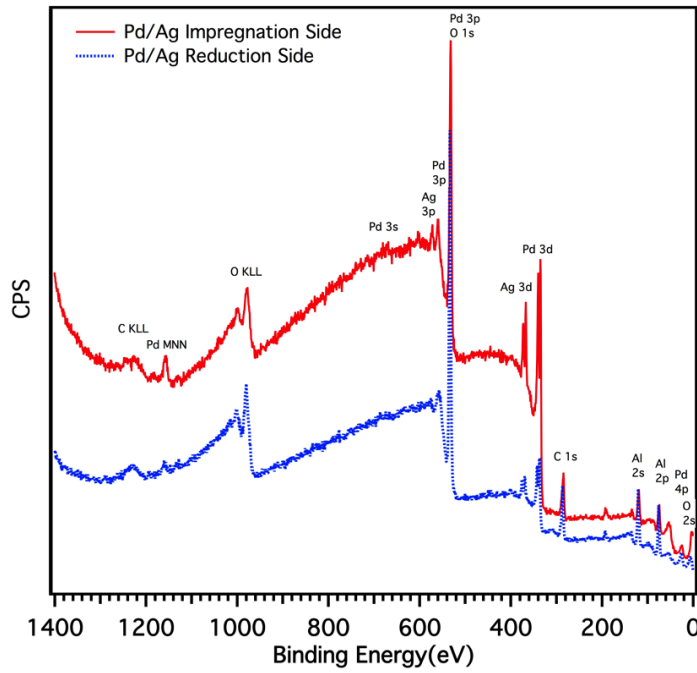


Figure 2.14 Full XPS spectra for the Ag₁₀Pd₉₀ sample

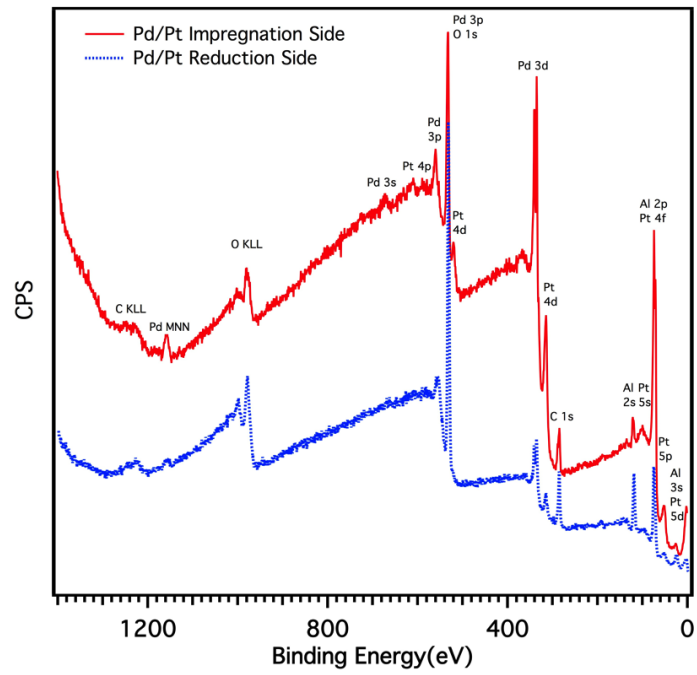


Figure 2.15 Full XPS spectra for the Pt₁₀Pd₉₀ sample

Element specific XPS spectra of the Ag₁₀Pd₉₀ sample (Figure 2.16A) show that Pd is predominantly in its elemental state with an intense 3d_{5/2} peak at 335.2 eV. A second small peak at 336.3 eV appears corresponding to an interaction with oxygen which could be physisorbed³⁷ (as studied in Chapter 6) or from the alumina support in thinner areas of the film³⁸. The Ag XPS spectrum has a low intensity 3d_{5/2} peak at 368.3 eV corresponding to pure Ag and a strong intense peak shifted approximately -0.6 eV. For Ag/Pd alloys, negative BE shifts have been reported with values between ~-0.7 and ~-1.0 eV for Ag:Pd ratios up to 10:90 due to hybridization of the Ag and Pd valence states.^{31,39-42} These XPS results agree with XRD results, and confirm that both metal precursors were reduced by SSR and that a partial alloy was formed between these two metals.

The Pt XPS spectrum of the Pt₁₀Pd₉₀ sample (Figure 2.17) shows the two characteristic 4f_{7/2} and 4f_{5/2} peaks at 71.1 eV and 74.5 eV respectively. The Pd XPS spectrum of the same sample has two peaks in the same positions as in the Ag₁₀Pd₉₀ sample. These results show that both metals were reduced by SSR without forming an alloy.

These results show that all the metal precursors studied were reduced by SSR. This is probably because anhydrous and low hydrated salts require a lower reduction energy than the hydrated precursors.⁴³ In addition, the standard reduction potential (E°) of Pt²⁺, Pd²⁺, and Ag⁺ are high (1.180 V, 0.915 V, and 0.799 V,⁴⁴ respectively), compared to sodium borohydride (1.20 V) which further explains why these cations were reduced by SSR.⁴⁵ Also, the fact that the reduction potentials of Pd²⁺ and Ag⁺ are close, could explain why they tend to make alloys.

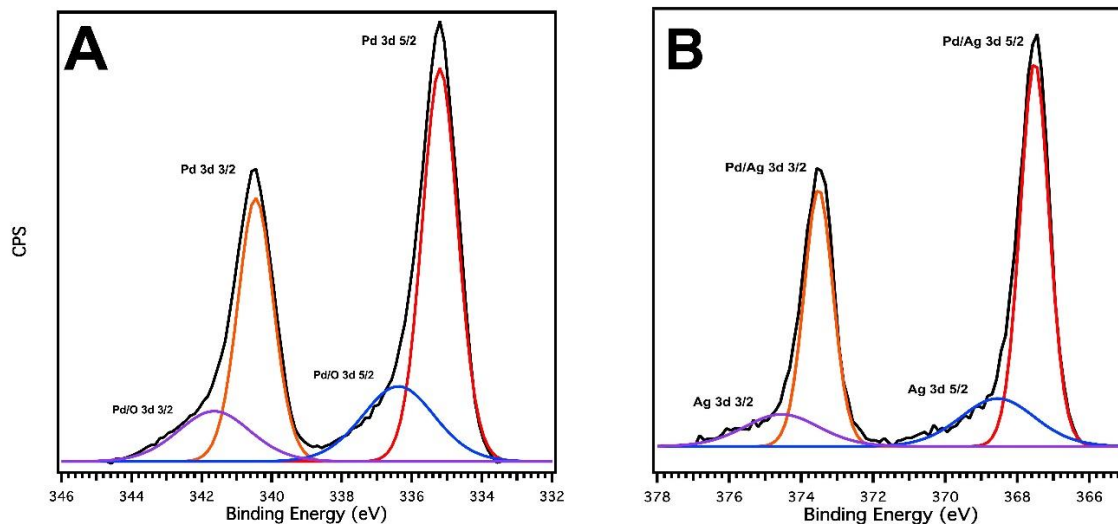


Figure 2.16 A) Pd and B) Ag XPS Spectra of the $\text{Ag}_{10}\text{Pd}_{90}$ sample

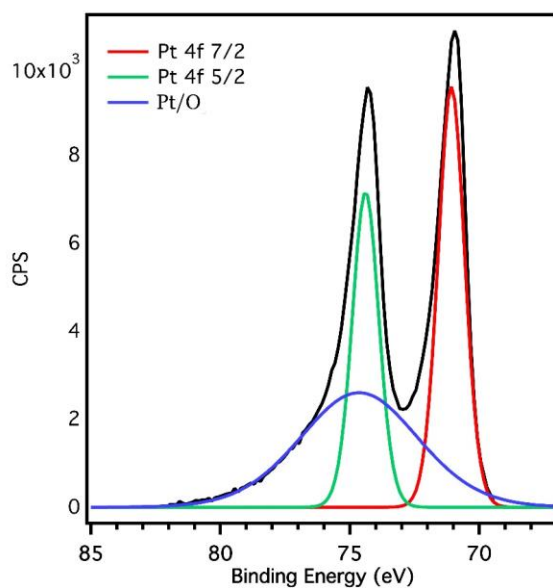


Figure 2.17 XPS spectrum for the Pt in the $\text{Pt}_{10}\text{Pd}_{90}$ sample.

The SSR is, thus, an alternate facile method to obtain bimetallic Pd/M films and nanowires for metals with a high reduction potential and precursors with low hydration shells.

2.4 CONCLUSIONS

The SSR is a facile synthesis method to obtain pure and bimetallic films supported on anodic alumina membranes. This technique is a cost-effective alternative to obtain films, as it does not require the use of excess amounts of reagents or solvents, sophisticated equipment, nor high temperatures or voltages.

Through this technique two films of different morphologies are formed on either side of the anodic alumina membranes membrane for both solid and liquid impregnation and for all metal combinations studied. A rough surface is formed as a consequence of the violent reaction of sodium borohydride with water at room temperature where the latter is at a higher concentration. One way the surface roughness could be controlled is by using ice-cold water for the precursor solution.

With solution impregnation it is possible to obtain more consistent films as the method relies less on human and environmental variability. It also yields a more even distribution of the metal. However, this method represses the growth of the nanowires and of the film on the reduction side presumably because diffusion of the metal is limited. In general, solution impregnation results in more reproducible film structures whereas solid impregnation produces longer nanowires. Moreover the solution form provides means for producing bimetallic films since the mixture of the two metal precursors can be easily achievable.

The incorporation of a second metal to the Pd films causes suppression in the expansion of the Pd lattice and a shift in the phase miscibility gap of the films. This technique works best with anhydrous metal precursors and for metals that have a positive standard reduction potential and is capable of making alloys.

2.5 REFERENCES

- (1) Rumiche, F.; Wang, H. H.; Hu, W. S.; Indacochea, J. E.; Wang, M. L. Anodized Aluminum Oxide (AAO) Nanowell Sensors for Hydrogen Detection. *Sensors & Actuators: B. Chemical* **2008**, *134* (2), 869–877.
- (2) Ramanathan, M.; Skudlarek, G.; Wang, H. H.; Darling, S. B. Crossover Behavior in the Hydrogen Sensing Mechanism for Palladium Ultrathin Films. *NanoTech* **2010**, *21* (12), 125501.
- (3) RaviPrakash, J.; McDaniel, A. H.; Horn, M.; Piloni, L.; Sunal, P.; Messier, R.; McGrath, R. T.; Schweighardt, F. K. Hydrogen Sensors: Role of Palladium Thin Film Morphology. *Sensors & Actuators: B. Chemical* **2007**, *120* (2), 439–446.
- (4) Hughes, R. C.; Schubert, W. K. Thin Films of Pd/Ni Alloys for Detection of High Hydrogen Concentrations. *J. Appl. Phys.* **1992**, *71* (1), 542–544.
- (5) Wang, M.; Feng, Y. Palladium–Silver Thin Film for Hydrogen Sensing. *Sensors & Actuators: B. Chemical* **2007**, *123* (1), 101–106.
- (6) Hoang, H. T.; Tong, H. D.; Gielens, F. C.; Jansen, H. V.; Elwenspoek, M. C. Fabrication and Characterization of Dual Sputtered Pd–Cu Alloy Films for Hydrogen Separation Membranes. *Materials Letters* **2004**, *58* (3-4), 525–528.
- (7) Dittmeyer, R.; Höllein, V.; Daub, K. Membrane Reactors for Hydrogenation and Dehydrogenation Processes Based on Supported Palladium. *Journal of Molecular Catalysis A: Chemical* **2001**, *173* (1–2), 135–184.
- (8) Gimeno, M. P.; Wu, Z. T.; Soler, J.; Herguido, J.; Li, K.; Menéndez, M. Combination of a Two-Zone Fluidized Bed Reactor with a Pd Hollow Fibre Membrane for Catalytic Alkane Dehydrogenation. *Chemical Engineering Journal* **2009**, *155* (1–2), 298–303.
- (9) Feng, D.; Wang, Y.; Wang, D.; Wang, J. Pd–Ag–Au–Ni Membrane Reactor for Methoxymethane Steam Reforming. *Journal of Chemical & Engineering Data* **2009**, *54* (9), 2444–2451.
- (10) Tong, J.; Matsumura, Y.; Suda, H.; Haraya, K. Experimental Study of Steam Reforming of Methane in a Thin (6 μm) Pd-Based Membrane Reactor. *Ind. Eng. Chem. Res.* **2005**, *44* (5), 1454–1465.
- (11) Shi, L.; Goldbach, A.; Zeng, G.; Xu, H. Direct H₂O₂ Synthesis Over Pd Membranes at Elevated Temperatures. *Journal of Membrane Science* **2010**, *348* (1–2), 160–166.
- (12) Joshi, R. K.; Krishnan, S.; Yoshimura, M.; Kumar, A. Pd Nanoparticles and Thin Films for Room Temperature Hydrogen Sensor. *Nanoscale Res Lett* **2009**, *4* (10), 1191–1196.
- (13) Ma, Z. A Palladium-Alloy Deposited Nafion Membrane for Direct Methanol Fuel Cells. *Journal of Membrane Science* **2003**, *215* (1-2), 327–336.
- (14) Tong, H. D.; vanden Berg, A. H. J.; Gardeniers, J. G. E.; Jansen, H. V.; Gielens, F. C.; Elwenspoek, M. C. Preparation of Palladium–Silver Alloy Films by a Dual-Sputtering Technique and Its Application in Hydrogen Separation Membrane. *Thin Solid Films* **2005**, *479* (1-2), 89–94.
- (15) Jewell, L.; Davis, B. Review of Absorption and Adsorption in the Hydrogen–Palladium System. *Applied Catalysis A: General* **2006**, *310*, 1–15.

- (16) Tung, Y.-L.; Tseng, W.-C.; Lee, C.-Y.; Hsu, P.-F.; Chi, Y.; Peng, S.-M.; Lee, G.-H. Synthesis and Characterization of Allyl(B-Ketoiminato)Palladium(II) Complexes: New Precursors for Chemical Vapor Deposition of Palladium Thin Films. *Organometallics* **1999**, *18* (5), 864–869.
- (17) Jun, C.-S.; Lee, K.-H. Palladium and Palladium Alloy Composite Membranes Prepared by Metal-Organic Chemical Vapor Deposition Method (Cold-Wall). *Journal of Membrane Science* **2000**, *176* (1), 121–130.
- (18) Elam, J. W.; Zinovev, A.; Han, C. Y.; Wang, H. H.; Welp, U.; Hryn, J. N.; Pellin, M. J. Atomic Layer Deposition of Palladium Films on Al₂O₃ Surfaces. *Thin Solid Films* **2006**, *515* (4), 1664–1673.
- (19) Mattox, D. M. *Handbook of Physical Vapor Deposition (PVD) Processing*, 1st ed.; Andrew, W., Ed.; William Andrew, 2010.
- (20) Hernández, S. C.; Yoo, B. Y.; Stefanescu, E.; Khizroev, S.; Myung, N. V. Electrodeposition of Iron–Palladium Thin Films. *Electrochimica Acta* **2008**, *53* (18), 5621–5627.
- (21) Gamburg, Y. D.; Zangari, G. *Theory and Practice of Metal Electrodeposition*; Springer Science & Business Media, 2011.
- (22) Quiñones, L.; Grazul, J.; Martínez-Iñesta, M. M. Synthesis of Platinum Nanostructures in Zeolite Mordenite Using a Solid-State Reduction Method. *Materials Letters* **2009**, *63* (30), 2684–2686.
- (23) Feliciano, J.; Martínez-Iñesta, M. M. Synthesis and Characterization of Pd, Cu, and Ag Nanowires in Anodic Alumina Membranes Using Solid State Reduction. *Materials Letters* **2012**, *82*, 211–213.
- (24) Hughes, R.; Schubert, W.; Buss, R. Solid- State Hydrogen Sensors Using Palladium- Nickel Alloys: Effect of Alloy Composition on Sensor Response. *J. Electrochem. Soc.* **1995**, *142*, 249–254.
- (25) Glavee, G. N.; Klabunde, K. J.; Sorensen, C. M.; Hadjapanayis, G. C. Borohydride Reductions of Metal Ions. a New Understanding of the Chemistry Leading to Nanoscale Particles of Metals, Borides, and Metal Borates. *Langmuir* **1992**, *8* (3), 771–773.
- (26) Yang, F.; Taggart, D. K.; Penner, R. M. Fast, Sensitive Hydrogen Gas Detection Using Single Palladium Nanowires That Resist Fracture. *Nano Lett.* **2009**, *9* (5), 2177–2182.
- (27) Penner, R. M. Electrodeposition of Nanowires for the Detection of Hydrogen Gas. *MRS Bulletin* **2010**, *35* (10), 771–777.
- (28) Wicke, E.; Brodowsky, H.; Züchner, H. Hydrogen in Palladium and Palladium Alloys. *Topics in Applied Physics* **1978**, *29*, 73–155.
- (29) Blackford, B. L.; Arnold, C. S.; Mulhern, P. J.; Jericho, M. H. A Scanning Tunneling Microscope Study of a Palladium Sphere in Hydrogen Gas: Expansion and Surface Topology. *J. Appl. Phys.* **1994**, *76* (7), 4054–4060.
- (30) Johansson, M.; Skúlason, E.; Nielsen, G.; Murphy, S.; Nielsen, R. M.; Chorkendorff, I. Hydrogen Adsorption on Palladium and Palladium Hydride at 1bar. *Surface Science* **2010**, *604* (7-8), 718–729.

- (31) Khan, N. A.; Uhl, A.; Shaikhutdinov, S.; Freund, H. J. Alumina Supported Model Pd–Ag Catalysts: a Combined STM, XPS, TPD and IRAS Study. *Surface Science* **2006**, *600* (9), 1849–1853.
- (32) Noordermeer, A.; Kok, G. A.; Nieuwenhuys, B. E. A Comparative Study of the Behaviour of the PdAg(111) and Pd(111) Surfaces Towards the Interaction with Hydrogen and Carbon Monoxide. *Surface Science* **1986**, *165* (2–3), 375–392.
- (33) Kok, G. A.; Noordermeer, A.; Nieuwenhuys, B. E. Effect of Alloying on the Adsorption of CO on Palladium; a Comparison of the Behaviour of PdAg(111), PdCu(111) and Pd(111) Surfaces. *Surface Science* **1985**, *152–153*, Part 1, 505–512.
- (34) Ossi, P. M. Surface Segregation in Transition Metal Alloys: Experiments and Theories. *Surface Science* **1988**, *201* (3), L519–L531.
- (35) Bosko, M. L.; Miller, J. B.; Lombardo, E. A.; Gellman, A. J.; Cornaglia, L. M. Surface Characterization of Pd–Ag Composite Membranes After Annealing at Various Temperatures. *Journal of Membrane Science* **2011**, *369* (1), 267–276.
- (36) Hughes, R. C.; Schubert, W. K.; Zipperian, T. E.; Rodriguez, J. L.; Plut, T. A. Thin-Film Palladium and Silver Alloys and Layers for Metal-Insulator-Semiconductor Sensors. *J. Appl. Phys.* **1987**, *62* (3), 1074–1083.
- (37) Kim, K. S.; Gossmann, A. F.; Winograd, N. X-Ray Photoelectron Spectroscopic Studies of Palladium Oxides and the Palladium-Oxygen Electrode. *Anal. Chem.* **1974**, *46* (2), 197–200.
- (38) Légaré, P.; Fritsch, A. XPS Study of Transition Metal/Alumina Model Catalysts: Equilibrium and Energy Referencing. *Surf. Interface Anal.* **1990**, *15* (11), 698–700.
- (39) Steiner, P.; Hüfner, S. Thermochemical Data of Alloys From Photoelectron Spectroscopy. *Acta Metallurgica* **1981**, *29* (11), 1885–1898.
- (40) Coulthard, I.; Sham, T. K. Charge Redistribution in Pd-Ag Alloys From a Local Perspective. *Phys. Rev. Lett.* **1996**, *77* (23), 4824–4827.
- (41) Abrikosov, I. A.; Olovsson, W.; Johansson, B. Valence-Band Hybridization and Core Level Shifts in Random Ag-Pd Alloys. *Phys. Rev. Lett.* **2001**, *87* (17), 176403.
- (42) Pervan, P.; Milun, M. Photoelectron Spectroscopy of the Ag/Pd(110) System. *Surface Science* **1992**, *264* (1–2), 135–146.
- (43) Raj, J. A.; Viswanathan, B. Synthesis of Nickel Nanoparticles with Fcc and Hcp Crystal Structures. *Indian J. Chem.* **2011**, *50*, 176–179.
- (44) Harris, D. C. *Exploring Chemical Analysis*; Freeman, W. H. & Company, 2005.
- (45) Rao, C.; Trivedi, D. Chemical and Electrochemical Depositions of Platinum Group Metals and Their Applications. *Coordination Chemistry Reviews* **2005**, *249* (5-6), 613–631.

3 BASIC SENSING CHARACTERIZATION OF Pd FILMS OBTAINED BY SSR: EFFECT OF ELECTRODE CONNECTIVITY, Pd CONCENTRATION, PARTIAL REDUCTION AND PHASE CHANGE

3.1 INTRODUCTION

As discussed in section 1.3.4, chemiresistors are materials that change their electrical resistance when exposed to a chemical environment to which they are sensitive. As these changes are easily measured, chemiresistors are ideal materials to detect chemical species. These chemiresistors must have a high solubility towards the analyte specie and are usually supported on a material with high thermal stability, high electrical resistance, and good adhesion properties¹, such as aluminum oxide (Al_2O_3). Thus, the composite Pd based materials developed through Solid State Reduction (Chapter 2) are good candidates as chemiresistors to detect hydrogen and their response is explored in this Chapter. The effects of electrode connectivity, partial reduction of the sample, metal content, and phase changes are discussed.

3.2 METHODOLOGY

Samples were synthesized following the solid impregnation method described in section 2.2.1. In a typical synthesis 0.0028 g, 0.0054 g and 0.0113 g of $\text{Pd}(\text{NO}_3)_2 \cdot x\text{H}_2\text{O}$ was deposited over different Anodic Alumina Membranes (Anodisc-25mm 0.02 μm) to obtain samples with 2.5%, 5% and 10% wt Pd, respectively.

The sensing chamber was a PVC cylinder with a 5.9 inches (15 cm) diameter and 15 inches (38.1 cm) length ($V \sim 7,000 \text{ cm}^3$) referred to as *Ch-7000*. A schematic of this chamber is shown in Figure 3.1. The electrical measurements were obtained using a

Keithley 2400 multimeter and the voltage used was 1V. Labview 2010 was used to monitor and record the changes in the electrical properties of the sensor. MKS gas flow controllers were used to regulate the flow of gas into the chambers. The electrical connections were made on the sample in the *Ch-7000* using tungsten needles or copper wires manipulated using KRN-09S micromanipulators.

For the experiments the chamber was first exposed to nitrogen until the current from the sample was stabilized at the desired voltage. Then the samples were exposed to continuous alternating cycles of different gas combinations at different concentrations using the same total volumetric flow. The sensitivities were calculated using Equation 1.1.

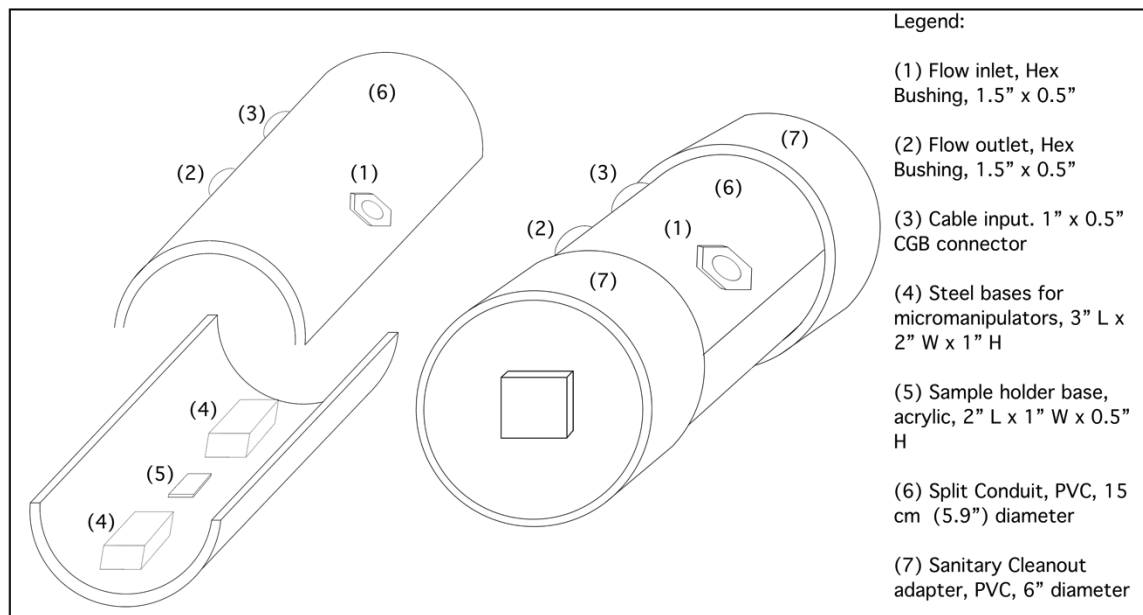


Figure 3.1 PVC chamber, ~7000 cm³.

3.3 RESULTS AND DISCUSSIONS

3.3.1 Effect of Electrode Connection

Films with two different morphologies are formed on either side of the AAM as discussed in Chapter 2. These morphologies affected the signals obtained. If the electrodes were connected to the rougher film, the signal was stable whereas if they were connected to the smoother film either no signal was detected or the signal was very noisy with very low currents. As discussed in Chapter 2, when using solid-state impregnation the rough films formed on the reduction side are also thicker. This morphology effect can be explained because the conductance of thin films increases with increasing metal content² and with increasing surface roughness if the correlation length is large.^{3,4} The effect of the film morphology on the signal is further discussed in Chapter 4.

The electrode connection used also affected the signal. Two types of connections were used; microprobe tungsten (W) needles and copper (Cu) wires attached by silver paste. Figures 3.2 A and B show that the samples exhibit the same sensing mechanism as bulk Pd described in Section 1.3.1, i.e., the current decreases upon hydrogen absorption. These results also show that using the copper wires the signal was significantly more stable than with the microprobe connection. The differences between a moveable and stationary electrical contacts have been described in the literature⁵ and silver is one of the preferred metals to reduce the contact transition resistance between two metals. Moreover, the connection of the Cu wires with the silver paste had more contact area with the sample than the microprobe needles that have a single contact point. This allows the formation of more α -spots, which are the contact points between the metal connector and the metal surface. Depending on the surface asperity or roughness, and the ductility

of the contact metal, these α -spots can increase in number providing better conduction paths. This is because the formation of α -spots depends on the force exerted on the connecting surface by the connector and the area for the connector to penetrate. The known ductility of Pd, the roughness of the film, and the increased contact area of the Cu wires promote the formation of many α -spots thus enhancing the electrical connectivity between the film and the wires.

Due to these results in the experiments described in the following sections the electrodes were connected with silver paste to the rougher film.

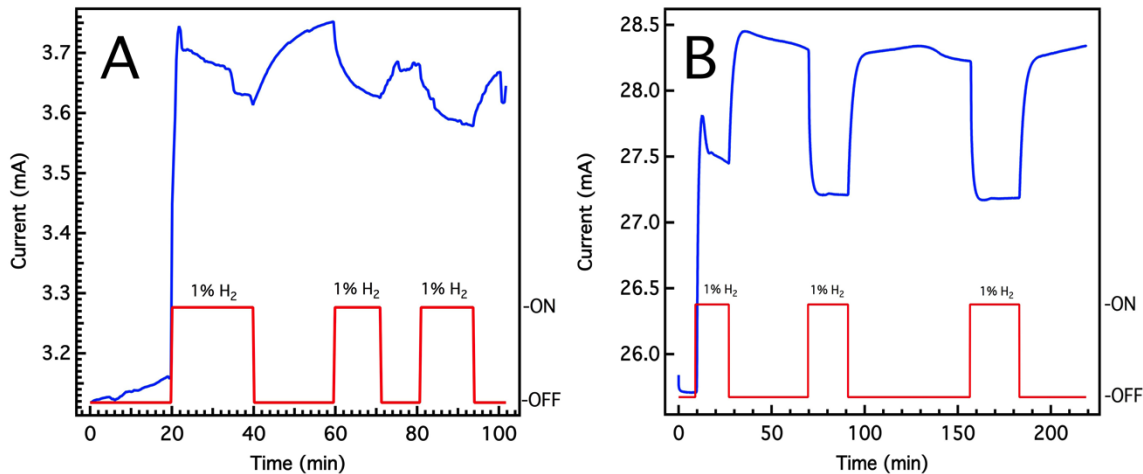


Figure 3.2 Hydrogen response of a 5%Pd sample rough film using a 4000 sccm total flow connected with (A) microprobe W needles and (B) Cu wires adhered with Ag paste.

3.3.2 Effect of Partial Reduction

As described in section 2.2.1, to promote the reduction of the precursor, a small amount of water is added during this step. Figure 3.3 shows that for samples where no water was added the baseline current drifted significantly to higher values as a function of time whereas the sample with added water had a stable baseline current. The increase in baseline current shows that, with continuous exposure to hydrogen, more metal is present

in the sample suggesting that hydrogen is acting as a reducing agent to any remaining unreduced Pd precursor. Adding water to the reduction step accelerates the reduction reaction (Equation 2.1) resulting in a significantly larger fraction of Pd metal leading to a stable baseline from the outset. Moreover, sensitivity is enhanced by 19% and response time is decreased by 8% at 1% v/v H₂. Alternatively pre-treating the samples with an on-site exposure to 5% v/v H₂ for 5 hours prior to the experiments also leads to a stable baseline as observed in Figure 3.2 C. However, this is a lengthy procedure and exposure of the samples this H₂ concentration can lead to structural changes as discussed below. These results show that the addition of water is a necessary and sufficient step for the efficient reduction of the Pd precursor. In the samples studied below, water was added during reduction to obtain a stable baseline.

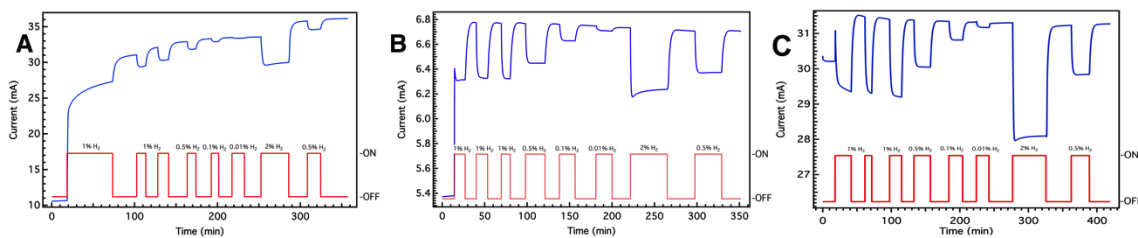


Figure 3.3 Response of 5%wt Pd sample rough film under a total flow of 4000 sccm (A) with no water added during reduction, (B) with water added during reduction, and (C) pretreated with 5%v/v H₂.

3.3.3 Effect of Pd Concentration

Figures 3.4, 3.5 and 3.6 show the hydrogen response of typical samples with 2.5%, 5% and 10%wt Pd, respectively. All samples are able to detect hydrogen at concentrations ranging from 0.01% to 2%, which are below the lower flammability limit of hydrogen (4% v/v). They show that the samples' current decreases upon hydrogen

absorption. This behavior is consistent with previously reported results for thin films with thicknesses higher than 10nm⁶.

There is an initial jump in current observed for all the samples after first exposure to hydrogen. This behavior will be discussed in Chapter 6.

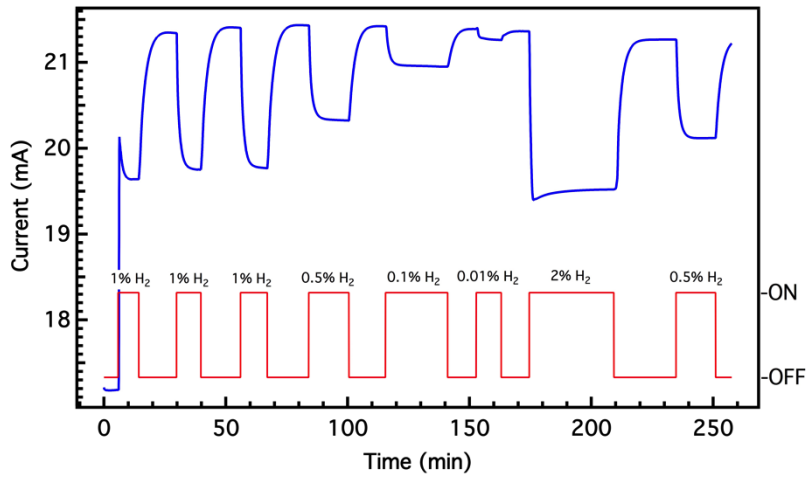


Figure 3.4 Hydrogen response to a 2.5% Pd sample

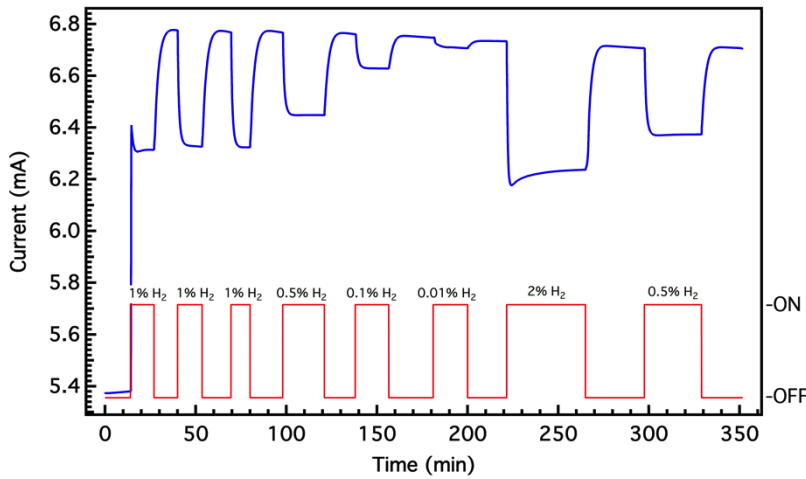


Figure 3.5 Hydrogen response to a 5% Pd sample

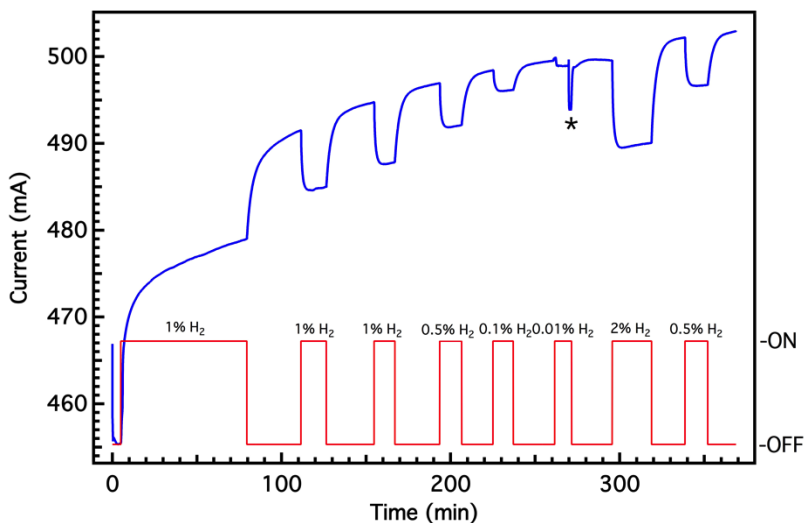


Figure 3.6 Hydrogen response to a 10% Pd sample. * There was a problem with the nitrogen flow control at this point.

These results show that, contrary to mesowires and discontinuous films, these samples do not need to undergo a phase transition to detect H_2 . Instead the signal relies on the resistivity changes that occur as hydrogen electrons fill holes in the Pd energy bands. This suggests that solid-state reduction yields fairly robust Pd films that will exhibit a similar sensing behavior before and after the phase transition at $\sim 1.5\%$ v/v.

Samples with 2.5% and 5% wt Pd show a stable response with minimal baseline drift showing that the addition of water during reduction was enough to obtain a stable baseline. Samples with 10% wt Pd, on the other hand, show a gradual and steady increase in the baseline, as was observed in partially reduced samples discussed in section 3.3.2. This suggests that these samples have a large fraction of unreduced metal precursor being reduced by the flowing hydrogen. This is probably because there is too much metal precursor in the sample and there is either insufficient reducing agent or insufficient contact between the reducing agent and the precursor leading to a reduced Pd film over

unreduced Pd precursor. Hydrogen, on the other hand, diffuses through the Pd film and keeps reducing the underlying Pd precursor.

Table 3.1 Sensitivity values for the different samples

H₂ Concentration	0.01%	0.1%	0.5%	1%	2%
Sample	Sensitivity (%)				
2.5%wt Pd	0.6	2.2	5.2	7.6	9.2
5%wt Pd	0.6	2.0	4.7	6.6	8.3
10%wt Pd	--	0.5	1.0	1.4	2.0

Hydrogen can diffuse through Pd membranes 25µm thick^{7,8} and it has been demonstrated that, in the absence of external diffusion limitations, the absorption process is internal diffusion limited.⁹ At each hydrogen concentration the samples can reach an equilibrium between the amount of hydrogen atoms being adsorbed, incorporated into the structure, and desorbed that dictates the solubility at those conditions.^{8,10} This solubility affects the sensitivity of the material used in sensing applications.

For samples used in sensor applications the sensitivity (S) is proportional to the hydrogen absorption which is defined by Sieverts' Law as:¹¹

$$S \propto \frac{H}{Pd} = \frac{1}{K_s} (p_{H_2})^{0.5} \quad (\text{Eq. 3.1})$$

where K_s is Sieverts' constant and p_{H_2} is the H₂ partial pressure. The sensitivity values for these samples at different concentrations are tabulated in Table 3.1. Overall the samples with the highest sensitivities are the ones with a 2.5%wt Pd loading while the samples

with 5%wt Pd have slightly lower sensitivity values and samples with 10%wt Pd have significantly lower sensitivities.

Lee et al.¹¹ observed sensitivities of ~6% at 1% H₂ for 100 nm Pd films synthesized by sputtering, while our 2.5%wt Pd samples showed an average sensitivity of 7.5% at the same concentration. On the other hand, Rumiche et al.¹² observed sensitivities of ~3% at 1% v/v H₂ on 8 nm thermal evaporated Pd thin films, 60% lower than our observed value for the 2.5%wt Pd sample. In addition the Pd films studied by Lu et al.¹³ supported on Anodized Aluminum Oxide (AAO) showed sensitivities close to 6% at 1% v/v H₂. It is evident that through Solid State Reduction highly sensitive H₂ sensing Pd films are obtained.

Figure 3.7 shows that our sensitivities are linearly dependent on the square of the hydrogen partial pressure, as suggested by Sievert's law. The slopes for samples 2.5%, 5%, and 10%wt Pd are 0.0022, 0.002, and 0.0004 Pa^{0.5} respectively (Figures 3.4-3.6). The two factors that affect the value of the sensitivity are the penetration depth of H atoms and the Pd effective exposed surface area.¹¹ The small slope of the 10% wt Pd sample further suggests that the H atoms had a shallow penetration due to remaining unreduced Pd precursor underneath the surface Pd film.

The agreement between Sieverts' law and our results shows that these films can be calibrated as hydrogen sensors to monitor hydrogen concentrations below 2%v/v H₂. The average sensitivity results and standard deviations of multiple samples that are shown in Figure 3.8 show that these results are reasonably reliable. These results also show that the sensitivities of the 2.5%wt Pd and the 5%wt Pd samples are within experimental error of each other at all hydrogen concentrations.

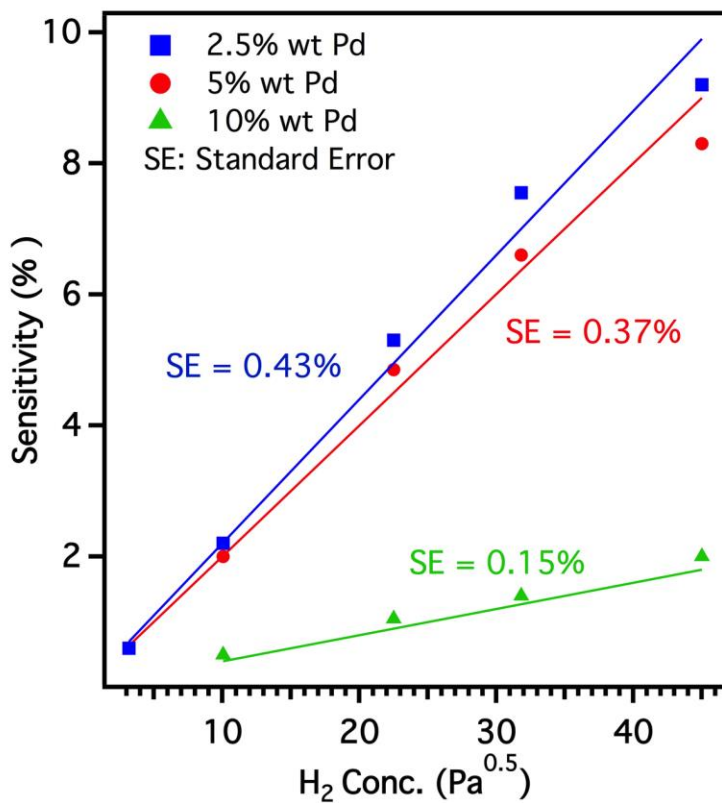


Figure 3.7 Sensitivity vs. square root of H₂ concentration.

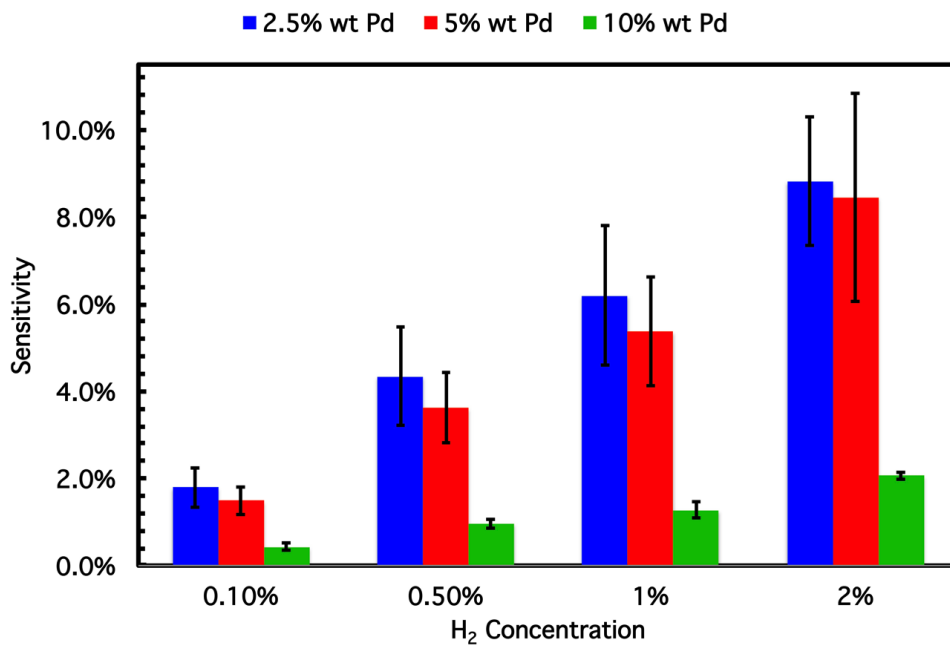


Figure 3.8 Average sensitivity variation at different H₂ concentrations between various samples.

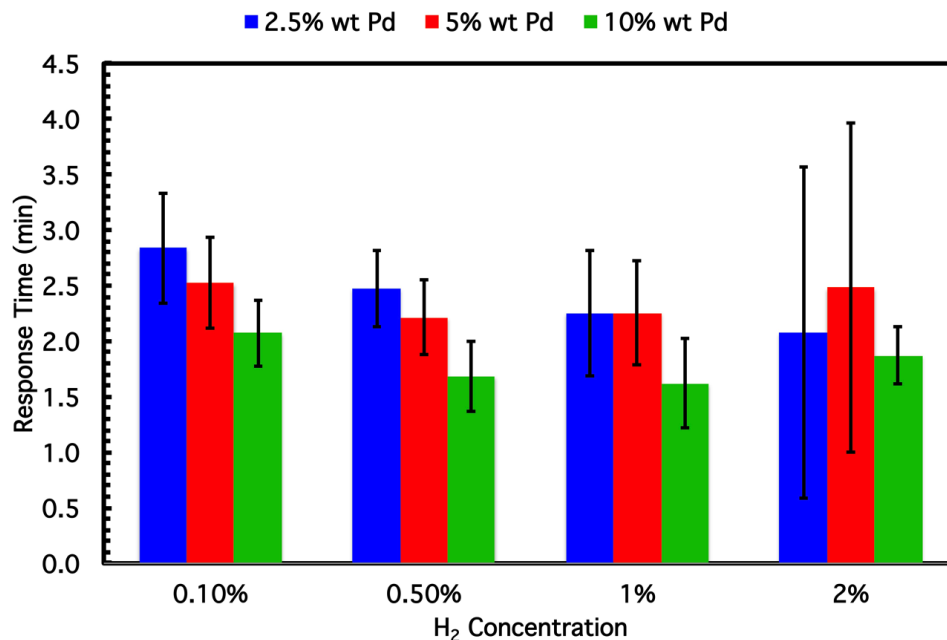


Figure 3.9 Average response time t_{90} and standard deviation at different hydrogen concentrations for samples with 2.5%, 5% and 10% wt Pd loadings.

Figure 3.9 shows that the average response time (t_{90}) for all the samples in this chamber are in the range of 1.7 min and 2.8 min. These response times are significantly higher than those reported by Lee¹¹, Rumiche¹² and Lu¹³. However, as explained in section 1.3.3 and further discussed in chapter 4, this variable depends heavily on the experimental conditions.

The fastest response times are for the samples with 10%wt Pd but their sensitivities are very low and the signal is unstable while, in general, samples with 2.5% Pd had higher sensitivities but slower responses. Samples with 5%wt Pd had similar characteristics as the 2.5%wt Pd samples; it had fast response time and high sensitivities. For subsequent experiments, this was the Pd concentration used as the precursor

quantities were more precisely measured at this concentration and it allowed the scale down to the smaller supports studied in Chapters 4 and 5.

3.3.4 Effect of Phase Change on the Response.

As discussed in section 2.3.1, the samples undergo a phase transition that starts at 1% v/v H₂ and it is completed at approximately 1.5% v/v H₂. This phase transition can cause structural changes that can affect the sensor response^{14,15} as discussed in section 1.3.4. Figure 3.10 shows a 2.5% Pd sample that was exposed to repeat cycles of H₂. It can be observed that when the sample is exposed to 2% v/v H₂ there is a steady increase in the value of the response current. At this H₂ concentration, Pd transitions to the β phase and the volume expansion associated with it closes void spaces or imperfections that may exist in the sample,¹⁶ this improves electrical continuity which can be observed as an increase in current. Afterwards, when the sample is exposed to nitrogen there is a decrease in the current baseline value but maintains the sensitivity in subsequent hydrogen exposures. This can be explained with the reported hysteric behavior of Pd samples where the resistance is higher upon hydrogen desorption than upon adsorption after transforming to the β -phase.¹¹

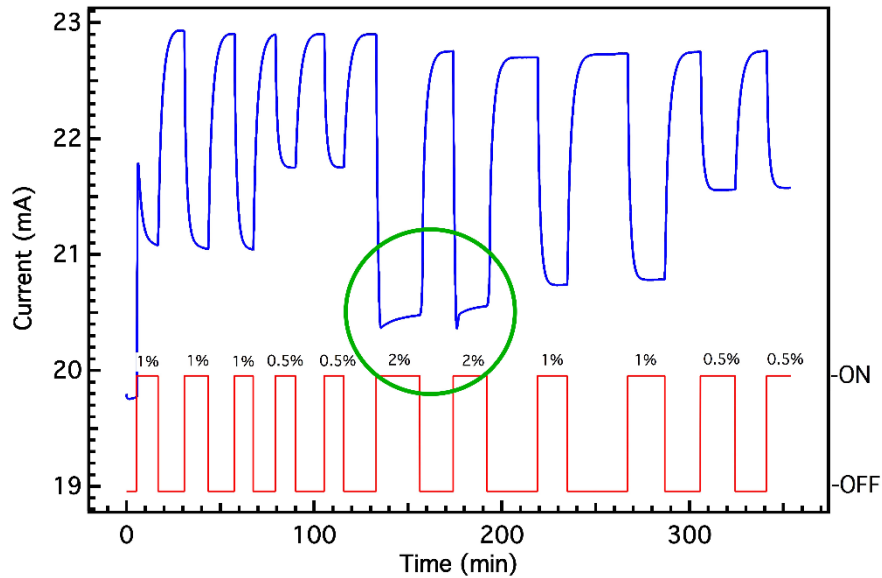


Figure 3.10 Sample exposed to various cycles of H₂ showing the effect of phase transition on the response in Ch-7000.

Figure 3.11 shows a curve of sensitivity vs. concentration upon hydrogen adsorption and desorption of our samples. As previously reported,^{11,17} the sensitivity follows a trend that can be related to the phase transition. At 1%v/v H₂ there is a significant change in sensitivity that can be identified as the start of the phase transition and at 3.5%v/v H₂ it appears to stabilize, signaling the end of the transition. However, upon desorption this sample did not return to the original sensitivity values suggesting that the morphology of the sample is affected by the phase transition through deformation or delamination as suggested by reports by Hughes and Choi.^{14,15} and discussed on Chapter 1. Exposing the sample to concentrations higher than 2% significantly affects the response suggesting film delamination and deformation as demonstrated in Figure 3.12.

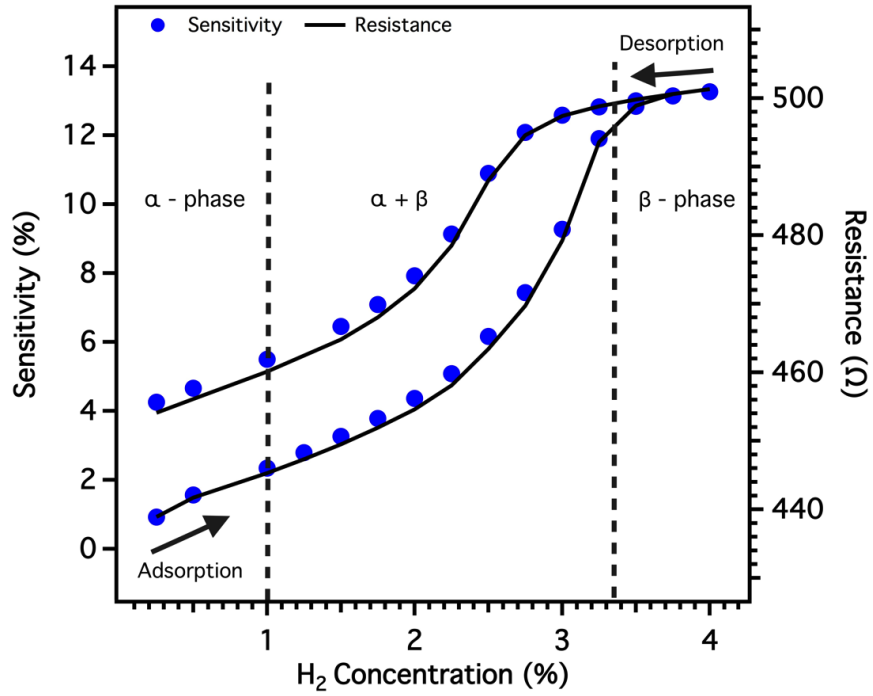


Figure 3.11 Hysteresis behavior of a 5% Pd sample.

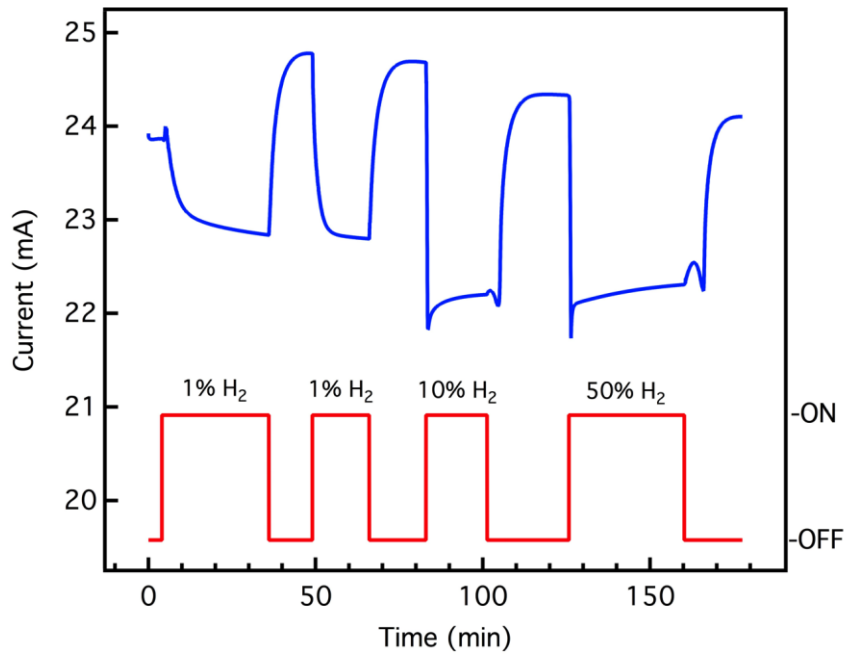


Figure 3.12 Sample exposed to H₂ concentrations higher than 2% v/v.

This effect was more pronounced in a 1.5% Pd sample (Figure 3.13), where the N₂ baseline did not recover from the exposure to 2%v/v H₂ probably due to deformation or delamination of the films caused by the exposure to high concentrations of H₂ (section 1.3.4).

The SSR method produces sensing elements that can accurately detect hydrogen concentrations below the explosion limit, however there are still obstacles that need to be conquered to be able to implement these sensing elements in actual devices.

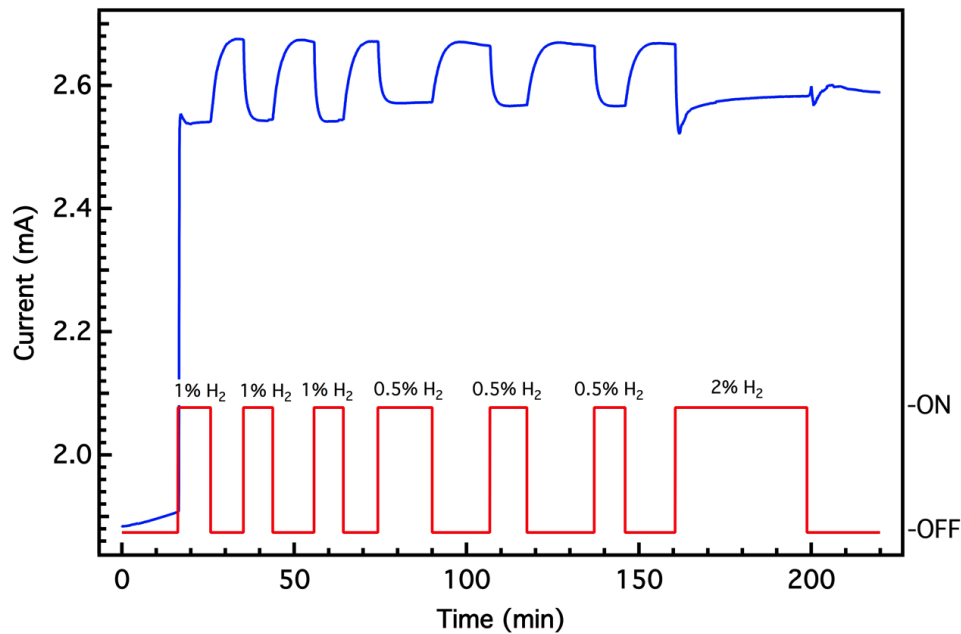


Figure 3.13 Response of a 1.5%wt Pd sample to different hydrogen concentrations.

3.4 CONCLUSIONS

The Pd samples obtained through the solid state reduction (SSR) method produces highly sensitive hydrogen sensing elements showing sensitivities as high as 7% for 1% v/v H₂ with stable signals for 2.5 and 5% wt Pd loadings and are able to detect in the 0.01% - 2% range. The samples follow with great accuracy Sieverts' law making them good candidates for hydrogen monitoring applications.

The electrode connectivity, film roughness, and reduction state of the sample affected significantly the stability of the sample signal. The electrode connection that yielded the more stable results were Cu wires adhered with Ag paste to the rougher film because of the increased α -spots (contact area) and decreased contact resistance. In addition, adding water during the reduction process not only increases the surface roughness but also the fraction of reduced metal leading to a stable baseline.

The addition of water during SSR can only reduce samples with a loading of less than 10% wt Pd. For practical purposes a 5% Pd loading is a good amount of metal to be used for the sensing elements because it shows a balance between sensitivity and response time. Finally, H₂ adsorption/desorption curves showed that the samples suffered morphological changes during phase transition that affects the responses above the phase transition concentration.

3.5 REFERENCES

- (1) Hübert, T.; Boon-Brett, L.; Black, G.; Banach, U. Hydrogen Sensors – a Review. *Sensors & Actuators: B. Chemical* **2011**, *157* (2), 329–352.
- (2) Ketenoğlu, D.; Ünal, B. Influence of Surface Roughness on the Electrical Conductivity of Semiconducting Thin Films. *Physica A* **2013**, *392* (14), 3008–3017.
- (3) Palasantzas, G.; Barnaś, J. Surface-Roughness Fractality Effects in Electrical Conductivity of Single Metallic and Semiconducting Films. *Phys. Rev., B Condens. Matter* **1997**, *56* (1), 7726–7731.
- (4) Palasantzas, G. Surface Roughness and Grain Boundary Scattering Effects on the Electrical Conductivity of Thin Films. *Physical Review B (Condensed Matter and Materials Physics)* **1998**, *58* (1), 9685–9688.
- (5) Braunovic, M.; Myshkin, N.; Konchits, V. Introduction to Electrical Contacts. In *Electrical Contacts; Fundamentals, Applications and Technology*; CRC Press, 2010; Vol. 20066652, pp 1–8.
- (6) Ramanathan, M.; Skudlarek, G.; Wang, H. H.; Darling, S. B. Crossover Behavior in the Hydrogen Sensing Mechanism for Palladium Ultrathin Films. *NanoTech* **2010**, *21* (12), 125501.
- (7) Elkina, I. B.; Meldon, J. H. Hydrogen Transport in Palladium Membranes. *Desalination* **2002**, 445–448.
- (8) Deveau, N. D.; Ma, Y. H.; Datta, R. Beyond Sieverts' Law: a Comprehensive Microkinetic Model of Hydrogen Permeation in Dense Metal Membranes. *Journal of Membrane Science* **2013**, *437*, 298–311.
- (9) Kay, B.; Peden, C.; Goodman, D. Kinetics of Hydrogen Absorption by Pd(110). *Phys. Rev., B Condens. Matter* **1986**, *34* (2), 817–822.
- (10) Conrad, H.; Ertl, G.; Latta, E. E. Adsorption of Hydrogen on Palladium Single Crystal Surfaces. *Surface Science* **1974**, *41* (2), 435–446.
- (11) Lee, E.; Lee, J. M.; Koo, J. H.; Lee, W.; Lee, T. Hysteresis Behavior of Electrical Resistance in Pd Thin Films During the Process of Absorption and Desorption of Hydrogen Gas. *International Journal of Hydrogen Energy* **2010**, *35* (13), 6984–6991.
- (12) Rumiche, F.; Wang, H. H.; Hu, W. S.; Indacochea, J. E.; Wang, M. L. Anodized Aluminum Oxide (AAO) Nanowell Sensors for Hydrogen Detection. *Sensors & Actuators: B. Chemical* **2008**, *134* (2), 869–877.
- (13) Lu, J.; Yu, S.; Wang, H. H. Ultrafast Pd/AAO Nanowell Hydrogen Sensor. *MRS Proceedings* **2005**, 0900–O10–09.1.
- (14) Choi, S. Y.; Takahashi, K.; Matsuo, T. No Blister Formation Pd/Pt Double Metal Gate MISFET Hydrogen Sensors. *IEEE Electron Device Lett.* **1984**, *5* (1), 14–15.
- (15) Hughes, R. C.; Schubert, W. K.; Zipperian, T. E.; Rodriguez, J. L.; Plut, T. A. Thin-Film Palladium and Silver Alloys and Layers for Metal-Insulator-Semiconductor Sensors. *J. Appl. Phys.* **1987**, *62* (3), 1074–1083.
- (16) Dankert, O.; Pundt, A. Hydrogen-Induced Percolation in Discontinuous Films. *Appl. Phys. Lett.* **2002**, *81* (9), 1618–1620.
- (17) Lee, E.; Lee, J. M.; Lee, E.; Noh, J.-S.; Joe, J. H.; Jung, B.; Lee, W. Hydrogen Gas Sensing Performance of Pd–Ni Alloy Thin Films. *Thin Solid Films* **2010**, *519* (2), 880–884.

4 OPTIMIZATION OF THE SENSING RESPONSE OF PD FILMS OBTAINED BY SSR: EFFECT OF RESIDENCE TIME, SOLUTION IMPREGNATION, AND VOLTAGE

4.1 INTRODUCTION

In Chapter 3 we discussed how the electrode connectivity, partial reduction of the sample, metal loading, and phase changes affected the response of our Pd chemiresistors to hydrogen. In this Chapter we discuss how the chamber flow dynamics, surface morphology, and voltage affect the sensor response.

Voltage is known to affect the sensitivity and response time of Pd nanowires^{1,2} and single nanowires³ and the morphology of films is also known to affect the response of Pd based chemiresistors^{4,5}. This Chapter describes the effect of voltage on the two different synthesis approaches covered in Chapter 2. Since our SSR method produces different film morphologies, their effect on the sensor response is also included in this Chapter.

According to Boon-Brett⁶ the response time is an important property for hydrogen safety sensors, however its value changes with experimental methods. Therefore this chapter includes experimental sensing results obtained in different chambers and the results are compared using residence time. The results of a simple Navier-Stokes simulation are included to illustrate how the flow dynamics of a chamber can affect the response of a sensor.

4.2 METHODOLOGY

Samples were synthesized following the solid and solution impregnation methods described in section 2.2.1. All the samples studied in this Chapter had a 5% wt Pd loading. The solid approach to the SSR will be referred as Solid-SSR and the solution approach as Solution-SSR. Water was added on both methods during the reduction step.

The samples were connected to copper wires using silver paste. All the results presented in this chapter were obtained using a 1% v/v H₂ concentration to avoid any structure damage related to the phase transition.

The samples' response to hydrogen was obtained in three sealed chambers constructed in house. The first chamber was a polycarbonate rectangular prism with dimensions 17 inches (43.2 cm) in length, 14 inches (35.6 cm) width, and 11 inches (27.9 cm) height (V~43,000 cm³). This chamber is referred to as **Ch-43000** and its configuration can be observed in Figure 4.1. The second chamber was a PVC cylinder with 5.9 inches (15 cm) in diameter and 15 inches (38.1 cm) in length (V~7,000 cm³). This chamber is referred to as **Ch-7000** and was described in Chapter 3 (Figure 3.1). The third chamber was a stainless-steel cylinder 1 inch (2.5 cm) in diameter and 7 inches (17.8 cm) in length (V~90cm³) with two side Swagelok 1" brass inlets. This chamber is referred to as **Ch-90** and can be observed in Figure 4.2. The electrical measurements were obtained using a Keithley 2400 multimeter. Labview 2010 was used to monitor and record the changes in the electrical properties of the sensor. MKS gas flow controllers were used to regulate the flow of gas into the chambers.

The electrical connections were made on the sample in the **Ch-43000** and **Ch-7000** using copper wires manipulated using KRN-09S micromanipulators. For the **Ch-90**

the Cu cables were connected to the sample through the sample holder specifically built for this chamber.

For the mathematical models presented in this Chapter, the numerical solution was found using MATLAB's built in PDE solver (pdepe) with a mesh of 200 points for the space and time variables. The routine can be found in Appendix C.

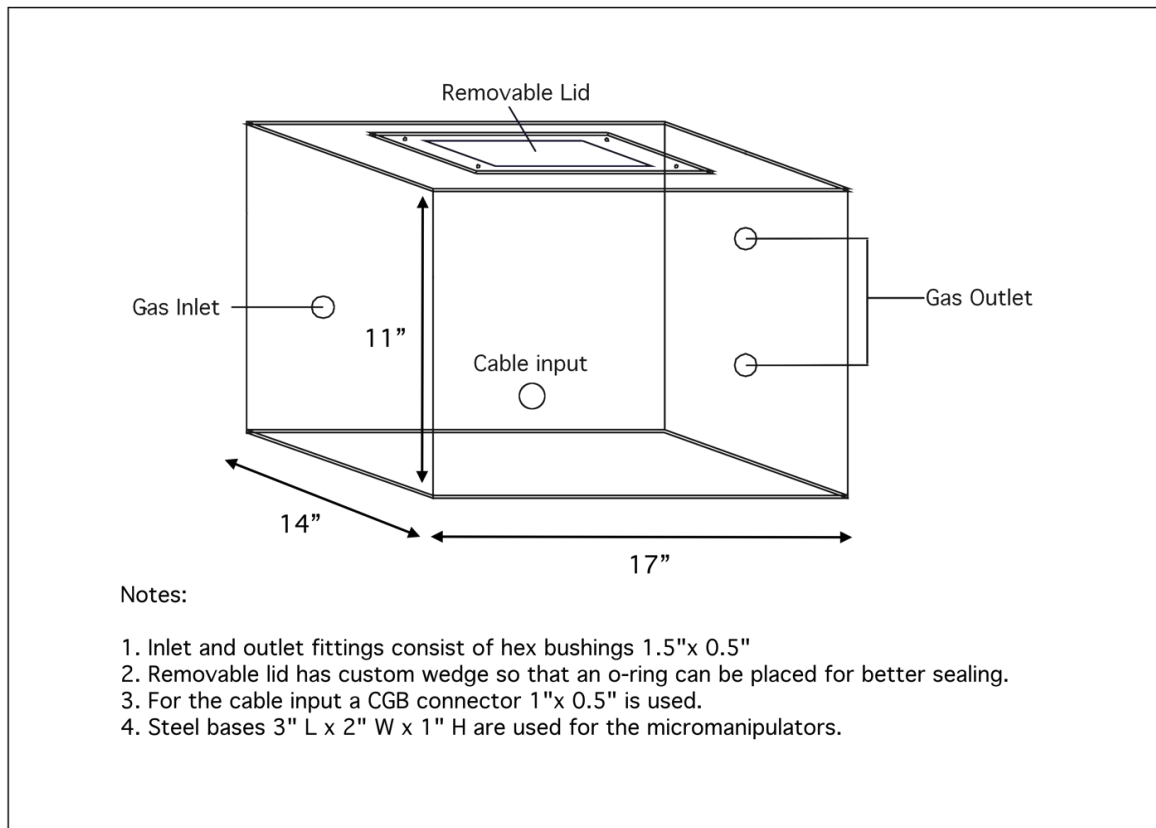


Figure 4.1 Polycarbonate Chamber, $V \sim 43,000 \text{ cm}^3$

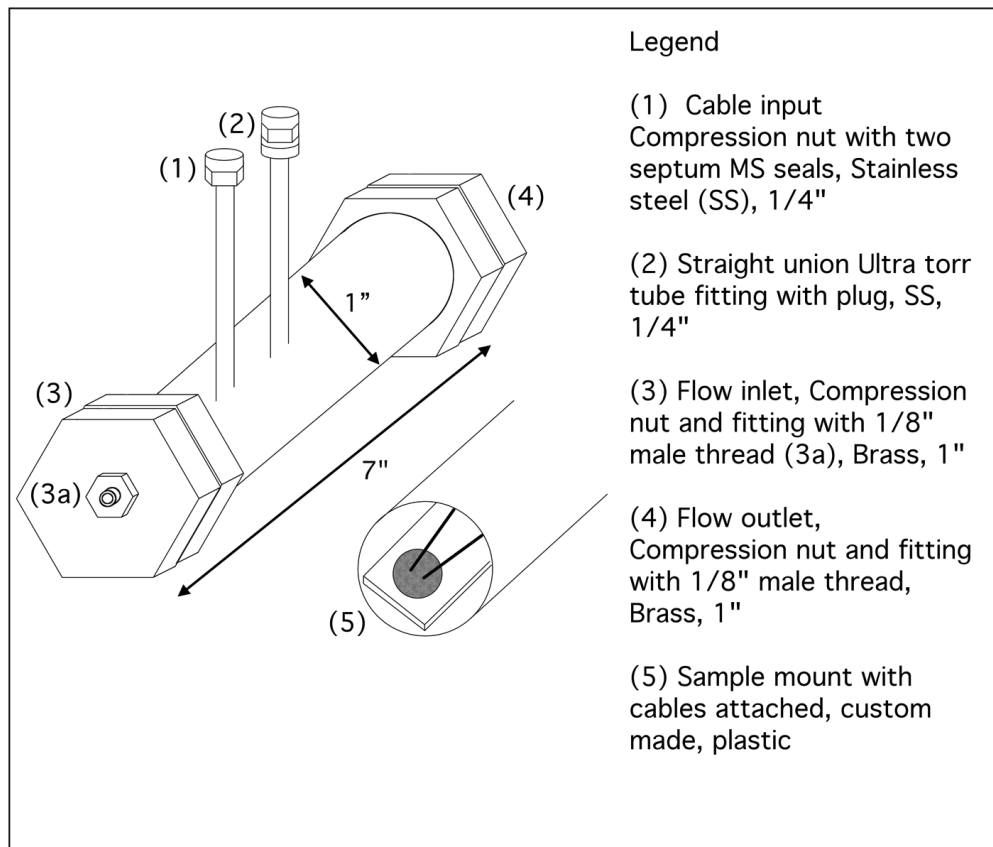


Figure 4.2 Stainless Steel Chamber, V~90 cm³

4.3 RESULTS

4.3.1 Effect of Voltage

The effect of voltage was studied for samples synthesized by Solid-SSR and Solution-SSR in the *Ch-90* chamber with a total flow of 300 sccm. Voltage was varied from 1000 mV to 15 mV.

Figure 4.3 shows that for the samples obtained by Solid-SSR the sensitivity increases but the response time is slowed as the voltage decreases. These results are consistent with a behavior first reported for Pd nanowires by Offermans et al.^{1,2} and later studied in more detail by Yang et al.³ The reduction in response time with higher voltages

is explained by the effect of self-heating of the Pd films known as Joule heating (Equation 4.1) which is proportional to the square of the current in a closed circuit where t is the time. As the voltage is increased the inner temperature of the metal increases due to the higher charge carrier flow therefore increasing the diffusion rate of the hydrogen atoms through the Pd structure.³

$$Q = i^2 R t \quad (\text{Eq. 4.1})$$

The reduction in sensitivity with increasing voltage is explained by taking a closer look to Sieverts' law (Eq. 3.1). The dependence of Sieverts' constant with temperature is given by:⁷

$$\ln K_s = -\frac{\Delta H}{2RT} + \frac{\Delta S}{2R} \quad (\text{Eq. 4.2})$$

where ΔH and ΔS are the standard molar enthalpy and standard molar entropy of desorption, respectively. Therefore, if the inner temperature of the sample increases, Sieverts' constant increases thus decreasing the solubility and decreasing the sensitivity.

This effect, however, is diminished when the sample is synthesized by Solution-SSR where the voltage variation on sensitivity and the response time (Figure 4.4) is negligible. An electrical current versus voltage analysis shows that the bulk resistance values for the Solid-SSR and Solution-SSR samples used in these experiments were 5 Ω and 172 Ω , respectively, a 189% difference. A high resistance (R) value implies that a sample would not significantly change its current (i) as the voltage (V) is changed as described by Ohm's law:

$$i = \frac{V}{R} \quad (\text{Eq. 4.3})$$

The insignificant changes in current as a function of voltage leads to a more stable self-heating, yielding more stable sensitivity and response times for the Solution-SSR samples. This suggests that the Solution-SSR method leads to more reliable samples than Solid-SSR. However, it is evident from the differences in the sensitivity values that the morphology of the films obtained by the two methods affect their response as will be discussed below.

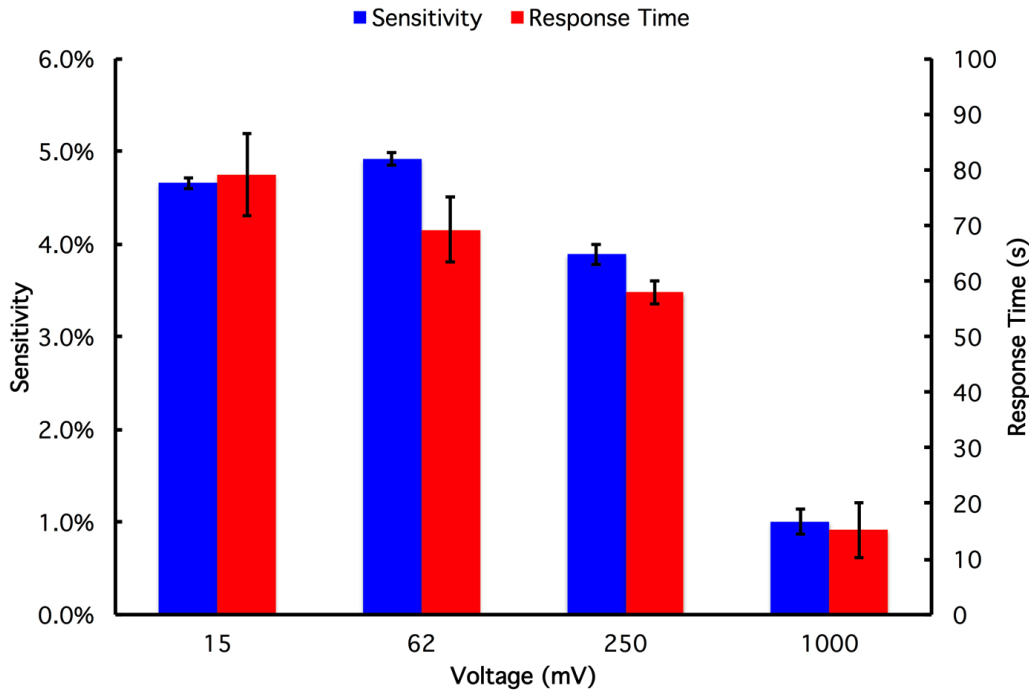


Figure 4.3 Voltage dependency on sensitivity and t_{90} for a 5%wt Pd sample obtained by Solid-SSR.

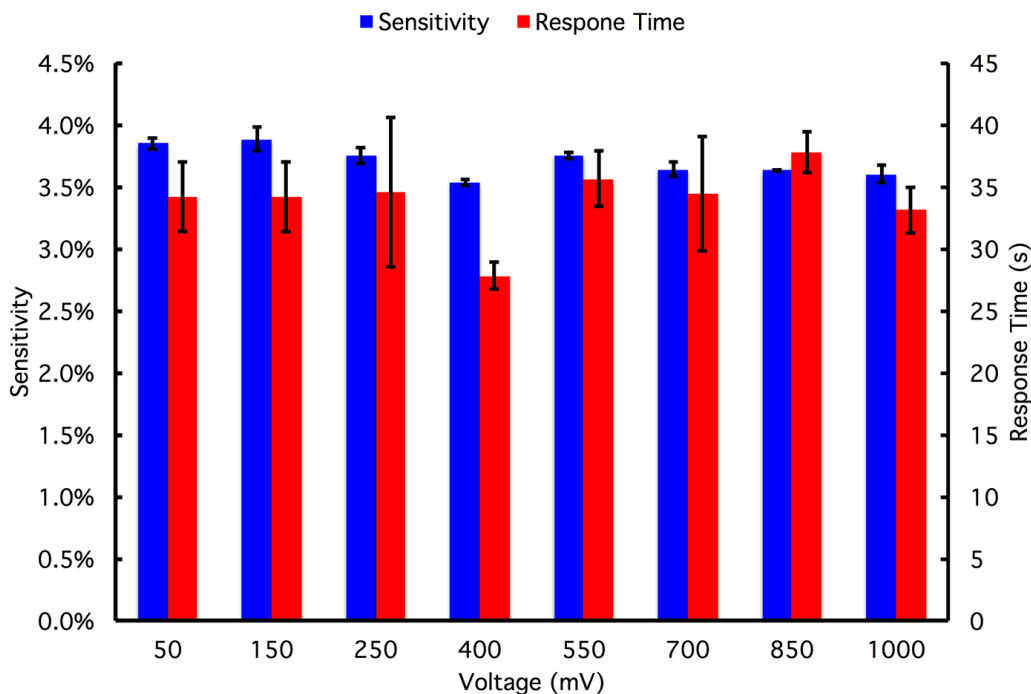


Figure 4.4 Voltage dependence on sensitivity and t_{90} for a sample synthesized by Solution-SSR.

4.3.2 Effect of Impregnation Form and Film Morphology

All surfaces are not perfectly smooth; they all have asperities even at the atomic level. The more defined these asperities are, the greater the roughness of the sample could be. It has been demonstrated that the roughness of the sample can change the response time and sensitivity of Pd film based chemiresistors.⁴

Significant differences were observed in the hydrogen responses of the samples obtained by Solid-SSR and Solution-SSR. The average sensitivity for different samples obtained with Solution-SSR is $4.4 \% \pm 0.7$ while with Solid-SSR it is $3.5 \% \pm 2.3$ at 1 V and 300 sccm in the *Ch-90*, where all samples were connected on their rougher side (Section 3.3.1). The Solution-SSR samples have a higher sensitivity to hydrogen and a lower standard deviation. This suggests that the Solution-SSR method leads to more

homogeneous samples that yield more consistent results and that the samples have a better electrical conductivity. Moreover, the smoother films of the samples obtained by Solution-SSR also lead to stable signals, as described below.

As discussed in Chapter 2, films with different surface roughness are obtained on either side of the AAM, which varies with the synthesis method (solid vs. solution impregnation). The effect of the roughness of the films on the sensitivity was studied in samples synthesized by solid and solution impregnation at 1% v/v H₂ and the results are shown in Figure 4.5. The results show for the Solution-SSR method the films on both sides of the samples respond to H₂. The smoother film had higher sensitivity values than the rougher films and lower initial electrical current values were observed for this side. Meanwhile, the rough films (impregnation side) of these samples have lower sensitivity values but have a lower standard deviation.

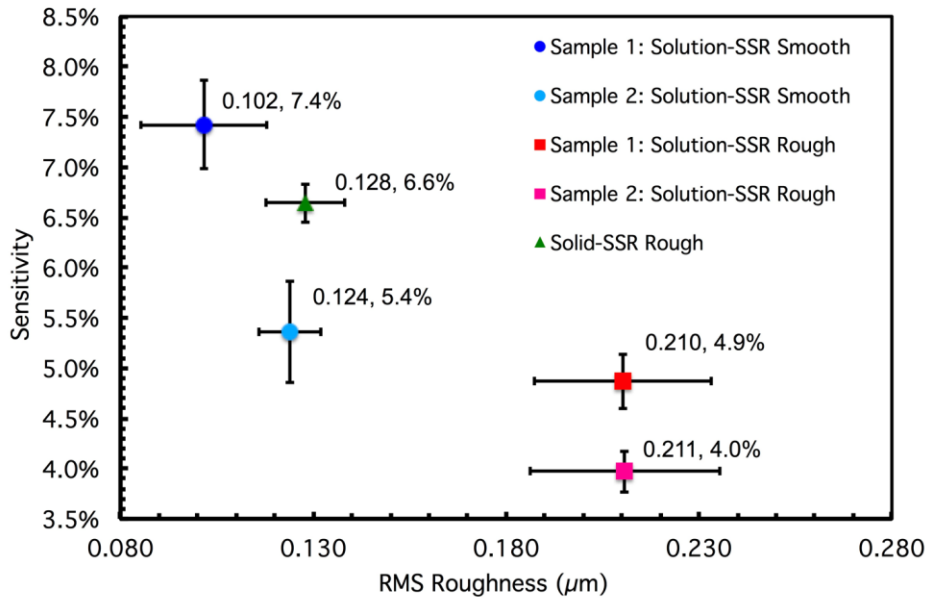


Figure 4.5 Sensitivity values compared to the surface RMS roughness. Various sensitivity and roughness measurements were performed on each sample.

The roughness of the films also affected the response times, t_{90} , of the solution-impregnated samples (Figure 4.6). Moreover the results for t_{90} were more consistent (18% difference vs. 71% difference) for this side when compared to the smooth side and faster when compared to the Solid-SSR's rough side.

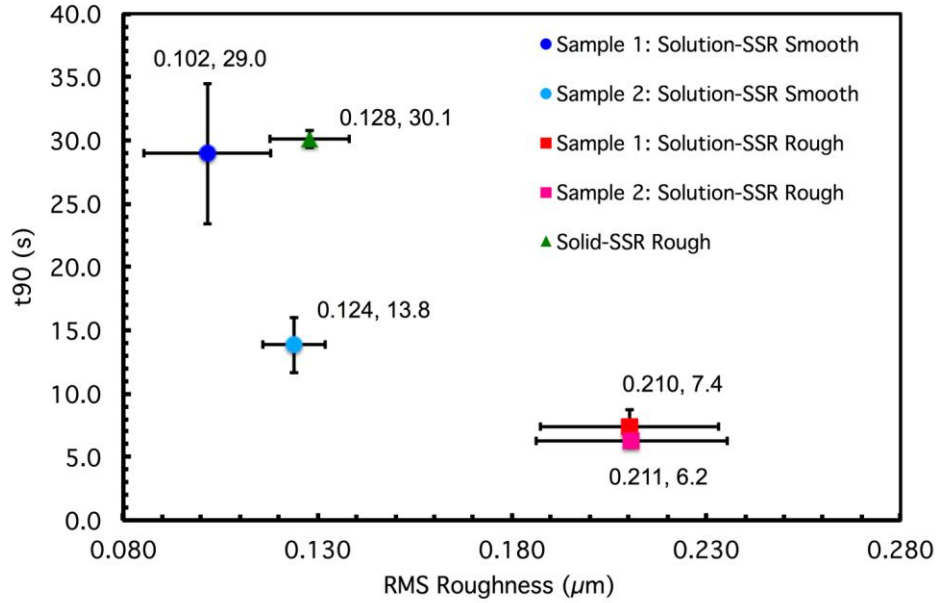


Figure 4.6 Response time values compared to the surface RMS roughness. Various sensitivity and roughness measurements were performed on each sample.

The possibility of having greater metal content on the rough side of the Solution-SSR and the interconnectivity between the grains of these samples produces fast responding sensing elements with fair sensitivities when compared to the smooth side of the same sample and to the rough side of the Solid-SSR sample. This high electrical current observed for this side causes the metal to raise its internal temperature by the phenomenon of Joule heating thus increasing the diffusivity of hydrogen through the film therefore decreasing the response time of this side. Meanwhile, the sensitivity for this

side is lower than the smooth side because the self-heating induced by the current, decreases Sieverts' constant thus reducing the solubility and therefore the sensitivity, however the high surface area for the rough side still gives fairly high sensitivities. Therefore, the rough film obtained by Solution-SSR yields more reliable H₂ sensing results than the smooth film obtained by the same method and the rough film obtained by Solid-SSR.

4.3.3 Effect of Residence Time on Response Time

The residence time τ is the ratio between chamber volume and total gas flow and it describes the average amount of time that a particle spends in a particular system.

$$\tau = \frac{V}{\nu} \quad (\text{Eq. 4.4})$$

Table 4.2 shows how the response times (t_{90}) changes in the different chambers described above by using the same volumetric flow rate using SSR-Solid samples at 1 V. As the chamber volume (and the residence time) decreased, the response time also decreased. For the **Ch-43000** the t_{90} was ~11 min whereas for the **Ch-90** the t_{90} was ~6 sec; this represents a 99.1% decrease in t_{90} . However the sensitivity is reduced significantly.

Table 4.1 Response time for 5%wt Pd samples to 1%v/v H₂ in chambers of different volumes

Chamber	V (cm³)	v (sccm)	v (cm³/min)	τ (min)	t₉₀ (min)	S
<i>Ch-43000</i>	~43,000	4000	1822	23.6	11	7.4%
<i>Ch-7000</i>	~7,000	4000	1822	3.8	2.5	7.2%
<i>Ch-90</i>	~90	4000	1822	0.05	0.1	2.7%

To further study the effect of flow on the response time, the chamber volume was fixed and the flow was varied. The chambers studied were the *Ch-7000* and *Ch-90* as they exhibited the fastest response times. Table 4.3 summarizes the response time of the sample response as a function of the residence time. As the total flow of the system increases, the residence time decreases and the response time of the sample decreases until almost a constant value is achieved. The sensitivity for the sample remains practically unchanged throughout the sensing cycles. This suggests that the response time is limited by external diffusion during low flows and tends to a stable value when the flows are increased. Also, the fact that the response time is reaching a plateau at high flows suggests that the system is reaching a condition where the system is no longer limited by external diffusion.

Table 4.2 Results for t_{90} and sensitivity in the *Ch-7000* of a 5%wt Pd sample at 1%v/v H_2 as a function of total flow. To reduce the experimental sample variances, this experiment was done on one sample with cycling of different flows.

v (sccm)	v (cm^3/min)	τ (min)	$\overline{t_{90}}$ (min)	\overline{S}
2000	911	7.6	4.7 ± 0.1	$7.2\% \pm 0.1$
4000	1822	3.8	2.5 ± 0.0	$7.2\% \pm 0.0$
8000	3643	1.9	1.2 ± 0.1	$7.3\% \pm 0.0$
10000	4554	1.5	1.0 ± 0.0	$7.3\% \pm 0.1$

To understand the effects of external diffusion of hydrogen on the response time, the fluid dynamics of a cylinder of length L and radius R where the gas flows in the z -direction were analyzed using the Navier-Stokes equation. This analysis assumes that the external diffusion is controlling the response time and does not include the adsorption and internal diffusion steps of hydrogen on the Pd structure. To solve the equation, it was assumed that there is no permeation through the walls of the cylinder and that there is no variation in the angular and radial velocity. The concentration profile of this system thus can be described with Equation 4.5:

$$\frac{\partial C}{\partial t} + V_z \frac{\partial C}{\partial z} = D \left[\frac{1}{r} \frac{\partial}{\partial r} \left(r \frac{\partial C}{\partial r} \right) + \frac{\partial^2 C}{\partial z^2} \right] \quad (\text{Eq. 4.5})$$

where D is the diffusivity of hydrogen in nitrogen which can be estimated with the Wilke-Lee model.⁸ As illustrated in Figure 4.7, C_{in} and C_{out} are the concentrations at the cylinder's inlet and outlet, respectively. For this analysis it was assumed that the concentration C_{out} changes with the concentration C inside the cylinder. These assumptions result in the boundary conditions depicted in Table 4.4.

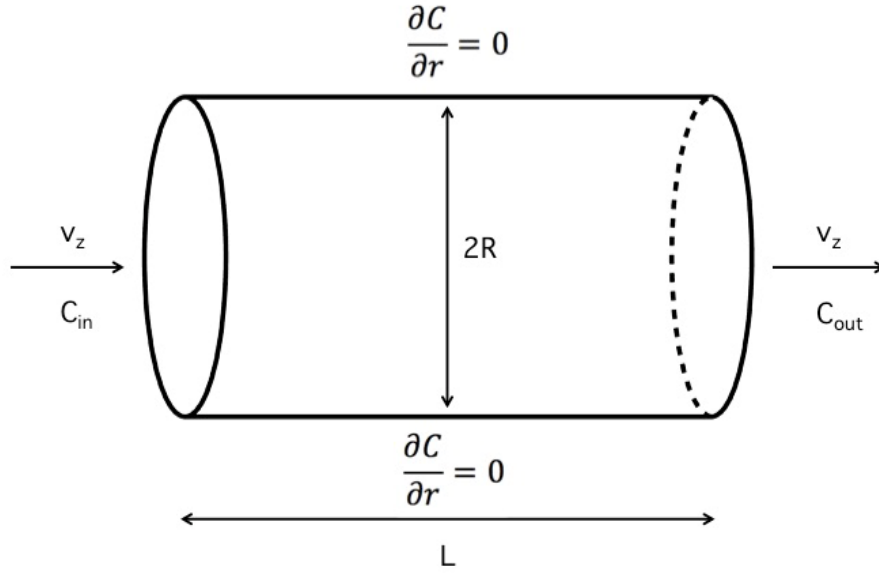


Figure 4.7 Cylinder of length L and radius R with gas flowing in z -direction.

Table 4.3 Initial and boundary conditions for equation 4.5

Initial Condition	Left Boundary Condition	Right Boundary Condition	Wall Boundary Condition
$C(\mathbf{z}, \mathbf{r}, \mathbf{0}) = C_{out} = \mathbf{0}$	$C(0, r, t) = C_{in}$	$C(L, r, t) = C_{out}$	$\frac{\partial C}{\partial r} = 0$ for $r = R$

To facilitate the analysis, Equation 4.5 can be expressed with the dimensionless parameters:

$$\theta = \frac{C_{in} - C}{C_{in} - C_{out}} \quad \rho = \frac{t}{t_f} \quad \eta = \frac{r}{R} \quad \Gamma = \frac{z}{L}$$

where C_{in} and C_{out} are the concentrations at the entrance and the exit of the cylinder, t_f is the time to reach steady state, and R and L are the radius and length of the cylinder. Using these parameters Equation 4.5 becomes:

$$\frac{1}{Fo} \frac{\partial \theta}{\partial \rho} + Pe \frac{\partial \theta}{\partial \Gamma} = \frac{K}{\eta} \frac{\partial}{\partial \eta} \left(\eta \frac{\partial \theta}{\partial \eta} \right) + \frac{\partial^2 \theta}{\partial \Gamma^2} \quad (\text{Eq. 4.6})$$

where Fo is the Fourier number, Pe is the Péclet number, and K is the ratio between length and radius:

$$Fo = \frac{Dt_f}{L^2} \quad Pe = \frac{V_z L}{D} = \frac{L^2}{\tau D} \quad K = \left(\frac{L}{R}\right)^2$$

The initial and boundary conditions for this system are now:

Table 4.4 Initial and boundary conditions for equation 4.6			
Initial Condition	Left Boundary Condition	Right Boundary Condition	Wall Boundary Condition
$\theta(\Gamma, \eta, 0) = 1$	$\theta(0, \eta, \rho) = 0$	$\theta(1, \eta, \rho) = 1$	$\frac{\partial \theta}{\partial \eta} = 0$ for $\eta = 1$

For $K \gg 1$, Equation 4.6 can be lumped by averaging each term for η . So $\bar{\theta}(\Gamma, \rho)$ can be defined as:⁹

$$\bar{\theta}(\Gamma, \rho) \equiv \frac{\int_0^1 \theta(\Gamma, \eta, \rho) \eta \, d\eta}{\int_0^1 \eta \, d\eta} = 2 \int_0^1 \theta(\Gamma, \eta, \rho) \eta \, d\eta \quad (\text{Eq. 4.7})$$

By integrating each term by $\int_0^1 \eta \, d\eta$ Equation 4.6 becomes:

$$\frac{\partial^2 \bar{\theta}}{\partial \Gamma^2} = Pe \frac{\partial \bar{\theta}}{\partial \Gamma} + \frac{1}{Fo} \frac{\partial \bar{\theta}}{\partial \rho} \quad (\text{Eq. 4.8})$$

The steady-state analytical solution for this equation is:

$$\bar{\theta}(\Gamma) = \frac{1}{e^{Pe} - 1} (e^{Pe\Gamma} - 1) \quad (\text{Eq. 4.9})$$

For this equation, Figure 4.8 shows that as the Pe number increases the profile goes from a linear to an exponential behavior. Moreover, as the Pe increases the concentration along the cylinder approaches the concentration at the inlet at steady state.

That is, at large flows the hydrogen concentration that reaches the sample is closer to the desired inlet concentration.

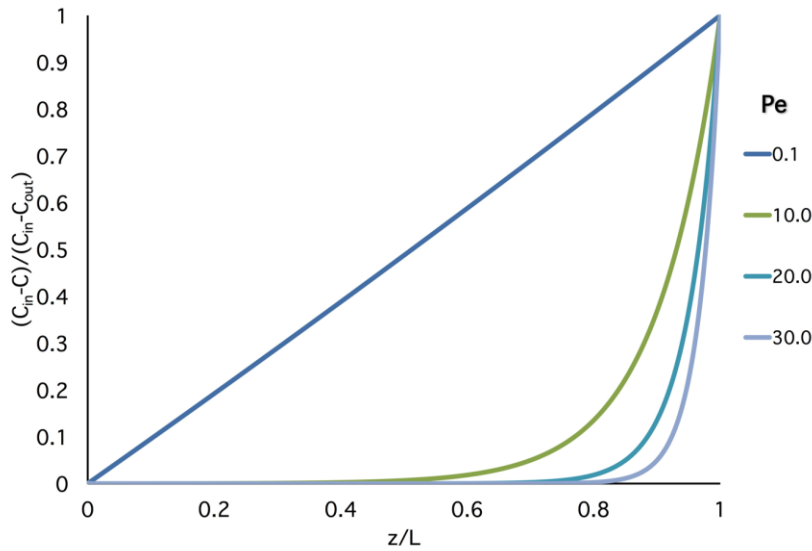


Figure 4.8 Steady-state concentration along z at different Pe numbers.

However, it is the unsteady solution to Equation 4.8 that can give a better indication on the effect of flow on the response time. The solution for Pe numbers equal to 0.1, 10, 20, and 30 with $Fo = 0.259$ are shown in Figure 4.9. The function reaches the steady state solution with time, as expected. For small Pe numbers the concentration in the chamber is controlled by the diffusion of hydrogen through nitrogen as the initial concentration along the cylinder approaches C_{out} . For large Pe numbers convection controls the concentration along the chamber and the steady state response is reached faster. These results show that by increasing the Pe number, the time it takes to expose the sample to the desired inlet concentration is significantly reduced, which helps explain the decreasing response time with increasing flow.

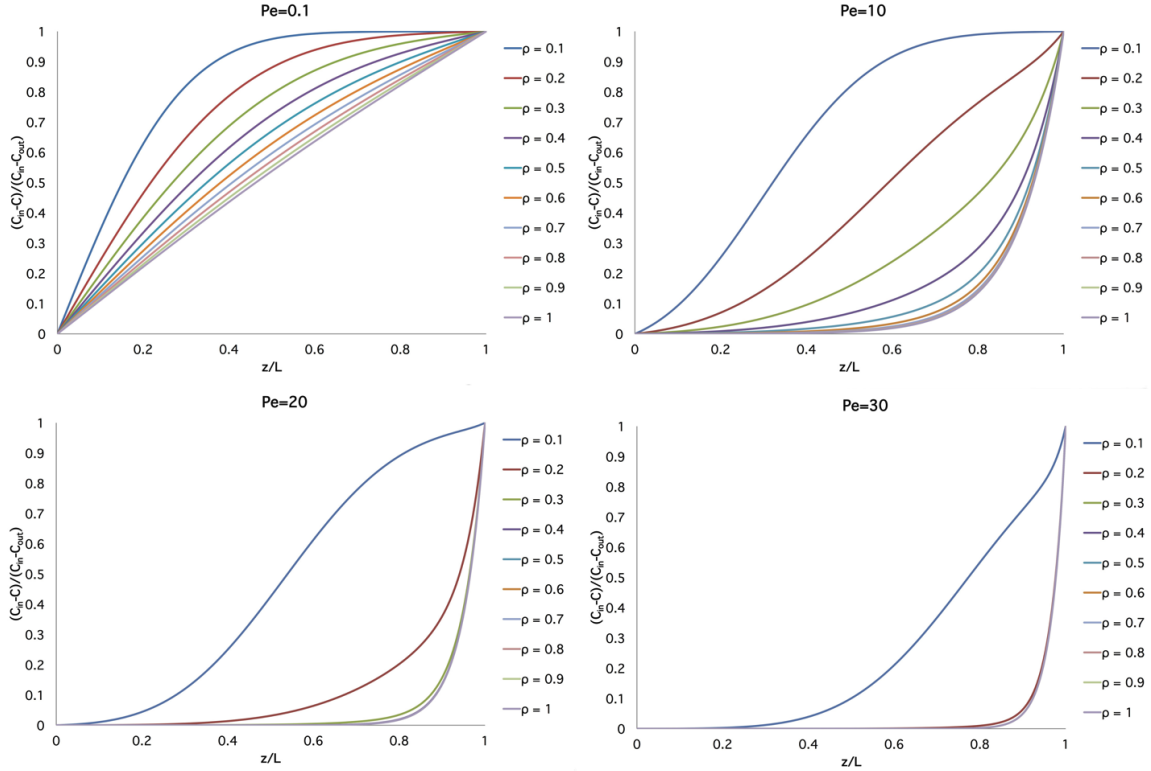
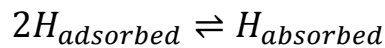
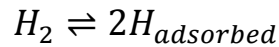


Figure 4.9 Changes in the cylinder concentration in z with time at different Pe and ρ .

Table 4.5 shows that on the *Ch-90* a different trend is observed, the sensitivity decreases as the residence time decreases. Note that in this chamber the residence time is on the order of seconds. This suggests that, in this range of residence times, a step other than external diffusion is controlling the response time. Other steps in the adsorption mechanism are:



The first step is the dissociative adsorption of hydrogen on the surface of Pd and the second step is the diffusion of the adsorbed hydrogen atoms inside the interstices of its structure. In clean samples the limiting step is the second step¹⁰ and, thus, the rate of

absorption depends on the concentration of adsorbed hydrogen atoms. Because the sensitivity depends on the concentration of adsorbed hydrogen atoms (Eq. 3.1) a decreasing sensitivity suggests that, in this limit, the decreasing residence time results in a decreasing number of adsorbed atoms. Furthermore, the response time also decreases but it is probably because there are fewer hydrogen atoms that need to be adsorbed to reach steady state.

These results suggest that there is an optimum residence time where the sensitivity is high and the response time is small. Figures 4.10 and 4.11 show that for samples Solid-SSR and Solution-SSR, there is an optimum at $\tau \sim 120$ s where the response times and sensitivities are 60 s, 6.6% and 61.5s, 6.1% for the Solid-SSR and Solution-SSR samples respectively. However, there is gap in the sensitivities due to a change in chambers and it was not possible to have a residence time where the two chambers coincided. Thus, the results might be affected by the different flow configurations of the chambers. It can be also observed that the gap between the high sensitivities and low sensitivities is larger for the SSR-Solid sample than for the SSR-Solution sample. This was due differences in current after the connection was made after changing from one chamber to the other. The percent difference in current for the Solution-SSR after changing chambers was 6%, whereas for the Solid-SSR was 121%. As discussed in section 4.3.1, big changes in base current can affect the sensitivity of the sample. Possibly the non-uniform nature of the Solid-SSR surface plus the fact that the two chamber connections are not identical, results in this bigger gap which affects the stability of the sample.

Table 4.5 Results for t_{90} and sensitivity varying total flow for the *Ch-90* chamber at 1% H_2 .

v (sccm)	v (cm^3/min)	τ (s)	$\overline{t_{90}}$ (s)	\overline{S}
500	228	23.7	60.9 ± 5.7	$5.1 \pm 0.0\%$
1000	455	11.9	26.7 ± 12.1	$4.6 \pm 0.1\%$
2000	911	5.9	12.8 ± 1.1	$3.1 \pm 0.1\%$
4000	1822	3.0	4.0 ± 0.58	$2.7 \pm 0.1\%$

Depending on the proposed application of the sensor, the chamber or casing for the sensing-element should be engineered to have a high sensitivity or fast response or a balance between the two. Furthermore, this shows that the guidelines set by the DOE for sensitivity and response times need to be balanced within a sample.

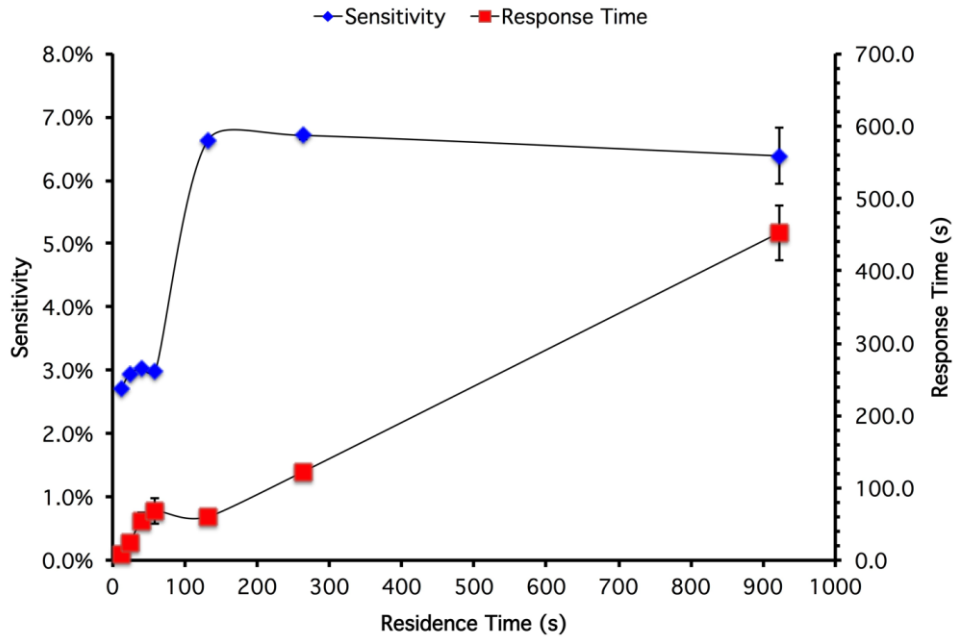


Figure 4.10 Sensitivity and response time dependence on residence time for a Solid-SSR sample at 1% H_2 .

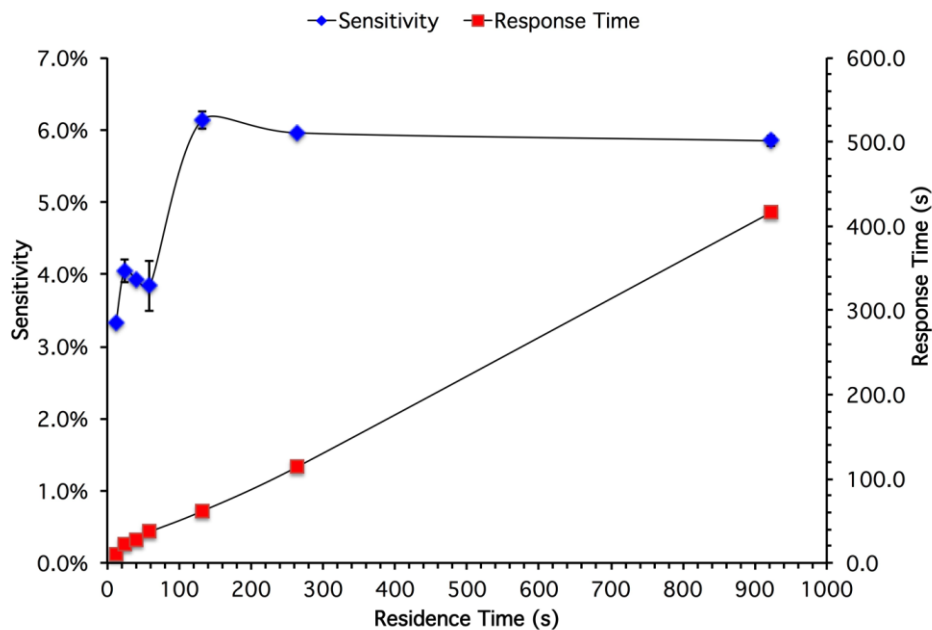


Figure 4.11 Sensitivity and response time dependence on residence time for a Solution-SSR sample at 1% H₂.

4.4 CONCLUSIONS

In this Chapter it was shown that the sensitivity and response time of the samples are affected by voltage applied, morphology of the film, and residence time. Changes in the voltage did not change the results of the Solution-SSR samples and the rough films of these samples yielded the more reliable results. These rough films also yield the fastest signal with good sensitivities because of the low resistance values that they show compared to the smooth surface of the same sample. The interconnectivity between the grains of the rough film results in high current which in turn increase the response time as described by the Joule heating effect.

Residence time was found to greatly affect the response time and sensitivity by shifting the rate-controlling step of the absorption process. When the residence time is in the order of minutes the external diffusion was the rate-limiting step; thus increasing the

flow of hydrogen yielded faster response times whilst maintaining the sensitivity. However, when the residence time was in the order of seconds the sensitivity decreased suggesting a decreased concentration of adsorbed hydrogen.

The best results were obtained at low residence times and 1 V with the rough films of samples synthesized by Solution-SSR. These samples yielded a sensitivity of 2.7% and a t_{90} of 4 s, which is close the specifications of DOE. However, this study shows that, in order to compare the performance of the different sensors reported in the literature, the DOE should standarize the testing conditions for the different applications. For example for hydrogen detection in enclosed facilities, probably a batch chamber is more appropriate where the location of the sensor and the hydrogen source are specified, whereas for hydrogen monitoring a flow through chamber is appropriate with specified flow and volume conditions as studied here.

4.5 REFERENCES

- (1) Offermans, P.; Crego-Calama, M.; Brongersma, S.; Tong, H.; van Rijn, C. Ultra-Low-Power Hydrogen Sensing with Palladium Nanowires. *Sensors, 2008 IEEE* **2008**, 98–101.
- (2) Offermans, P.; Tong, H. D.; van Rijn, C. J. M.; Merken, P.; Brongersma, S. H.; Crego-Calama, M. Ultralow-Power Hydrogen Sensing with Single Palladium Nanowires. *Appl. Phys. Lett.* **2009**, *94*, 223110.
- (3) Yang, F.; Taggart, D. K.; Penner, R. M. Joule Heating a Palladium Nanowire Sensor for Accelerated Response and Recovery to Hydrogen Gas. *Small* **2010**, *6*, 1422–1429.
- (4) RaviPrakash, J.; McDaniel, A. H.; Horn, M.; Pilione, L.; Sunal, P.; Messier, R.; McGrath, R. T.; Schweighardt, F. K. Hydrogen Sensors: Role of Palladium Thin Film Morphology. *Sensors & Actuators: B. Chemical* **2007**, *120*, 439–446.
- (5) Ramanathan, M.; Skudlarek, G.; Wang, H. H.; Darling, S. B. Crossover Behavior in the Hydrogen Sensing Mechanism for Palladium Ultrathin Films. *NanoTech* **2010**, *21*, 125501.
- (6) Boon-Brett, L.; Black, G.; Moretto, P.; Bousek, J. A Comparison of Test Methods for the Measurement of Hydrogen Sensor Response and Recovery Times. *International Journal of Hydrogen Energy* **2010**, *35*, 7652–7663.
- (7) Wicke, E.; Brodowsky, H.; Züchner, H. Hydrogen in Palladium and Palladium Alloys. *Topics in Applied Physics* **1978**, *29*, 73–155.
- (8) Wilke, C. R.; Lee, C. Y. Estimation of Diffusion Coefficients for Gases and Vapors. *Ind. Eng. Chem.* **1955**, *47*, 1253–1257.
- (9) Deen, W. M. *Analysis of Transport Phenomena*; Oxford University Press: New York, 1998.
- (10) Kay, B.; Peden, C.; Goodman, D. Kinetics of Hydrogen Absorption by Pd(110). *Phys. Rev., B Condens. Matter* **1986**, *34*, 817–822.

5 SENSING CHARACTERIZATION OF Pd/Pt AND Pd/Ag FILMS OBTAINED BY SSR

5.1 INTRODUCTION

In previous chapters it was discussed that Pd films formed by SSR undergo an α to β phase transition that starts at $\sim 1\%$ v/v H_2/N_2 and is complete at 2% v/v H_2/N_2 (Figure 2.5). The volume expansion associated with this phase transition closes voids that exist between the metal grains which increases the electrical current but also causes instability in the films as it can lead to morphology deformations.¹ As discussed in Chapter 1, the addition of a second metal such as Ni,² Ag,³ or Pt⁴ can delay the phase transition to higher H_2 concentrations thus improving the detection range of the Pd based sensing films.

In Chapter 2 we studied the lattice expansion for $Pt_{10}Pd_{90}$ and $Ag_{10}Pd_{90}$ films obtained by SSR. For $Pt_{10}Pd_{90}$ (Figure 2.13) a lattice expansion starts at $\sim 1\%$ and, while at 3% v/v H_2/N_2 the lattice is apparently still expanding, it is less than the α to β expansion of pure Pd. For $Ag_{10}Pd_{90}$ (Figure 2.12) a lattice expansion seems to start at 0.5% v/v H_2/N_2 and by 1.5% v/v H_2/N_2 it has reached the maximum lattice expansion but, as $Pt_{10}Pd_{90}$, the lattice does not reach the Pd β -phase lattice parameter. These constraints in the lattice expansion can reduce the instability on the sensor signal caused by hydrogen adsorption, such as delamination, film peeling, and embrittlement,^{5,6} thus improving the detection range for the films. Researchers believe that the changes in the phase transition behavior of Pd alloys can be explained mainly by the geometric effect that causes structural changes within the metal lattice.⁷⁻¹⁰ However, while our $Ag_{10}Pd_{90}$ film formed

an alloy, our Pt₁₀Pd₉₀ film did not.¹¹ These different interactions between Pd and the second metal challenges the understanding of the behavior of these films when exposed to H₂.

In this chapter the response of these bimetallic films to hydrogen is described and discussed.

5.2 METHODOLOGY

Samples were synthesized following the solution impregnation method described in section 2.2.1. All the samples studied in this Chapter had a 5%wt total metal loading.

Two solutions with a 90:10 ratio of the Pd:M metals were made. The solution for the Ag₁₀Pd₉₀ sample had 0.0016 g of silver nitrate [AgNO₃, Alfa Aesar] and 0.0200 g of Pd(NO₃)₂•H₂O dissolved in 42 μL of deionized water. The solution for the Pt₁₀Pd₉₀ film had 0.0013 g of tetraammineplatinum(II) nitrate [Pt(NH₃)₄(NO₃)₂, Sigma Aldrich] and 0.0068 g of Pd(NO₃)₂•H₂O dissolved in 16 μL of deionized water. For each sample 3 μL of each bimetallic solution was impregnated over a 13mm Anodic Alumina Membrane to achieve the desired concentrations. The 90:10 ratio was chosen because it has been suggested in the literature that this ratio is the one suited for hydrogen sensing applications.^{2,12} The reduction was carried out using solid NaBH₄ and adding ~2μL of water as described in Chapter 2.

The sensing response was measured in the *Ch-90* described in section 4.2 using the methodology described in sections 3.2 and 4.2.

5.3 RESULTS AND DISCUSSION

As discussed in section 3.3.4, the signal of the Pd films becomes unstable with increasing hydrogen concentration. This instability is first evidenced in the hydrogen

response as an increase in the initial hydrogen baseline current as is observed at 4% v/v H₂/N₂ in Figure 5.1. This increase suggests that the phase change is closing void spaces in the film. At concentrations higher than 4% v/v H₂/N₂ the signal becomes unstable probably due to irreversible morphological changes caused directly by the phase change such as hydrogen embrittlement and film delamination.

The Pt₁₀Pd₉₀ sensor, on the other hand, can detect H₂ at a wider range of concentrations than the pure Pd sensor. In this film the first increase in current is first observed at 8% v/v H₂/N₂ (Figure 5.2). This delay to a higher concentration can be explained by the restriction in the lattice expansion of this sample at this concentration compared to pure Pd. The XRD patterns in Figure 2.13 suggest that above 3% v/v H₂/N₂ the lattice expansion continues; therefore there is a possibility that at 8% the lattice expansion has reached the Pd β-phase value. Furthermore, no instabilities, i.e. N₂ baseline drift, are observed in the response to higher concentrations up to 50% v/v H₂/N₂ suggesting that this sample does not suffer from irreversible morphological changes.

The results shown in Table 5.1 and a Pt₁₀Pd₉₀ hydrogen adsorption/desorption experiment (Figure 5.3) show that the sensitivity of the Pt₁₀Pd₉₀ sample increases almost linearly with respect to hydrogen concentration up to 4% v/v H₂/N₂ and reaches a sensitivity plateau at 8% v/v H₂/N₂. Earlier studies on Pt₁₀Pd₉₀ alloys also show a linear increase in normalized resistance as the hydrogen loading is increased¹³ and Ni-Pd alloys show a similar linear behavior.¹⁰ The maximum probably occurs as the hydride vacancies are filled as suggested by Sakamoto et al.¹⁴ This can produce a “blocking effect”¹⁵ as the number of vacancies is reduced therefore limiting absorption of hydrogen.

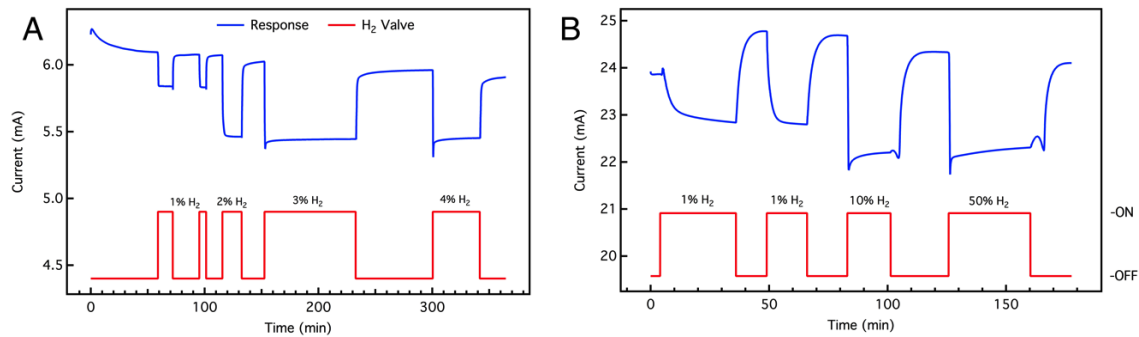


Figure 5.1 Sensing response of a pure Pd sample to hydrogen concentrations ranging from 1% to 4% (A) and the sensing response of a sample up to 50% v/v H₂/N₂ (B).

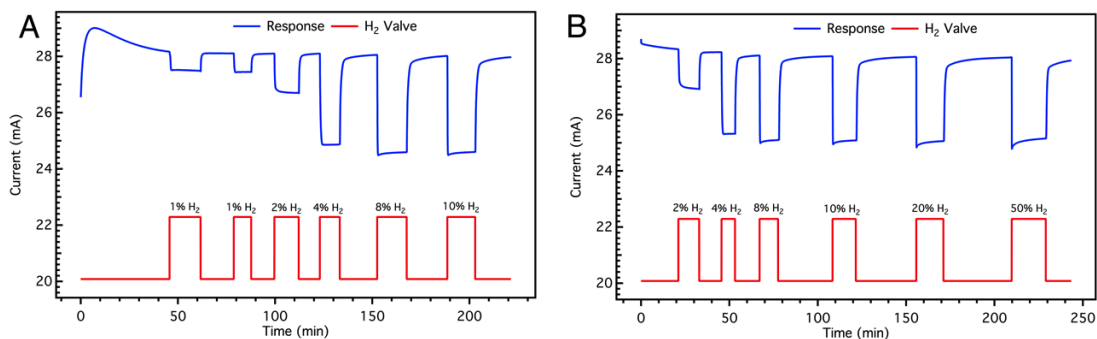


Figure 5.2 Sensing response of a Pt₁₀Pd₉₀ sample to hydrogen concentrations ranging from (A) 1% to 10% and (B) 2% to 50% v/v H₂/N₂

Table 5.1 Sensitivity at various concentrations for the Pd-M samples (NS = Not Stable).

	Sensitivity						
	1% H ₂	2% H ₂	4% H ₂	8% H ₂	10% H ₂	20% H ₂	50% H ₂
Pd	4.0%	10.1%	8.5%	NS	NS	NS	NS
Pt₁₀Pd₉₀	2.3%	5.0%	10.9%	11.5%	11.5%	10.7%	10.3%
Ag₁₀Pd₉₀	1.7%	3.4%	5.9%	6.6%	5.7%	5.0%	4.5%

The shape of the adsorption/desorption curve (Figure 5.3) is different than for pure Pd (Figure 3.11) suggesting that there are changes in the thermodynamics of the phase transition. The smaller hysteresis of this type of sample when compared to pure Pd

has been previously reported⁹ as was the bigger slope of the desorption curve owing to the faster desorption kinetics that result from the addition of a non adsorbing element. Also, the sensitivity during desorption almost reaches the initial value of 0% compared to 4% for pure Pd suggesting that the structural changes in this sample are reversible and that there is minimal irreversible gas absorption.

The structural stability of this sample at increasing hydrogen concentrations is also evident in the nitrogen current baseline value.^{16,17} In pure platinum, hydrogen can exist in either a negatively or positively polarized state depending on the surface morphology of the film.¹⁸ A negatively polarized subsurface state tends to increase the surface work function, thus decreasing the electrical conductivity.¹⁸⁻²⁰ The small N₂ baseline drift suggests that only positively charged hydrogen states are present in the sample. The stable response of these samples makes them reliable for detecting a wide range of hydrogen concentrations. Moreover, Pt does not suffer hydrogen embrittlement⁶ possibly adding further stability to the sample.

The Pt₁₀Pd₉₀ sample has a higher sensitivity than pure Pd at 4% v/v H₂/N₂ (Table 5.1). Early studies done by Lewis¹³ show that Pt₁₀Pd₉₀ alloys gradually increase their sensitivity with hydrogen loading by a larger factor than pure Pd due to a decrease in the chemical potential for hydrogen adsorption, that also reflects as a decrease in the heat of adsorption. Platinum alone however, does not dissolve hydrogen as effectively as pure palladium since it does not form hydrides even though the chemical potential for hydrogen adsorption is decreased.²¹

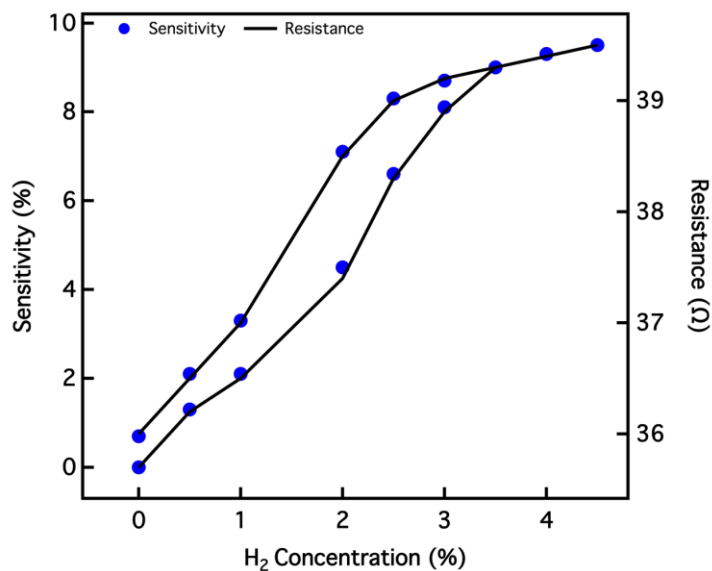


Figure 5.3 Hysteresis during hydrogen absorption and desorption of a Pt₁₀Pd₉₀ sample.

The response time of this sample, however, is slower than for pure Pd under the same experimental configuration at 4% v/v H₂ which coincides with the concentration at which the sensitivity increases (Table 5.2). As the sensitivity increases, the time required to reach absorption equilibrium increases thus increasing the response time. Moreover, studies have shown that the rate of diffusion of hydrogen in Pt/Pd systems decreases as the amount of Pt is increased.²² As the H₂ concentration increases, the response time increases as described with relaxation time theory.²³

Compared to other Pd/Pt hydrogen sensors studies, the response of our samples is as stable and fast as those reported in the literature. Similar stability has been observed in other Pd/Pt nanowire based hydrogen sensors that were studied up to 4% v/v.^{24,25} Phan et al.²⁴ report high sensitivities of 50% at 4% v/v H₂/N₂ and ~3 min response times. In contrast Li et al.²⁵ report faster response times for Pt₁₀Pd₉₀ nanowire based sensors (4 s at 4% v/v H₂/N₂) but with a lower sensitivity (10% at 4% v/v H₂/N₂). However, as

demonstrated in Chapter 4, the response time is highly dependent on testing conditions. Even though the morphologies are very different, our Pt₁₀Pd₉₀ film obtained through SRR is very competitive in terms of their stability, sensitivity, and response time.

Table 5.2 Response time at various concentrations for the Pd and Pd-M samples (NS = Not Stable)

	Response Time (s)						
	1% H ₂	2% H ₂	4% H ₂	8% H ₂	10% H ₂	20% H ₂	50% H ₂
Pd	33.3	79.5	12.8	NS	NS	NS	NS
Pt₁₀Pd₉₀	37.0	73.3	37.5	11.8	9.7	4.3	2.1
Ag₁₀Pd₉₀	15.7	22.4	13.9	4.3	3.2	2.1	1.1

The hydrogen sensing response of the Ag₁₀Pd₉₀ sample is shown in Figures 5.5 and 5.6. As Pt₁₀Pd₉₀, this sample was also able to withstand 50% v/v H₂/N₂ exposures. The sensitivity of this sample however, was lower than for pure Pd and Pt₁₀Pd₉₀ because the addition of Ag lowers its hydrogen adsorption capacity.³ Moreover, the nitrogen current baseline drifts significantly to lower values with increasing concentrations starting at 4% v/v H₂/N₂. Theoretical studies^{26,27} have shown that hydrogen absorption in Ag₁₀Pd₉₀ alloys can cause the segregation of Ag to the surface which could be causing this shift. Scharnagl et al.²⁸ showed this experimentally with Auger Electron Spectroscopy and Scanning Electron Microscopy. They also reported baseline drifts in gate field effect transistors with Ag₁₀Pd₉₀ thin films and attributed it to this particle migration; this drift eventually stabilizes when hydrogen is completely desorbed. The baseline in Figure 5.5 seems to approximate to a stable value after various cycles. Pre-treatment with hydrogen could stabilize the sample if the segregation reaches a limit where it does not occur any longer with hydrogen exposure.

This baseline drift affects the calculations of sensitivity for this sample. In Figure 5.4a, the sensitivity of the film to the first exposure to 4% v/v H₂/N₂ is 14%, whereas the sensitivity to the second exposition decreases to 10%. This decrease in sensitivity is probably due to the larger fraction of Ag on the surface after the hydrogen induced particle segregation that is decreasing the hydrogen absorption capacity. However, the sensitivity to 1%v/v H₂/N₂ remains unchanged after the sample being exposed to high hydrogen concentrations possibly because this low H₂ concentration does not induce Ag particle segregation.

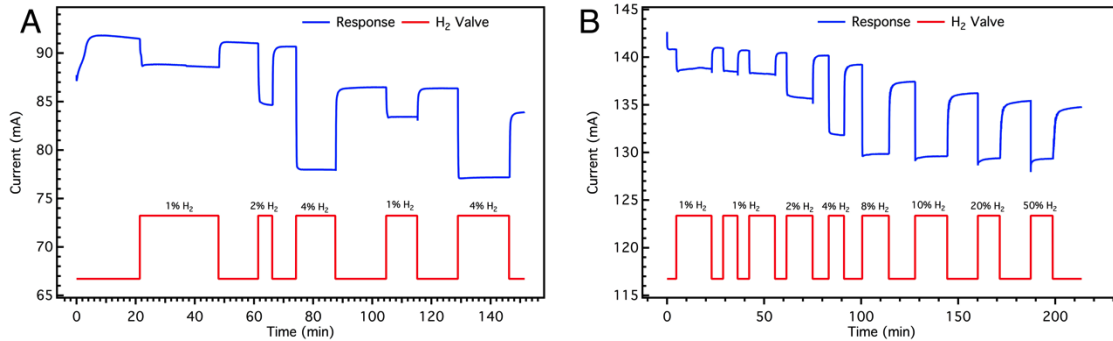


Figure 5.4 Sensing response of a Ag₁₀Pd₉₀ film (A) from 1% to 4% v/v H₂/N₂ and (B) 1% to 50% v/v H₂/N₂.

The response time of this sample is faster than the Pt₁₀Pd₉₀ sample and to the pure Pd sample (Table 5.2). This agrees with the high H₂ permeability of Ag₁₀Pd₉₀ which is comparable to pure Pd (2.46 cm³/cm² s for Ag₂₀Pd₈₀ vs. 1.43 cm³/cm² s for pure Pd).²⁹ It has been said that Ag can enhance the H₂ permeation through Pd films^{7,29,30} Higher permeation would mean higher hydrogen content penetrating the sample per unit time. Therefore, the system would achieve the final resistance base value faster thus decreasing response time.

The trends of our Ag₁₀Pd₉₀ hydrogen sensors are similar to those published in the literature. Palladium-silver thin film based hydrogen sensors reported by Wang et al.³¹ have smaller sensitivities when compared to pure Pd but respond faster possibly due to the decreased absorption capacity^{2,3} and high permeability of hydrogen through Ag₁₀Pd₉₀ alloys, respectively. They show response times of ~15 s for a 2% v/v H₂/N₂ exposure which is close to our observed value of 22 s at the same concentration. In contrast, they report 1.5% sensitivity at 2% H₂, whereas our sensor shows 3.4% at this concentration.

5.4 CONCLUSIONS

Our results show that addition of Pt and Ag increase the range of hydrogen concentration detection of our samples. Both the Pt₁₀Pd₉₀ and Ag₁₀Pd₉₀ samples were able to respond to up to 50% v/v H₂/N₂ concentrations. Of the three samples studied, the Pt₁₀Pd₉₀ sample had the most stable nitrogen baseline and high sensitivity across all the hydrogen concentrations tested due to a higher adsorption capacity, but was slower than pure Pd films due to increased absorption equilibrium time. The Ag₁₀Pd₉₀ films, on the other hand, have lower sensitivities than pure Pd films but faster response times at all hydrogen concentrations tested probably due to increased H₂ permeation and lower adsorption capacity. However, they have an unstable N₂ baseline at concentrations higher than 4% v/v H₂/N₂ due to Ag segregation.

Overall, SSR is able to produce bimetallic films that expand the range of detection and applications of pure Pd films for hydrogen sensing that is comparable or better than similar sensors in the literature.

5.5 REFERENCES

- (1) Kufudakis, A.; Čermák, J.; Lewis, F. A. Reversible and Irreversible Diffusion-Elastic Deformation Effects Resulting From Absorption and Desorption of Hydrogen by Palladium. *Surface Technology* **1982**, *16* (1), 57–66.
- (2) Hughes, R. C.; Schubert, W. K. Thin Films of Pd/Ni Alloys for Detection of High Hydrogen Concentrations. *J. Appl. Phys.* **1992**, *71* (1), 542–544.
- (3) Hughes, R. C.; Schubert, W. K.; Zipperian, T. E.; Rodriguez, J. L.; Plut, T. A. Thin-Film Palladium and Silver Alloys and Layers for Metal-Insulator-Semiconductor Sensors. *J. Appl. Phys.* **1987**, *62* (3), 1074–1083.
- (4) Choi, S. Y.; Takahashi, K.; Matsuo, T. No Blister Formation Pd/Pt Double Metal Gate MISFET Hydrogen Sensors. *IEEE Electron Device Lett.* **1984**, *5* (1), 14–15.
- (5) Adams, B. D.; Chen, A. The Role of Palladium in a Hydrogen Economy. *Materials Today* **2011**, *14* (6), 282–289.
- (6) Barnoush, A. Hydrogen Embrittlement. *Saarland University* **2011**.
- (7) Kibria, A.; Sakamoto, Y. The Effect of Alloying of Palladium with Silver and Rhodium on the Hydrogen Solubility, Miscibility Gap and Hysteresis. *International Journal of Hydrogen Energy* **2000**, *25* (9), 853–859.
- (8) Sakamoto, Y.; Yuwasa, K.; Hirayama, K. X-Ray Investigation of the Absorption of Hydrogen by Several Palladium and Nickel Solid Solution Alloys. *Journal of the Less Common Metals* **1982**, *88* (1), 115–124.
- (9) Łukaszewski, M.; Hubkowska, K.; Czerwiński, A. Electrochemical Absorption and Oxidation of Hydrogen on Palladium Alloys with Platinum, Gold and Rhodium. *Phys. Chem. Chem. Phys.* **2010**, *12* (43), 14567–14572.
- (10) Lee, E.; Lee, J. M.; Lee, E.; Noh, J.-S.; Joe, J. H.; Jung, B.; Lee, W. Hydrogen Gas Sensing Performance of Pd–Ni Alloy Thin Films. *Thin Solid Films* **2010**, *519* (2), 880–884.
- (11) Valentín-Estevés, K.; Mendez-Colberg, H.; Martínez-Iñesta, M. M. Synthesis of Pure and Bimetallic Pd Films Supported in Anodic Alumina Membranes by Solid State Reduction. *Materials Letters* **2015**, *156*, 65–68.
- (12) Hughes, R.; Schubert, W.; Buss, R. Solid- State Hydrogen Sensors Using Palladium- Nickel Alloys: Effect of Alloy Composition on Sensor Response. *J. Electrochem. Soc.* **1995**, *142*, 249–254.
- (13) Lewis, F. A. The Hydrides of Palladium and Palladium Alloys. *Platinum Metals Rev* **1961**, *5* (1), 21–25.
- (14) Sakamoto, Y.; Takai, K.; Takashima, I.; Imada, M. Electrical Resistance Measurements as a Function of Composition of Palladium-Hydrogen (Deuterium) Systems by a Gas Phase Method. *J. Phys.: Condens. Matter* **1996**, *8*, 3399–3411.
- (15) Tong, X. Q.; Sakamoto, Y.; Lewis, F. A.; Bucur, R. V. “Uphill” Hydrogen Diffusion Effects and Hydrogen Diffusion Coefficients in Palladium. *International journal of ...* **1997**, *22* (2-3), 141–144.
- (16) Pundt, A. Hydrogen in Nano-Sized Metals. *Adv. Eng. Mater.* **2004**, *6* (12), 11–21.

- (17) Lee, E.; Lee, J. M.; Koo, J. H.; Lee, W.; Lee, T. Hysteresis Behavior of Electrical Resistance in Pd Thin Films During the Process of Absorption and Desorption of Hydrogen Gas. *International Journal of Hydrogen Energy* **2010**, 35 (13), 6984–6991.
- (18) Lisowski, W.; Duś, R. Formation of Surface and Subsurface Hydrogen States on Thin Palladium and Platinum Films Precovered with Methane. *Applied surface science* **1994**, 78 (4), 363–372.
- (19) Felter, T. E.; Foiles, S. M.; Daw, M. S.; Stulen, R. H. Order-Disorder Transitions and Subsurface Occupation for Hydrogen on Pd (111). *Surface Science Letters* **1986**, 171 (1), L379–L386.
- (20) Lewis, F. A.; McKee, S. G. Structures of Hydrided Palladium at Interfaces: Evidence of Subsurface Quasi-B(A') Phase Hydride Formation at Very Low Hydrogen Chemical Potentials at 25 °C. *Surface Technology* **1985**, 24 (4), 355–363.
- (21) Antonov, V. E.; Belash, I. T.; Malyshev, V. Y. The Solubility of Hydrogen in the Platinum Metals Under High Pressure. *Platinum Met ...* **1984**, 28 (4), 158–163.
- (22) Lewis, F. A. The Palladium-Hydrogen System. *Platinum Metals Rev* **1982**, 26 (3), 121–128.
- (23) Laidler, K. J. *Chemical Kinetics*; 1965.
- (24) Phan, D.-T.; Uddin, A. S. M. I.; Chung, G.-S. Sensors and Actuators B: Chemical. *Sensors & Actuators: B. Chemical* **2015**, 220, 962–967.
- (25) Li, X.; Liu, Y.; Hemminger, J. C.; Penner, R. M. Catalytically Activated Palladium@Platinum Nanowires for Accelerated Hydrogen Gas Detection. *ACS Nano* **2015**, 9 (3), 3215–3225.
- (26) Løvvik, O. M.; Opalka, S. M. Reversed Surface Segregation in Palladium-Silver Alloys Due to Hydrogen Adsorption. *Surface Science* **2008**, 602 (17), 2840–2844.
- (27) Gonzalez, S.; Neyman, K. M.; Shaikhutdinov, S.; Freund, H. J.; Illas, F. On the Promoting Role of Ag in Selective Hydrogenation Reactions Over Pd-Ag Bimetallic Catalysts: a Theoretical Study. *J. Phys. Chem. C* **2007**, 111 (18), 6852–6856.
- (28) Scharnagl, K.; Eriksson, M.; Karthigeyan, A. Hydrogen Detection at High Concentrations with Stabilised Palladium. *Sensors and Actuators B ...* **2001**, 78, 138–143.
- (29) Knapton, A. G. Palladium Alloys for Hydrogen Diffusion Membranes. *Platinum Metals Review* **1977**, 21 (2), 44–50.
- (30) Uemiya, S.; Matsuda, T.; Kikuchi, E. Hydrogen Permeable Palladium-Silver Alloy Membrane Supported on Porous Ceramics. *Journal of Membrane Science* **1991**, 56 (3), 315–325.
- (31) Wang, M.; Feng, Y. Palladium–Silver Thin Film for Hydrogen Sensing. *Sensors & Actuators: B. Chemical* **2007**, 123 (1), 101–106.

6 REDUCTION OF THE EFFECT OF ADSORBED OXYGEN ON THE Pd BASED HYDROGEN SENSOR RESPONSE BY ADDITION OF A ZEOLITE LAYER

6.1 INTRODUCTION

Oxygen can dissociatively adsorb on Pd surfaces at temperatures above 200 K as a physisorbed and a chemisorbed precursor for the formation of PdO.¹⁻⁴ This ability of Pd is used in applications such as catalytic converters in cars for carbon monoxide (CO) oxygenation^{2,5,6} and fatty acid deoxygenation.⁷

Shaikhutdinov et al.⁸ demonstrated with TPD that Pd surfaces that were pre-exposed to oxygen inhibited the adsorption of hydrogen due to a site-blocking effect caused by the oxygen ad-atoms. This adsorption competition represents a problem in hydrogen sensing applications since the signal of the sensing element depends directly on the absorption of hydrogen. Similarly, other gases such as CO, SO₂, and H₂S can poison the Pd surface decreasing the ability of the sensing element to reliably detect hydrogen.⁹ Molecular sieves are an alternative to minimize this adsorption competition and increase the selectivity of hydrogen-sensing elements.

Zeolites are crystalline porous aluminosilicate materials with a tetrahedral connected framework with cavities occupied by ions or water molecules¹⁰. The size of the pores of these materials, which are in the angstrom range, allow them to act as molecular sieves. There are a variety of zeolite frameworks that are classified according to their structure and symmetry that give them different separation capacities.

Among available zeolites, Zeolite P (Figure 6.1) has a Gismondine-like framework (GIS) with intersecting channels of $3.1 \times 4.4 \text{ \AA}$ and $2.6 \times 4.9 \text{ \AA}$ along $[100]$ and $[010]$ directions, respectively.^{11,12}

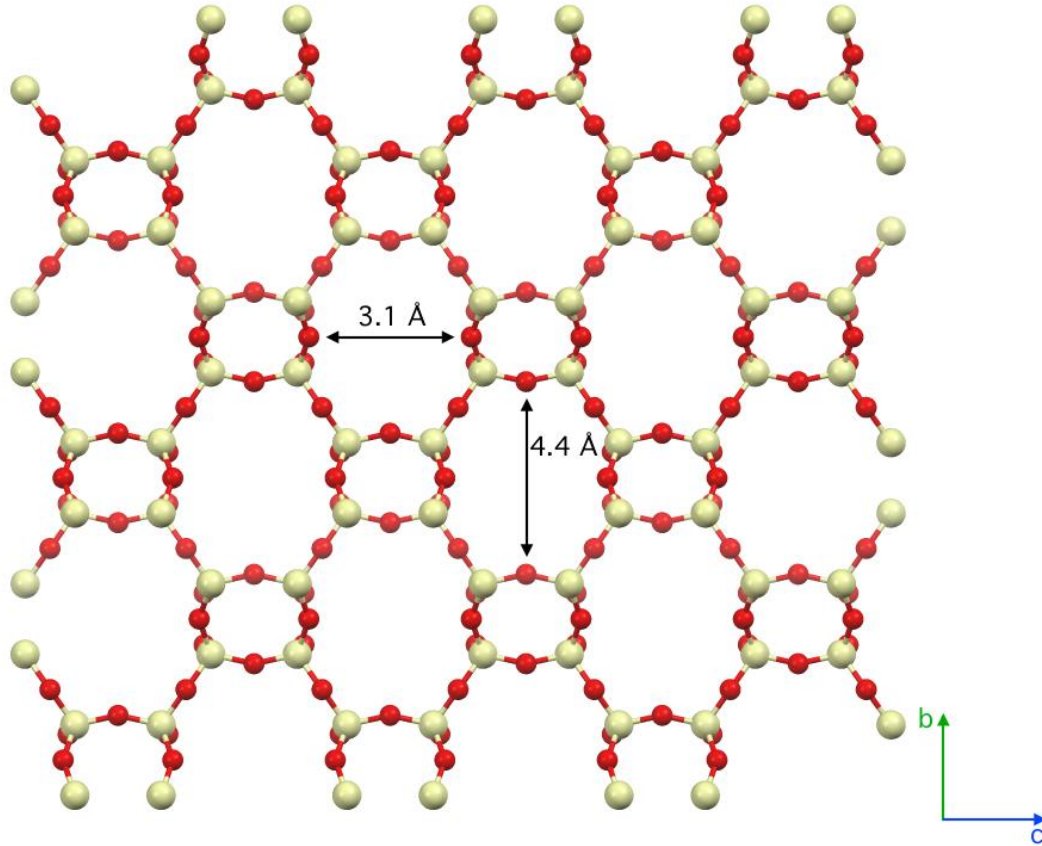


Figure 6.1 Gismondine framework viewed along the a -axis¹³

According to the International Zeolite Association (IZA) the maximum diameter of a sphere that can diffuse through axis a , b , and c of this framework is 3.32 \AA . The kinetic diameters of oxygen and hydrogen are 3.46 \AA and 2.89 \AA , respectively.¹⁴ Therefore zeolite P with GIS framework can potentially be used for H_2/O_2 separation. In this Chapter we report the results of the effect of oxygen on the hydrogen response of our Pd sensor and how a layer of zeolite type Na-P1 with GIS framework can help their hydrogen selectivity.

6.2 METHODOLOGY

6.2.1 Synthesis and Characterization of Pd sensors

The Pd samples were synthesized with the solid impregnation method as described in section 2.2.1 with 5% wt Pd and adding water during reduction. The sensing was tested in the *Ch-7000* chamber described in section 3.2.

6.2.2 Synthesis and Characterization of Zeolite P

The zeolite synthesis gel was produced following the procedure described by Dong et al.¹¹ For this synthesis 6.4 mL of sodium silicate and 0.5130 g of sodium aluminate were dissolved on 25 mL and 14.7 mL of NaOH 0.472 M respectively. The clear solution of sodium aluminate was added into the sodium silicate solution under vigorous stirring to obtain a homogeneous synthesis gel. The solution was left under continuous stirring for 20 hours before use. The solution was deposited inside of a 60 mL Teflon-lined autoclave. Then the autoclave was placed inside of an oven at 100°C for 12 hours. The characterization was carried out using X-ray diffraction with a Rigaku Ultima III diffractometer unit using CuK α radiation operating at 40 kV and 44 mA.

6.2.3 Deposition of Zeolite P

The deposition of the zeolite powder was done by suspending ~0.04 g of zeolite Na-P1 in 20 mL of deionized water. The Pd ensemble was immersed in the suspension for 10 minutes and dried at 60 °C for 30 minutes. This procedure was repeated three times. Afterwards, zeolite Na-P1 was further deposited on the sample by suspending 0.04 g of zeolite type Na-P1 in 3 mL of deionized water and pipetting the suspension on top of the sample. An attempt was made to synthesize a zeolite membrane by the traditional hydrothermal treatment but components in the sensor ensemble such as the silver epoxy

that was used to fabricate the electrodes was reacting with the reactive mixture and destroying the sample.

6.3 RESULTS AND DISCUSSION

6.3.1 Effect of Oxygen on the Response

For all the properly reduced samples there is an initial sudden jump in the current values when the sensor is first exposed to H₂ that quickly stabilizes. This phenomenon has been previously reported on the response to hydrogen of a PdO sample¹⁵ and is attributed to its reduction to Pd. As shown in Chapter 2 with XRD and XPS, our samples are pure Pd, therefore the presence of this initial jump is due to either desorption of oxygen from the surface of the sample or the reaction of adsorbed oxygen with the flowing hydrogen. The reaction between oxygen and hydrogen is thought to occur through the following reaction mechanism where adsorbed atomic oxygen reacts with adsorbed atomic hydrogen to produce water at T > 200K.¹⁶⁻¹⁸



Figure 6.2 shows the response of a sample exposed to cycles of H₂/N₂ and O₂/N₂. The sample responds as expected to hydrogen when it is mixed with nitrogen, i.e. the current decreases when exposed to H₂ and increases when exposed to N₂. However when the sample is in N₂ and is exposed to different O₂/N₂ concentrations, the current also decreases. This decrease can be attributed to an increase in the Pd surface work function due to changes to the dipole layer by the strongly adsorbed negatively charged oxygen atoms.¹⁹ The correlation between a decrease in electrical conductivity with increasing

work function was shown by Heras et al.²⁰ who also reported an increase in the work function of a Pd(111) surface by 0.8 eV as the surface is exposed to oxygen at 300 K.

When the sample is reexposed to 1% H₂/N₂, after been exposed to O₂, the current jumps up and then slowly decreases which is similar to what is observed in the first hydrogen cycle in a nitrogen and hydrogen only environment. Conrad et al.²¹ reported an increase in work function of 0.2 eV for adsorption of hydrogen at room temperature, which is a smaller change in work function than during oxygen adsorption. The current values during the 1% H₂/N₂ flow are lower than those during O₂/N₂ flow. The discrepancy between the change in work function and the current values is due to that hydrogen is adsorbed on the Pd surface in two different forms: negatively and positively polarized atoms.²² Negatively charged ad-species increase the work function, whereas positively charged ad-species decrease the work function. Positively charged ad-species can penetrate into the bulk leading to the formation of hydride species, which are mainly responsible for the decrease in electrical current of the bulk. Therefore the higher decrease in current due hydrogen absorption does not happen mainly because of changes in work function, rather the effect of the positively polarized ad-species.

The increase in current that occurs with hydrogen exposure after being exposed to oxygen shows that the presence of hydrogen reduces the amount of adsorbed oxygen. The adsorption energy of oxygen in Pd at room temperature is higher than that of hydrogen (~55 kcal/mol²³ vs. ~21 kcal/mol²¹), thus the adsorption of the oxygen and the hydrogen is very competitive. Thus, the reduction of adsorbed oxygen likely occurs through two mechanisms: desorption of weakly adsorbed oxygen and reaction with hydrogen. The observed jump in the response when exposed to H₂/N₂ after air can be explained by the

desorption of weakly adsorbed oxygen. The slow decrease in the signal can be explained by the subsequent simultaneous reduction reaction and adsorption/absorption of hydrogen into the structure.

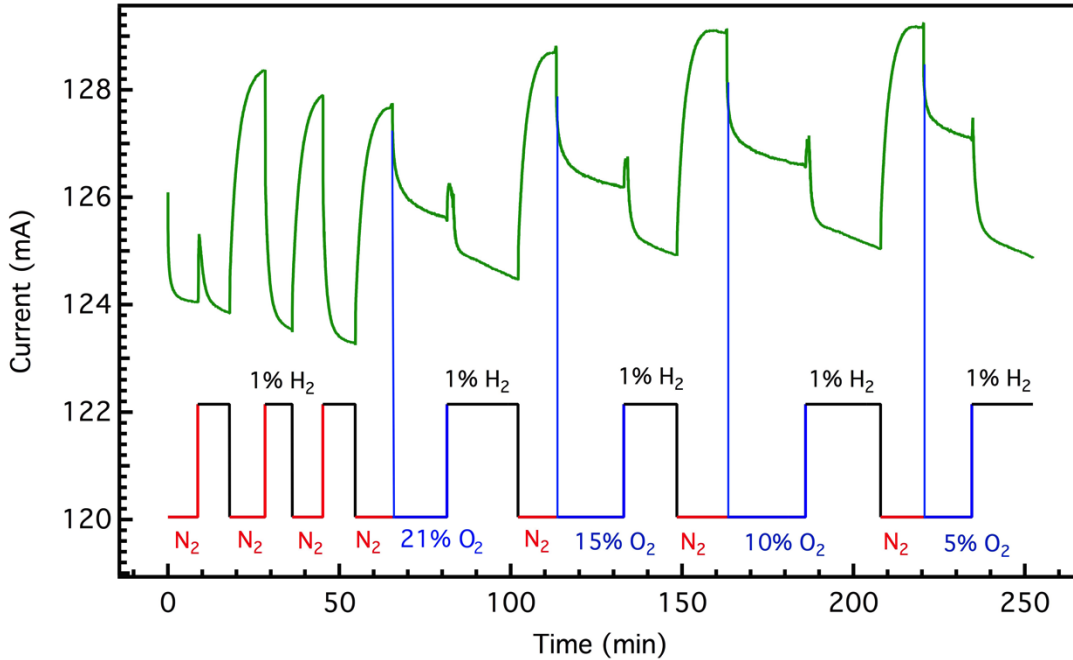


Figure 6.2 Sample with 5%wt Pd exposed to O₂ after hydrogen exposure.

To further understand the effect of oxygen in the sensing results we studied the response of a sample exposed to 0.5% v/v H₂ in compressed air when previously exposed to compressed air (Figure 6.3). Contrary to the response to H₂/N₂ after exposition to O₂/N₂, the current increases and then slowly decreases with no initial jump. The fact that there is no jump is explained by the fact that in this system there is a continuous adsorption and desorption of oxygen. The increase in current can be explained by the decrease in surface oxygen atoms by their reaction with hydrogen and the slow decrease in current can be explained by the slow absorption of hydrogen in this system.

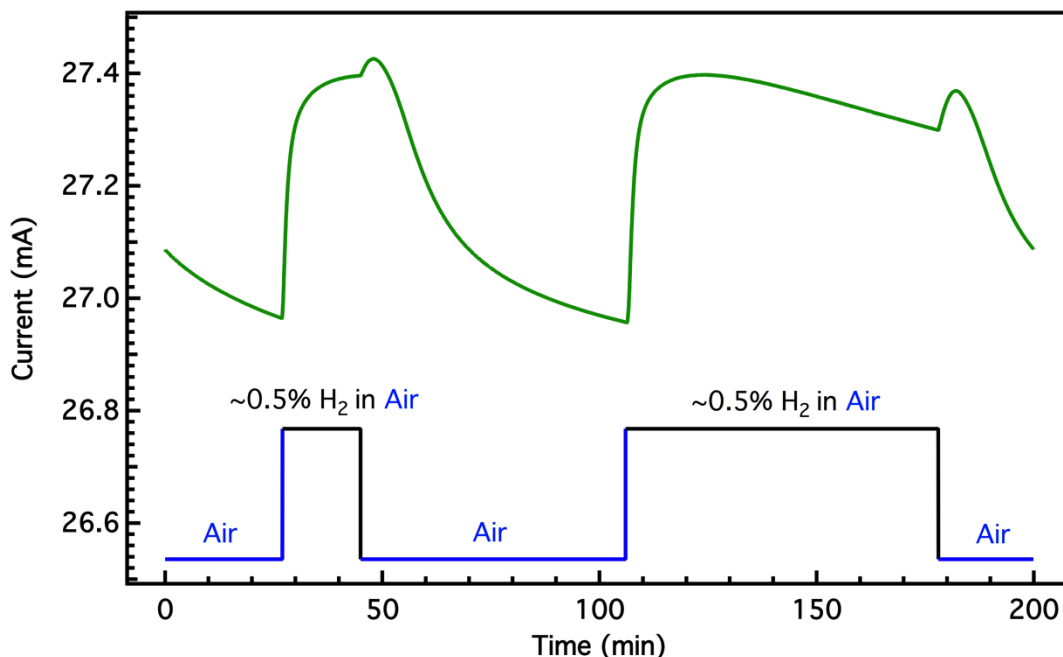


Figure 6.3 Sample with 5%wt Pd exposed to H₂/ N₂ and H₂/compressed air cycles.

The response time (time to reach 90% of the final change in current after exposure to hydrogen) for the 0.5%v/v H₂/air after exposure to air (Figure 6.3) was ~5 minutes which was significantly slower when compared to other samples exposed to 0.5%v/v H₂/N₂ (~2.5 minutes). In the presence of oxygen it is more difficult for the hydrogen to adsorb. The jump in current observed when the sample is reexposed to oxygen after being exposed to hydrogen is possibly due to the fast desorption of hydrogen.

These results might suggest that Pd could function as an oxygen sensor as well as a hydrogen sensor. Figure 6.4 shows that when a sample is on a nitrogen environment and is initially exposed to oxygen the current decreases due to oxygen adsorption. However, this adsorption is very strong and, unlike reexposure to H₂/N₂, the reexposure of the sample to N₂ does not change the current significantly since nitrogen does not react with oxygen nor it promotes its desorption.

Nitrogen (N_2) is known to dissociatively chemisorb at room temperature and above on transition metals such as Ti, Zr, Nb, among others to form metal nitrides. However, nitrogen does not chemisorb on noble metals such as Pd and Pt either dissociatively or molecularly.²⁴ Due to its inertness, N_2 is used on the testing of noble metal based H_2 sensing devices. Therefore, the decrease in current of the sample when exposed to oxygen occurs notably in an oxygen free surface, that is, after the sample has been exposed to hydrogen and all the oxygen has been removed. The increase in current when the sample is exposed to nitrogen after being exposed to hydrogen diluted in nitrogen, appears to occur because nitrogen drags away the hydrogen molecules as the atoms associatively desorb from the Pd surface since the adsorption of hydrogen is reversible at room temperature.²⁵⁻²⁹

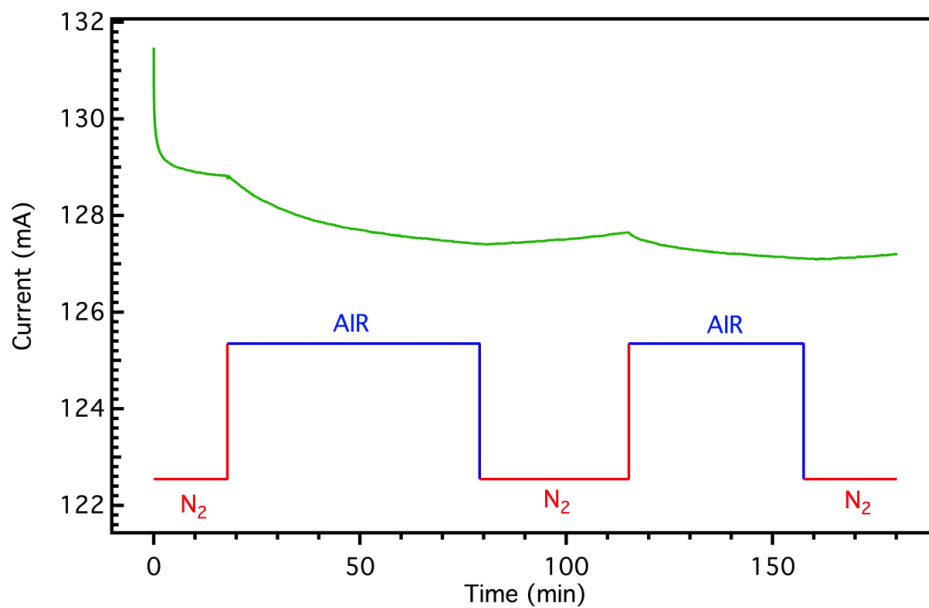


Figure 6.4 Sample with 5%wt Pd exposed to N_2 and Air cycles.

6.3.2 Effect of Zeolite P on the Hydrogen/Oxygen Pd Sensor Selectivity

Figure 6.5 shows that the X-ray diffraction pattern of our synthesized zeolite corresponds to zeolite Na-P1 (GIS). Figures 6.6A and B show the response of a 5% wt Pd sample without zeolite deposition, and with two zeolite depositions, respectively. The samples were exposed to cycles of 1% H₂/N₂ and O₂/N₂ and Table 6.1 shows the results of the current change associated with these results calculated as:

$$\Delta i = \frac{|i_0 - i_g|}{i_0} \times 100 \quad (\text{Eq. 6.3})$$

where i_0 is the initial current value and i_g is the final current value when the sample has been exposed to a gas (H₂ or O₂). Because the current does not reach a steady state value, to be consistent, the final current value has been defined as the value after ten minutes of exposure.

As before, these figures show that there is a decrease in current upon exposure to oxygen for both the sample without and with a zeolite layer. Table 6.1 shows that the Δi for the sample without a zeolite layer upon oxygen adsorption at different concentrations is very similar while for the sample with the zeolite layer the Δi decreases with oxygen concentration. Moreover, the Δi for the sample with the zeolite layer upon H₂/N₂ exposure is significantly increased and for O₂/N₂ is significantly decreased.

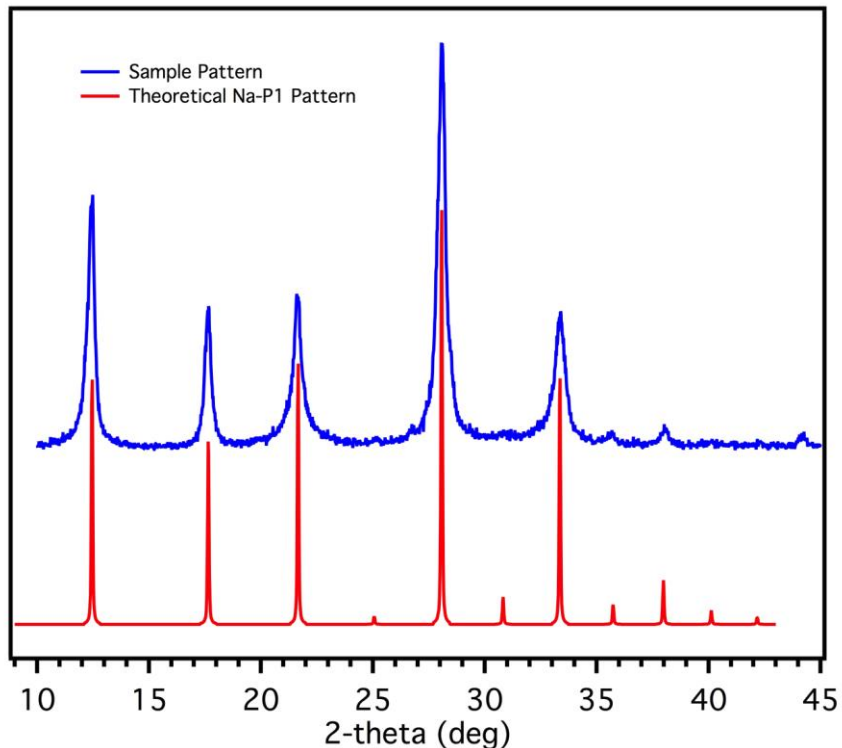


Figure 6.5 XRD Patterns for Zeolite type Na-P1 sample compared to theoretical pattern.

The sample without the zeolite layer had a Δi of 7.1% for an exposure to 1%v/v H_2/N_2 . After the zeolite deposition, the initial Δi to 1%v/v H_2/N_2 decreased to 5.9%, a 17% reduction. However the most change was observed during oxygen adsorption; the Δi for 10% O_2 exposure decreased from 3.8% to 1.9% (a 50% reduction) and for 0.5%v/v O_2 the Δi decreased from 3.0% to 1.1% (a 63% reduction) before and after zeolite deposition.

Moreover the Δi due to hydrogen exposure after oxygen exposure before and after zeolite deposition increased. Evidently the zeolite layer enhances the response of the sample to H_2 when in an oxygen environment. These results can be explained by a decrease of adsorbed oxygen in the Pd surface such that the hydrogen can more readily

adsorb. The response time to H₂/N₂ in the sample before and after the zeolite deposition is similar suggesting that diffusion through the zeolite layer does not slow the response and that the limiting step is still the removal of the adsorbed oxygen atoms.

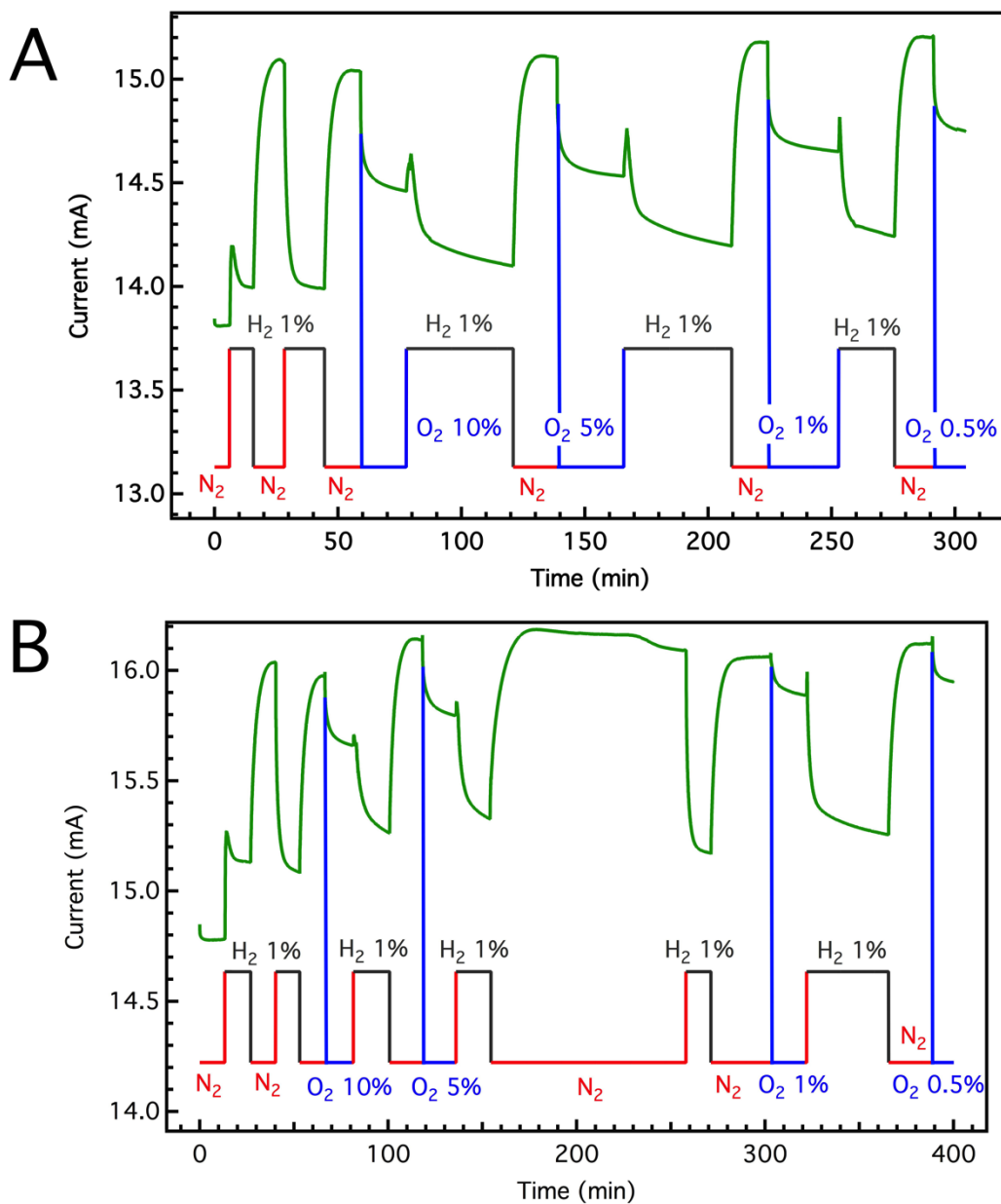


Figure 6.6 Sample with 5%wt Pd exposed to cycles of 1%v/v H₂, N₂ and O₂ diluted with N₂, (A) No zeolite deposited, and (B) zeolite layer deposited.

Table 6.1 Current changes for the sample with and without zeolite deposition. Response times are shown for hydrogen cycles after oxygen exposure.

Gas Concentration	t_{90} (min)	Δi
No zeolite deposited		
Initial exposure H₂ 1% in	2.9	7.1%
N ₂		
O ₂ 10%	--	3.8%
H ₂ 1% in N ₂	8.4	1.6%
O ₂ 5%	--	3.8%
H ₂ 1% in N ₂	7.6	1.4%
O ₂ 1%	--	3.5%
H ₂ 1% in N ₂	5.2	2.5%
O ₂ 0.5%	--	3.0%
Zeolite deposited		
Initial exposure H₂ 1% in	3.2	5.9%
N ₂		
O ₂ 10%	--	1.9%
H ₂ 1% in N ₂	7.3	2.2%
O ₂ 5%	--	2.1%
H ₂ 1% in N ₂	6.4	2.7%
O ₂ 1%	--	1.1%
H ₂ 1% in N ₂	4.9	3.4%
O ₂ 0.5%	--	1.1%

These results show that the layer of zeolite Na-P1 acts as a barrier for oxygen adsorption. The pores of the zeolite are acting as a molecular sieve to oxygen allowing the faster diffusion of hydrogen. However, the fact that there is still a response to oxygen suggests that the deposition method used is not 100% effective by providing void spaces for the oxygen to penetrate to the sample. Nevertheless, these results demonstrate the potential of using zeolite coatings for producing highly selective hydrogen sensors.

6.4 CONCLUSIONS

This work is a proof of concept that a local zeolite coating can make Pd based sensors more selective to hydrogen. The zeolite Na-P1 used in this work suppressed the diffusion of oxygen onto Pd based chemiresistors presumably by size selectivity. This work suggests that this method is viable as an alternative to also prevent poisoning to other gases, such as carbon monoxide, and that through optimization of the deposition method, more selectivity is possible.

Moreover, this work gives more insight into the effect of oxygen in the response of Pd based sensors, which is important as oxygen is ubiquitous in land based environments. The competition between oxygen with hydrogen for adsorption in Pd can affect the sensor response since it decreases the response time and the sensitivity as well. Moreover exposure to oxygen decreases the current of the sample, which could be misinterpreted as response to hydrogen and affect the viability of the sensing elements.

Another phenomenon that was explored were the jumps in current when going from oxygen to hydrogen environments and vice versa which can have applications in hydrogen safety sensors because these changes are faster and larger before achieving a steady state change.

6.5 REFERENCES

- (1) Imbihl, R.; Demuth, J. E. Adsorption of Oxygen on a Pd(111) Surface Studied by High Resolution Electron Energy Loss Spectroscopy (EELS). *Surface Science Letters* **1986**, *173* (2), A390–A391.
- (2) Meusel, I.; Hoffmann, J.; Hartmann, J.; Heemeier, M.; Bäumer, M.; Libuda, J.; Freund, H. J. The Interaction of Oxygen with Alumina-Supported Palladium Particles. *Catalysis Letters* **2001**, *71* (1-2), 5–13.
- (3) Sjøvall, P.; Uvdal, P. Oxygen Sticking on Pd(111): Double Precursors, Corrugation and Substrate Temperature Effects. *Chemical Physics Letters* **1998**, *282*, 355–360.
- (4) Guo, X.; Hoffman, A.; Yates, J. T. Adsorption Kinetics and Isotopic Equilibration of Oxygen Adsorbed on the Pd(111) Surface. *J. Chem. Phys.* **1989**, *90* (10), 5787–5792.
- (5) Peterson, E. J.; DeLaRiva, A. T.; Lin, S.; Johnson, R. S.; Guo, H.; Miller, J. T.; Hun Kwak, J.; Peden, C. H. F.; Kiefer, B.; Allard, L. F.; et al. Low-Temperature Carbon Monoxide Oxidation Catalysed by Regenerable Atomically Dispersed Palladium on Alumina. *Nat Commun* **2014**, *5*, 4885.
- (6) Rumpf, F.; Poppa, H.; Boudart, M. Oxidation of Carbon Monoxide on Palladium: Role of the Alumina Support. **1988**, *4* (3), 722–728.
- (7) Ford, J. P.; Immer, J. G.; Lamb, H. H. Palladium Catalysts for Fatty Acid Deoxygenation: Influence of the Support and Fatty Acid Chain Length on Decarboxylation Kinetics. *Top Catal* **2012**, *55* (3-4), 175–184.
- (8) Shaikhutdinov, S. Interaction of Oxygen with Palladium Deposited on a Thin Alumina Film. *Surface Science* **2002**, *501*, 270–281.
- (9) Hübert, T.; Boon-Brett, L.; Black, G.; Banach, U. Hydrogen Sensors – a Review. *Sensors & Actuators: B. Chemical* **2011**, *157* (2), 329–352.
- (10) Lobo, R. F. Introduction to the Structural Chemistry of Zeolites. *Handbook of Zeolite Science and Technology* **2003**.
- (11) Dong, J.; Lin, Y. S. In Situ Synthesis of P-Type Zeolite Membranes on Porous A-Alumina Supports. *Industrial & engineering chemistry research* **1998**, *37* (6), 2404–2409.
- (12) Yin, X.; Zhu, G. S.; Yang, W.; Li, Y.; Zhu, G. Q.; Xu, R.; Sun, J.; Qiu, S.; Xu, R. R. Stainless-Steel-Net-Supported Zeolite NaA Membrane with High Permeance and High Permselectivity of Oxygen Over Nitrogen. *Adv. Mater.* **2005**, *17* (16), 2006–2010.
- (13) Macrae, C. F.; Bruno, I. J.; Chisholm, J. A.; Edgington, P. R.; McCabe, P.; Pidcock, E.; Rodriguez-Monge, L.; Taylor, R.; van de Streek, J.; Wood, P. A. Mercury CSD 2.0 - New Features for the Visualization and Investigation of Crystal Structures. *Journal of Applied Crystallography* **2008**, *41* (2), 466–470.
- (14) Baker, R. W. *Membrane Technology and Applications*; John Wiley & Sons, 2012.
- (15) Lee, Y. T.; Lee, J. M.; Kim, Y. J.; Joe, J. H.; Lee, W. Hydrogen Gas Sensing Properties of PdO Thin Films with Nano-Sized Cracks. *NanoTech* **2010**, *21* (16), 165503.

- (16) Mitsui, T.; Rose, M. K.; Fomin, E.; Ogletree, D. F.; Salmeron, M. Coadsorption and Interactions of O and H on Pd (111). *Surface Science* **2002**, *511*, 259–266.
- (17) Demchenko, D. O.; Sacha, G. M.; Salmeron, M.; Wang, L. W. Interactions of Oxygen and Hydrogen on Pd(111) Surface. *Surface Science* **2008**, *602* (14), 2552–2557.
- (18) Clay, C.; Cummings, L.; Hodgson, A. Mixed Water/OH Structures on Pd(111). *Surface Science* **2007**, *601* (2), 562–568.
- (19) Huang, W.; Zhai, R.; Bao, X. Direct Observation of Subsurface Oxygen on the Defects of Pd(100). *Surface Science* **1999**, *439* (1), L803–L807.
- (20) Heras, J. M.; Estiu, G.; Viscido, L. Annealing Behaviour of Clean and Oxygen Covered Polycrystalline Palladium Films: a Work Function and Electrical Resistance Study. *Thin Solid Films* **1990**, *188*, 165–172.
- (21) Conrad, H.; Ertl, G.; Latta, E. E. Adsorption of Hydrogen on Palladium Single Crystal Surfaces. *Surface Science* **1974**, *41* (2), 435–446.
- (22) Duś, R.; Nowakowski, R.; Nowicka, E. Chemical and Structural Components of Work Function Changes in the Process of Palladium Hydride Formation Within Thin Pd Film. *Journal of Alloys and Compounds* **2005**, *404-406*, 284–287.
- (23) Conrad, H.; Ertl, G.; Küppers, J.; Latta, E. E. Interaction of NO and O₂ with Pd (111) Surfaces. II. *Surface Science* **1977**, *65* (1), 245–260.
- (24) Miyazaki, E.; Kojima, I.; Kojima, S. Chemisorption of Molecular Nitrogen on Palladium Surfaces at and Above Room Temperature. **1985**, *1* (2), 264–266.
- (25) Li, Y.; Cheng, Y. T. Hydrogen Diffusion and Solubility in Palladium Thin Films. *International Journal of Hydrogen Energy* **1996**, *21* (4), 281–291.
- (26) Wicke, E.; Brodowsky, H.; Züchner, H. Hydrogen in Palladium and Palladium Alloys. *Topics in Applied Physics* **1978**, *29*, 73–155.
- (27) Everett, D.; Nordon, P. Hysteresis in the Palladium+ Hydrogen System. *Proceedings of the Royal Society of London. Series A. Mathematical and Physical Sciences* **1960**, *259* (1298), 341–360.
- (28) Lee, E.; Lee, J. M.; Koo, J. H.; Lee, W.; Lee, T. Hysteresis Behavior of Electrical Resistance in Pd Thin Films During the Process of Absorption and Desorption of Hydrogen Gas. *International Journal of Hydrogen Energy* **2010**, *35* (13), 6984–6991.
- (29) Deveau, N. D.; Ma, Y. H.; Datta, R. Beyond Sieverts' Law: a Comprehensive Microkinetic Model of Hydrogen Permeation in Dense Metal Membranes. *Journal of Membrane Science* **2013**, *437*, 298–311.

7 CONCLUSIONS AND RECOMMENDATIONS

The solid-state reduction (SSR) is a facile synthesis method to obtain Pd and Pd based bimetallic films that are stable, sensitive, and fast resistor-type hydrogen sensors. This technique is cost-effective, as it does not require excess metal reagents, sophisticated equipment, high temperatures or high voltages.

The SSR method can successfully reduce the Pd, Pt, and Ag precursors: $\text{Pd}(\text{NO}_3)_2 \cdot x\text{H}_2\text{O}$, $\text{Pt}(\text{NH}_3)_4(\text{NO}_3)_2$, and AgNO_3 . Using anodic alumina membranes as a support two films of different morphologies are formed on either side for all metal combinations studied. A rough film is formed due to the aggressive reaction of sodium borohydride with water on the side where the latter is at a higher concentration whereas a smooth film is formed on the water deficient side. Solution impregnation yielded a more consistent and even distribution of the metal on the support as it relies less on human and environmental variability and is also appropriate for producing bimetallic films.

As a hydrogen sensing element, the Pd films obtained through the SSR method had stable signals at 2.5 and 5% wt Pd loadings and were able to detect 0.01% - 2% v/v H_2/N_2 with sensitivities as high as 7%. The Pd films followed with great accuracy Sieverts' law making them good candidates for hydrogen monitoring applications. A 5% wt Pd loaded sample is a good candidate for hydrogen sensing applications since it showed a balance between response time, sensitivity, and signal stability along with good reproducibility.

To optimize the stability of the signal, the electrical connection, film roughness, and reduction state were studied. The best configuration for obtaining a stable signal was

using Cu wires with silver paste connected on the rough surface of the sample since better contact area (increased α -spots) were achieved. Adding water in the reduction step during synthesis increases the roughness of the film and the fraction of reduced metal leading to a more stable signal.

The sensitivity and response time of the samples were affected by the voltage applied, morphology of the film, and residence time. The sensitivity and response time of the films synthesized by solution impregnation were not affected by changes in voltage, as it did for solid impregnation films, because of the small bulk resistance the former has. This leads to small changes in current which stabilize the self-heating of the films.

The Joule heating effect and the increased α -spots are probable reasons why the rough films yielded faster response times with good sensitivities when compared to the smooth surface. The residence time significantly affected the response time and sensitivity of the Pd films by shifting the rate-controlling step from the hydrogen adsorption to the hydrogen convection to the sample.

Hydrogen adsorption/desorption curves showed along with the hydrogen response plots, that the samples suffered morphological changes during phase transition that affects the responses above the phase transition concentration. The incorporation of Pt and Ag to the Pd films caused suppression in the expansion of the Pd lattice and increases the range of hydrogen concentration detection of our samples. Both the Pt₁₀Pd₉₀ and Ag₁₀Pd₉₀ samples were able to respond to up to 50% v/v H₂/N₂ concentrations. The Pt₁₀Pd₉₀ films had the most stable nitrogen baseline and high sensitivity across all the hydrogen concentrations tested, but was slower than pure Pd films due to slow diffusion. Ag₁₀Pd₉₀ films, on the other hand, have smaller sensitivities than pure Pd films but faster

response times at all hydrogen concentrations tested due to increased H₂ permeation. However, they have an unstable N₂ baseline at concentrations higher than 4%v/v H₂/N₂ possibly due to the segregation of Ag particles with H₂ absorption.

This work provided insight into the effect of oxygen in the response of Pd based sensors, which is important, as oxygen is ubiquitous in land-based environments. Exposure to oxygen decreases the current of the sample, which could be misinterpreted as response to hydrogen and affect the viability of the sensing elements. A zeolite type Na-P1 coating on top of the films made them more selective to hydrogen presumably by suppressing the diffusion of oxygen by size selectivity. This work suggests that this method is viable as an alternative to also prevent poisoning from other gases, such as carbon monoxide, and that through optimization of the deposition method, better selectivity is possible.

Overall, films obtained through the SSR synthesis method can be engineered to meet the specifications of the DoE for indoor fueling facility monitoring (response time of 30 s at 1% H₂) By optimizing the sensing conditions a Pd films had a 2.7% sensitivity and a t_{90} of 4 s and the bimetallic films that expanded the range of detection to 50%v/v H₂. This performance is comparable or better than similar sensors in the literature.

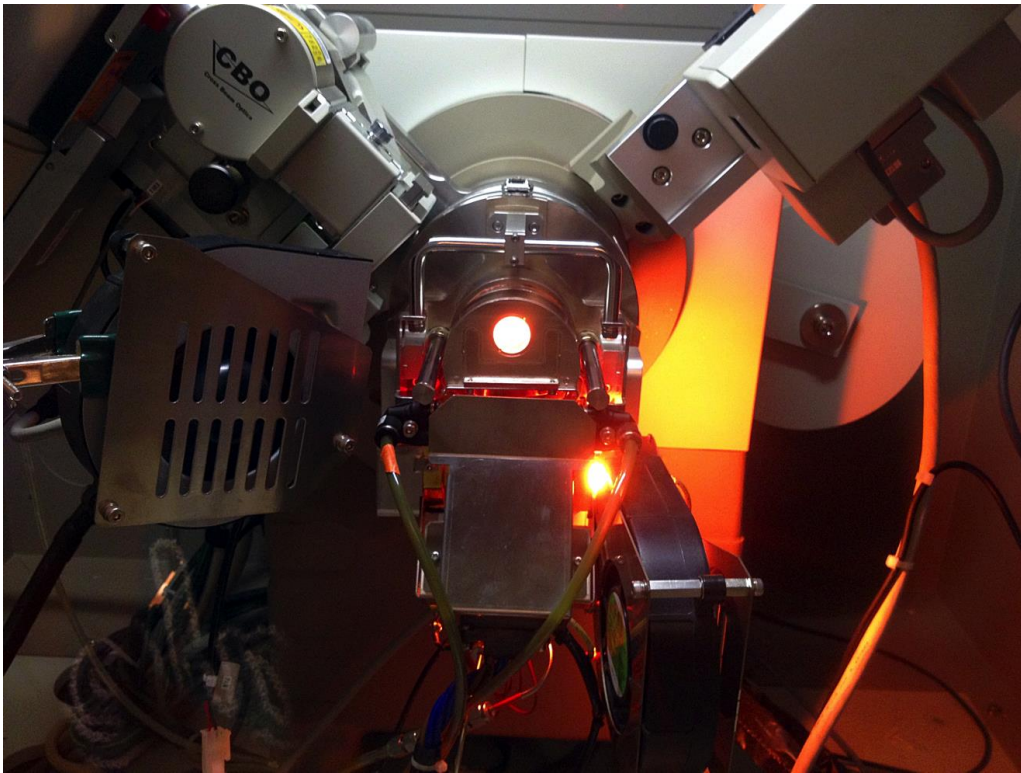
As recommendations, the solution incorporation of the metal precursor in SSR method could be improved by using techniques such as spin coating to achieve better precursor distribution by preventing localized high concentration spots. With spin coating, the SSR could yield more uniform films. With uniform films along with the addition of the sample onto a strong support, techniques such as SEM, AFM, and Profilemeters could be used to effectively characterize the delamination and

embrittlement of the samples. If a uniform film is obtained for the bimetallic samples, Auger Electron Spectroscopy with depth profiling could be used to effectively characterize the distribution of species within the sample. Moreover, the addition of a third metal could be studied.

The testing of the samples can be improved by using a specialized testing chamber intended for this purpose, where the position of the sensor can be varied to study the effect this has on the response. This would allow us to perform location validations to be able to accurately locate the sensor if the source for leaks or monitoring is well established. Also, with this chamber, the effect that conditions such as temperature and humidity have on the response could be studied.

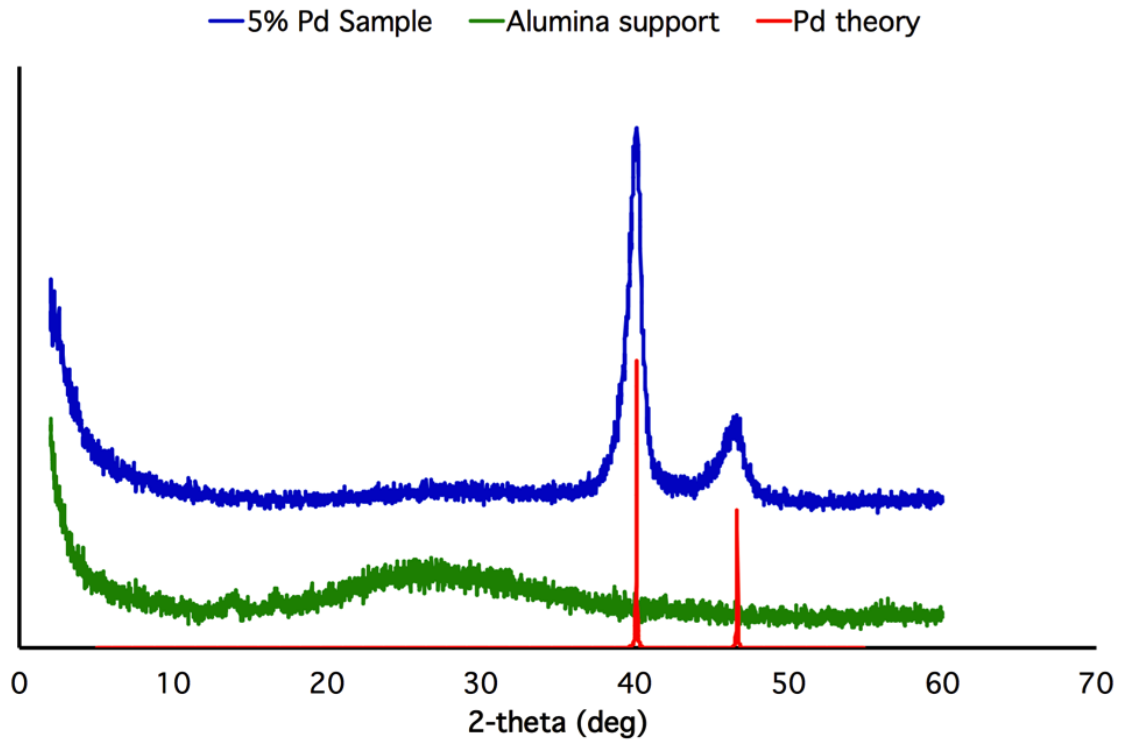
APPENDIX A

Attachment used for the characterization of the phase changes for Pd
(Reactor X)



APPENDIX B

XRD pattern for a 5% wt Pd sample without the Reactor X attachment.



APPENDIX C

Matlab routines for solving the Navier-Stokes equation:

Please see <http://www.mathworks.com/help/matlab/ref/pdepe.html> for more information on the pdepe solver.

A. *icfun.m*

```
function u0=icfun(x)
%icfun: MATLAB function M-file that specifies the initial condition
%for a PDE in time and one space dimension.
u0=0;
end
```

B. *bcfun.m*

```
function [pl,ql,pr,qr]=bcfun(xl,ul,xr,ur,t)
%bcfun: MATLAB function M-file that specifies boundary conditions
%for a PDE in time and one space dimension.
pl=ul;
ql=0;
pr=ur-1;
qr=0;
end
```

C. *pdefun.m*

```
function [c,b,s] = pdefun(x,t,u,DuDx)
%pdefun: MATLAB function M-file that specifies
%a dimensionless PDE in time and one space dimension.
inch=7;
L=inch*0.0254; %meters
tf=1.5*60; %seconds
flow=1; %cm^3/min
Qf=flow*1e-6*(1/60); %m^3/s conversion
area=(3.1416*(1/2)^2)*0.00064516; %meters^2
vel=Qf/area; %meters/seconds
D=9.089e-5; %meters^2/seconds
Fo=D*tf/L^2; %fourier number
Pe=L*vel/D; %pecllet number
c=1/Fo; %c, b, and s are the PDE.m function parameters,
b=DuDx; %See http://www.mathworks.com/help/matlab/ref/pdepe.html
s=-Pe*DuDx;
end
```

D. PDE.m

```
%PDE:MATLAB script M-file that solves and plots
%solutions to the PDE stored in pdefun.m
clear all
close all
m=0;
%Define solution mesh
x=linspace(0,1,200);
t=linspace(0,1,200);
%Solve the PDE
u = pdepe(m,@pdefun,@icfun,@bcfun,x,t);
for i=20:20:200
    set(gca, 'FontName', 'Geneva');
    set(gca, 'FontSize', 14);
    figure (1);
    plot(x,u(i,:), 'LineWidth', 1.25);
    xlabel('z/L', 'FontSize', 14);
    ylabel('(C0-C)/(C0-Cf)', 'FontSize', 14);
    axis tight

hleg=legend('t1','t2','t3','t4','t5','t6','t7','t8','t9','t10','t11','t
12','t13','t14','t15','t16','t17','t18','t19','t20');
    set(hleg, 'FontSize', 14);
    hold on
    filename3='u.xls';
    j=(20:20:200);
    xlswrite(filename3,u(j,:),1);
end
```